UNIVERSITAT POLITÈCNICA DE CATALUNYA
BARCELONATECH
Escola Superior d'Enginyeries Industrial, Aeroespacial i Audiovisual de Terrassa

Air distribution in street canyons: a CFD study

BACHELOR FINAL THESIS

Document:
Report

Author:
Pau Garcia Moreno

Director /Co-director:
Ivette María Rodríguez Pérez

Degree:
Bachelor in Industrial Technologies Engineering

Examination session:
Spring, 2021

DECLARATION

Project Title	Air distribution in street canyons: a CFD study
Author	*Pau Garcia Moreno*
Direcor	Ivette María Rodríguez Pérez

I declare that this thesis entitled *Air distribution in street canyons: a CFD study* is the result of my own work except as cited in the references.

Pau Garcia Moreno

Department of Heat engines and machines
Polytechnic University of Catalonia, ESEIAAT

Date: June 22, 2021

ACKNOWLEDGEMENTS

First of all I would like to express my deep and sincere gratitude to my director and research supervisor, *Ivette María Rodríguez Pérez*, for giving me the opportunity to work in a project that has given to me much more knowledge than I would have never thought. I really appreciate her professionalism, her passion, not just for science but for teaching, the immense amount of knowledge and work ethics transferred to me and, obviously, her trust on me for carrying out this project.

I want to thank to all the people who I have met during these four amazing years, professionals who have taught me uncountable exciting subjects, have instilled in me priceless values at the same time that have made from this journey an unforgettable experience. I would like to emphasise the help provided to me by students who introduced me Ivette, by the fluid mechanics professors and by my teammates of *Open Source Computational Fluid Dynamics* subject.

Last but not least I want to express my most sincere gratitude to my parents for their unconditional support and trust, to *M.C.R.*, my relatives and friends for their kind care, and to all the people who have supported me, directly or indirectly, during this final stage of my Bachelor's Degree in Industrial Engineering Technologies.

Pau Garcia Moreno
Polytechnic University of Catalonia, ESEIAAT
Date: June 22, 2021

—- Pau Garcia Moreno —-

ABSTRACT

Nowadays, it is a fact that one of the most important and harmful problems, that all of us have to deal with, is pollution. Despite of pollutants generation issue goes quite further and needs to be solved from the root, this study allows us to have a deep understanding of how passive gaseous pollutants move around our cities and lets us conclude how cities parameters, such as urban street canyons' width and street's aspect ratio, among others, affect the airflow and pollutant transport and diffusion.

The study of the air flow has been made by using *OpenFoam*, an open source CFD (Computational Fluid Dynamics) software that combined with some meshing and post-processing tools, such as *Ansa*, *ParaView* and *Matlab*, has allowed us to obtain all the valuable information mentioned before. All the initial results obtained from an *RNG k-epsilon* simulation have been validated with LES (Large Eddy Simulations) and experimental data, and once 2D results are validated for an aspect ratio *(AR)* equal to the unit, other street canyons configurations have been implemented in order to obtain more detailed results and visualize and comprehend the pollutants movement and the direct relation in between it and the canyon's configuration.

After all these simulations are done, important conclusion have been obtained and cities improvements could be proposed, referring to the improvement of air circulation in street canyons, in order to reduce the harmful effects of pollution.

Keywords: pollution, street canyons, CFD, OpenFoam, LES, experimental data, 2D, Matlab, Ansa, ParaView

SUMMARY

English version

The presented thesis entitled *Air distribution in street canyons: a CFD study*, developed by Pau Garcia Moreno and directed by Ivette Maria Rodríguez Pérez, is the result of a research project related to the study of airflow and pollutant distribution in modern cities. This study is interesting as the configuration and characteristics of nowadays cities around the world drive the pollutant generated in street canyons to be retained in them, creating one of the worst pollutant removal scenario possible. Some of these remarkable characteristics are: tall buildings and narrow streets, low velocity airflows, buildings' repetition patterns with small distance in between them, among others.

Given this situation and all the health and environmental problems that pollution generates, the main objective of this thesis is to study the airflow and distribution of pollutant generated by cars in street canyons by using computational fluid dynamics (CFD) simulations. With this purpose we have conducted many different simulations with OpenFoam using a simplified 2D computational domain that consists on a different number of buildings in a row, depending on the aspect ratio, obtaining many useful street canyons for conducting our studies. This geometry can be found in uncountable cities around the world and, for its importance, it has been studied in many occasions, with computational and experimental methods, giving use the opportunity to use the literature results to validate our own results.

The described geometry has been used for conducting different simulations that can be classified in two parts: the first one, where there has not been implemented any pollutant source, being the main purpose of it the obtaining of validated velocity and pressure maps in order to have a strong basis for performing the second part of this thesis. In this second part a lineal pollutant source in the middle of the street canyon at ground-level has been implemented, being a passive scalar pollutant source. The distribution and transport of the gaseous pollutant source has been studied for three different street canyons depending on the aspect ratio (AR): AR=0.50, AR=1.00 and AR=2.00. All the results obtained from these *OpenFoam* simulations have been post-processed using *Matlab* and *ParaView* in order to interpret and analyse all the data obtained and later get valuable conclusions. With this purpose we have used velocity and pressure maps, streamlines, mean concentration and

pollutant flux maps, etc. It cannot be omitted the fact that after conducting all these steps we have validated all the results with the available data in the literature.

Finally, after having followed all the process for doing a CFD simulation, we have obtained some conclusions that allow us to perfectly appreciate the relation in between the pollutant retention and recirculation in street canyons and the canyons' and flow's parameters. It has been shown that for an airflow with Reynolds and Schmidt numbers of 12 000 and 0.72, respectively, the relation in between the canyons' aspect ratio and the pollutant retention is direct, with values of 95, 97 and 99% of retention in canyons of an aspect ratio of 0.50, 1.00 and 2.00, respectively. These results give us the opportunity to continue the work done in this thesis in a wide variety of ways: improve the mesh and configuration of the cases, implement a second pollutant source, change the way how the pollutant source is modelled, among others.

SUMMARY

Catalan version

La present tesis titulada "Air distribution in street canyons: a CFD study", realitzada per Pau Garcia Moreno i dirigida per Ivette Maria Rodríguez Pérez, és el resultat d'un projecte d'investigació sobre la circulació de l'aire i distribució de contaminants a les ciutats. Aquest estudi és d'especial interès donada la configuració i característiques de les ciutats modernes d'arreu del món, les quals tenen una sèrie de propietats que fan que els seus carrers siguin ideals per l'estancament i recirculació dels contaminants generats pels cotxes. Algunes d'aquestes característiques són: edificis alts i carrers estrets, circulació d'aire a poca velocitat, existència de patrons de repetició d'edificis amb poca distància de separació, entre d'altres.

Donada aquesta situació i els greus problemes que la contaminació genera, tant a la nostra salut com al medi ambient, el principal objectiu d'aquesta tesis és l'estudi de la circulació de l'aire i distribució dels contaminants generats pels cotxes, mitjançant tècniques de CFD (mecànica de fluids computacional). Amb aquest propòsit s'han fet diverses simulacions en OpenFoam amb un domini d'estudi simplificat en dues dimensions que consta de diversos edificis en fila, generant així diversos canons regulars, ideals pel nostre estudi. Aquesta geometria la podem trobar en innumerables ciutats i ha sigut estudiada en diverses ocasions, tant experimentalment com amb tècniques de CFD, el que ens permet validar els resultats obtinguts en el nostre projecte.

La geometria descrita s'ha fet servir per dur a terme vàries simulacions, les quals podem separar en dues parts: la primera, on s'ha fet un estudi sense generació de contaminants per canons urbans de diverses relacions d'aspecte entre l'altura de l'edifici i l'amplada del carrer; aquesta primera part s'ha fet amb el propòsit d'obtenir uns resultats de velocitat i pressió validats i tenir així una base sòlida d'on partir en la segona part de l'estudi. En aquesta altra s'ha afegit una font de contaminants lineal al canó, simulant així la generació de gasos dels cotxes. Aquesta font és de contaminants escalars i passius, i s'ha fet servir per estudiar la seva distribució i transport en canons de relació d'aspecte de 0.50, 1.00 i 2.00 (mateixes relacions que s'han fet servir a la primera part). Els resultats d'aquestes simulacions s'han post-processat, amb Matlab i ParaView, per tal de poder interpretar i analitzar la informació obtinguda i obtenir així unes conclusions mitjançant mapes de velocitat i pressió, línies de

corrent, mapes de concentració i flux de contaminants, entre d'altres. No podem obviar el fet de que aquests, posteriorment, han sigut validats amb la informació trobada en la literatura.

Finalment, després de seguir tot el procés necessari per realitzar correctament una simulació amb CFD, hem extret conclusions que ens permeten apreciar perfectament la relació que hi ha entre la retenció i recirculació dels contaminants als nostres carrers i els paràmetres del canons i del flux d'aire. Hem vist que per un flux amb números de Reynolds i de Schmidt de 12 000 i 0.72, respectivament, la relació d'aspecte té una relació directe amb la retenció del contaminants al canó, amb una retenció del 95, 97 i 99% en canons de relació d'aspecte de 0.50, 1.00 i 2.00, respectivament. Aquest resultats donen pas a possibles futurs estudis, com ara: millora de la malla i configuració dels casos, incorporació d'una segona font de contaminants, canvi en el modelat de la font de contaminants, entre d'altres.

GLOSSARY

- **CFD:** Computational Fluid Dynamics
- **AR:** Aspect Ratio
- **DNS:** Direct Numerical Simulation
- **LES:** Large Eddy Simulation
- **RANS:** Reynolds-Averaged Navier-Stokes
- **RNG:** Re-Normalization Group
- **FVM:** Finite Volume Method
- **PDE:** Partial Differential Equation
- **EVM:** Eddy Viscosity Model
- **LDA:** Laser Doppler Anemometer
- **CAD:** Computer-Aided Design
- **TKE:** Turbulent Kinetic Energy
- **PID:** Property Identifier
- **ACH:** Air Exchange Rate
- **PCH:** Pollutant Exchange Rate

Contents

List of Figures

List of Tables

Chapter 1

Introduction

1.1 Aim

The aim of this project is to do a CFD study of air distribution and pollutant transport in street canyons continuing some previously done studies related to this field, such as the thesis presented in *ESEIAAT* two years ago by *Jordi Galí*[14]. With this project a deep understanding of pollution distribution in cities will be obtained and a study about how cities, buildings and air flows parameters can affect to it, will be carried out.

1.2 Scope

The scope can be defined as follows:

- Learn how to work with Ansa and how to use the software to mesh the case geometry.
- Apply the previously mentioned knowledge in order to do the mesh.
- Learn how to use the open source software OpenFoam (v7/v8) to do a CFD simulation.
- Run the first 2D simulation in order to obtain similar results to the ones previously obtained by experimental studies and LES simulations, using the case setup that *Jordi Galí* obtained during his thesis.
- Learn how to use ParaView as a post-processing tool.
- Study the results obtained in the first 2D simulation using ParaView and compare them with the LES and experimental results.
- If the results are coherent and appropriate, we move to the next step, if not, we prepare the case setup again and run simulations until we obtain appropriate results.

- Add pollution transport to the case set up in order to model the pollutants diffusion and transport in street canyons and the direct relation that it has with the aspect ratio.
- Study the results in order to obtain significant information about the pollution distribution and retention in street canyons.
- Apply geometry and boundary conditions changes and see how the results are affected.
- Propose suitable improvements for improving air circulation in street canyons.

1.3 Requirements

This investigation thesis has some requirements that should be fulfilled in order to achieve all this study's goals:

- Obtain simulated results according to the experimental and LES information in order to validate the first simulations.
- Be able to do a detailed study of certain street canyons of interest.
- Find an appropriate method to model a pollutant source.
- Propose feasible solutions or improvements that take into account the cities technical requirements and people's needs.
- Obtain coherent simulation results according to the available computational resources.
- Be able to appreciate the differences in between airflow structures in urban street canyons of different aspect ratios.

1.4 Background

It is a fact that one of the most important dangers that our society has to deal with is pollution, and that all the problems that it generates are main issues that must be solved in the next years to come. These aspects make this project so significant and important in order to improve the air circulation through cities and to reduce the pollution that affects population in a wide variety of ways: health problems, ecosystems damaging, etc.

This project was started two years ago, in 2019, by *Jordi Galí*[14], an ESEIAAT student whose final year thesis was also directed by *Ivette María Rodríguez*. Using the case implementation results that Jordi obtained, and by adding the model of a lineal pollutant source at ground-level, we will be able to know how all these harmful substances move around our cities. Moreover, we will be able to visualize and understand how the city parameters, such as buildings aspect ratio, and gaseous inert pollutant properties, such as the diffusion coefficient, affect to the pollution distribution.

After all these studies are conducted we will obtain very important conclusions that will be so useful to improve the air circulation in cities, understanding the flow structures of different street canyons configurations and preventing the recirculations (vortexes) effects that originate a pollution concentration and retention in our streets. To obtain significant data it is critical that the results of the CFD simulations, using a *RNG k-epsilon* model coincide with the LES and experimental results (many previous simulations, experiments and studies in this field have been carried out along the years) and that the pollution transport equations properly model the phenomena that we want to study.

Finally, it is important to mention the fact that for being able to carry out this project I have been learning (extracurricular) fluid mechanics, focusing on learning how CFD simulations work, and that the start point of this study is the previous work done by *Jordi Galí*, as he found the appropriate turbulence models, simulation parameters, mesh size... During these months we will be working on the CFD simulations that will allow us to understand how, something as important as pollution, moves around and how we can improve the air circulation and reduce the effects among us.

Chapter 2

Problem definition

2.1 State of the art

Because of the importance and direct effect that pollutants have in our health and in the environment preservation, airflow and pollutant transport in street canyons have been widely studied during the last few decades. These studies include several variations in case studies, geometries, techniques... but all of them have the same pursuit: find the answer to something that concerns everyone. In this section we are just focusing on the studies which are related to symmetric street canyons, with and without pollutant transport, as it is the objective of our thesis.

Related to the flow and vortex structure in symmetric street canyons, many studies have been carried out since the XX Century. *Oke*[4], in 1988 analysed the literature and did a review of regular canyons, finding the different flow regimes that are mentioned and used during the following sections . Later on, in 1996, *Sini*[15] performed CFD simulations using RANS (Reynold-Averaged Navier-Stokes equations), obtaining initial numerical results to the analysis previously done.
Later on, during the first decade of the XXI Century, some other studies have been done, including the work done by *Yujun, Li and Lee*, among others[16][15][17]. In these studies, more advanced CFD techniques and experiments were used, such as Large Eddy Simulations and wind tunnel tests; some of the obtained results include the finding of the two vortexes generated in street canyons of AR=2.00, and the relationship in between the AR (aspect ratio) and the number of vortexes generated in a canyon.

Regarding to the pollutant dispersion in symmetric canyons, there are many studies that need to be remarked. In 1999, *Pavageau*[18] performed some wind tunnel experiments

in order to study the pollutant concentration in regular street canyons. *Liu*[19], in 2005, performed LES simulations for obtaining information about the relationship about the AR of the canyon and the level of pollutant removal. More recently, in 2011 and 2013, *Banerjee & Christian*[20] and *Chung*[21], respectively performed CFD simulations in order to study the pollutant concentration in the different parts of canyons, as well as its connection with the geometry configuration.

Finally, we can mention some recent studies. In 2015 *Gallagher*[22] published a study about passive methods for improving the air quality in built areas, which could be a good starting point for further studies after performing the pollutant transport investigation of this thesis .
A year later, in 2016, *Lateb*[23] published a paper where many valuable information about how to perform street canyons studies is summarized, taking into account from experiments to CFD simulations.

All these papers and studies [24] provide a priceless amount of information, some of which will be used during this thesis in order to establish the theoretical fundamentals and the basis for carrying out the CFD simulations and the OpenFoam case setup. In addition, some other researches will be presented during this study and mentioned in the corresponding section and some others could be so helpful for developing and extending this project

2.2 Problem description

Modern cities are the result and perfect description of thousands of years of evolution with: tall modern buildings that allow countless people to life in few square meters, roads that communicate every point of the city, park slots at every street, etc. We could think that this has just began and that are all advantages but, if we go deeper and perform a close analysis, we can detect high pollution levels in these street canyons. This is an accumulation of many circumstances and characteristics: traffic, lack of ventilation, narrow streets and tall buildings, among others.

This thesis has the main aim of studying and analysing the air flow and pollutant transport in street canyons, both strongly affected by cities' geometry. That is the reason

why in this section we are focusing on it, in order to have a deep understanding of how it affects to air flow and help us obtain valuable conclusions after all the studies.

All the factors mentioned before can be summarized by using the so-called canyon effect; this effect states that the highest part of pollutant remains concentrated in street canyons, resulting in health and environmental impacts. This pollutant retention, added to the air flow through street canyons, which originates pollutant concentration gradients, creates some sub-microenvironments where the pollutant can be considered uniform. Starting from this point, and taking into account that for having a good city planning some objectives, that cannot be achieved at the same time, should be fulfilled, we are focusing on the main objective that at the same time is the key part of our study: maximize the air pollutants dispersion[25] and reduce its retention in urban street canyons.

For this study we are going to use a geometry inspired in cities with clear repetition patterns, such as China or Barcelona, see *Figure 2.1* and *Figure 2.2*, for increasing the accuracy and representativeness of the geometry presented in the following section. It is needed to mention that in order to simplify the complex geometry of a real city, elements such as trees, balconies, parked and on road vehicles, radiation, among others, are not represented and symmetric canyons are considered.

Figure 2.1: Aerial image of Barcelona where clear repetition patterns can be identified [1]

Figure 2.2: Aerial image of China where clear repetition patterns and similar geometries, as the ones simulated, can be identified [2]

2.2.1 Urban geometry

Before defining the geometry, some basic concepts, about urban geometry and air flow through them, are going to be explained in order to have a deep understanding of all the presented information.

- **Aspect ratio:** is the division of the buildings' height (H) and street canyons' width (W). Usual cities have street canyons with an aspect ratio in between 0.50 and 2.00 and a canyon is considered regular if its AR is equal or close to 1.00 [26].
- **Windward and leeward sides of the building:** are the side in which the wind is directly blowing and the opposite, respectively, and can be appreciated in *Figure 2.3*.

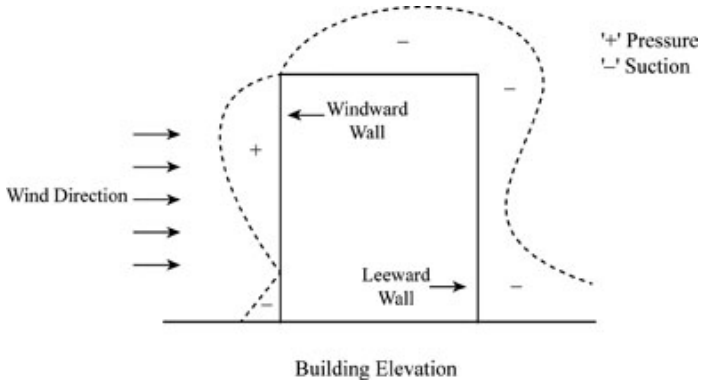

Figure 2.3: Different parts of a building, referring to the air flow distribution [3]

- **Flow regimes depending on the buildings' separation:**
  1. **Isolated roughness flow:** when the aspect ratio is low (H/W<0.30) the street canyon's width is enough for allowing the air to travel sufficient distance and there is no wake interference with the next building; then we could consider the building isolated (see *Figure 2.4*).
  2. **Wake interference flow:** if the buildings are closer, with an approximate aspect ratio of 0.50, and the flow cannot be readjusted before the next windward face, the flow is totally affected by the wake created by the previous building (see *Figure 2.6*).
  3. **Skimming flow:** when the AR is around the unit *(regular street canyons)* the biggest part of airflow flows over the following canyon and the other part

generated a vortex in it. This study will be focused on this flow regime but some other situations will be also presented (see *Figure 2.5*).

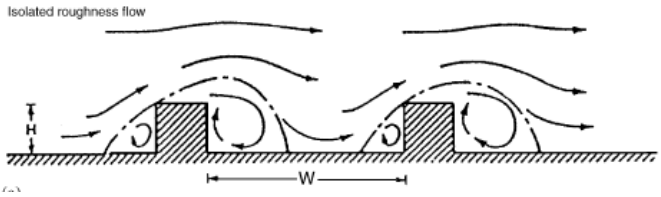

Figure 2.4: Isolated roughness flow through buildings [4]

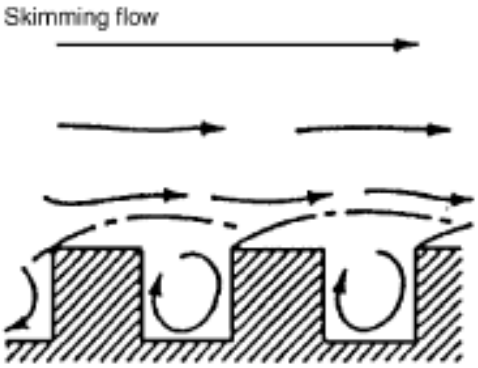

Figure 2.5: Skimming flow through buildings [4]

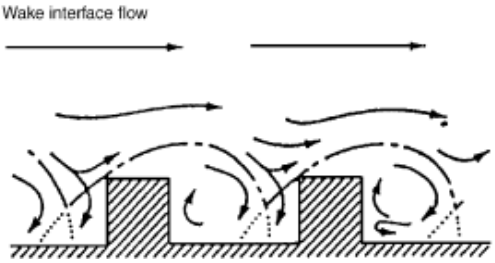

Figure 2.6: Wake interference flow through buildings [4]

All these information can be properly summarized in *Figure 2.7*.

As will be deeply explained later, the flow, apart from being in the skimming region in the main cases, will be incompressible (air flow through cities usually is slow and then $Ma < 0.30$), considered perpendicular to the buildings, constant thermophysical properties (density and temperature), homogeneous (despite of having a lineal pollutant source when implementing pollutant transport in the studies), it is initially supposed to be carried out the 2D study of a Newtonian and non-stationary flow (buildings create turbulence and it cannot be considered stationary as we are deeply interested in the transient phenomena given at roof-level for studying the polluted air removal).

Once defined the flow, we can explain the different study zones generated in the air distribution in street canyons[25].

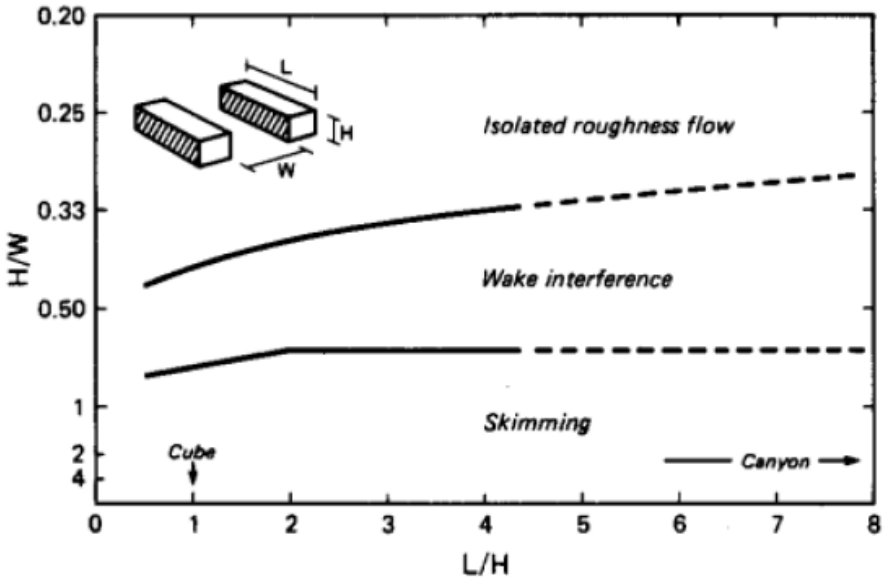

Figure 2.7: Flows around buildings classification depending on canyons parameters [5]

- **Airflow around buildings:** it is obvious that a building modifies several aspects of the environment surrounding the construction, but in this chapter we will just focus on the effect that it has on the air flow, more specifically on the different parts of it.

  For this analysis of the flow we are just using an isolated building with the flow perpendicular to its windward face, the one that receives the highest pressure levels. The highest force is generated in the upper middle part (at the stagnation point, where the velocity is zero), as the air in the outside accelerates and is deflected over the top, to the bottom and sides of the building. This situation is perfectly described by *Figure 2.8 and Figure 2.9*. These images allow us to perfectly visualize the four most important parts of the airflow around buildings:

  1. **Free stream (zone A):** this zone is far enough from the building to be undisturbed.
  2. **Deflection zone (zone B):** in this part the air is deflected by the building and moves over it. In there we can appreciate that at one point (stagnation point) the streamline is completely stopped by the building and as the *Bernoulli's principle* states, when the velocity is minimum the pressure is maximum.

3. **Suction zone (zone C):** this is the most chaotic part as because of the low pressure, we have high velocities and turbulence. The drastic pressure change at the leeward generates reverse flow and this increases the instability of the flux.
4. **Wake (zone D):** in this part the flow is still affected by the building but it is starting to stabilize (it has residual turbulence)[27].

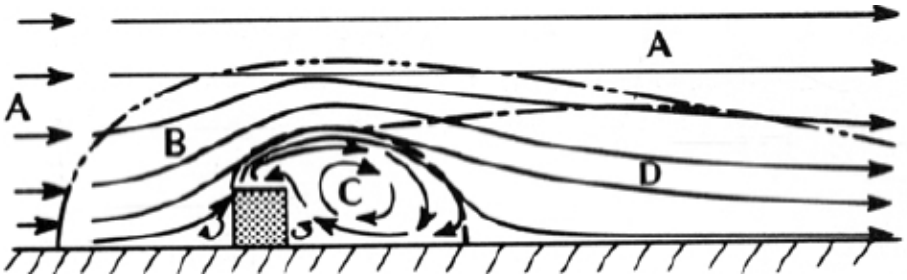

Figure 2.8: Flows zones around a building, side view [4]

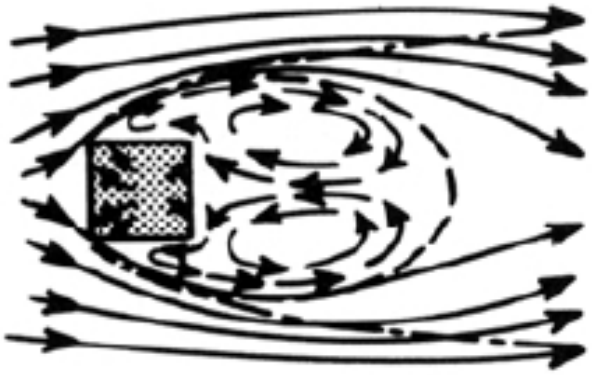

Figure 2.9: Flows zones around a building, top view [4]

Chapter 3

Theoretical framework

3.1 Fluid mechanics fundamentals

The problem presented before can be studied in many different ways, each one with its pros and cons. Throughout history the flow and pollution transport in street canyons case has been studied numerically or empirically using different experiments and methods (the one used for our case validation will be explained later during *Chapter 4: Validation of numerical results. No pollutant transport*).

In the last decades, Computational Fluid Dynamics studies have been carried out, reducing the time and money invested in these studies. This technique's main drawback is the fact that fluids (air in this study) are so complex and difficult to faithfully represent, as it is so difficult to exactly define the fluid properties and state. These characteristics vary in the space and time and, as the fluid is composed by countless particles that move in the 3D space, very complex differential equations (that cannot be solved by hand) are needed to define the velocity, pressure and temperature fields, among others. As if it was not enough, all these equations are coupled, which means that are strongly related and if one changes, it affects to the others.

On the other hand, we have to mention the fact that in some studies, if aspects, such as the geometry, are not complex, simplifications can be done. In the pollutant transport study done in this thesis some simplifications have been chosen, for example: the case is considered incompressible (as the velocities and characteristics of the street canyons flows does not lead to a density change) and 2D simulations are carried out. These simplifications increase the error committed during the study and despite of it, we would never be able to solve the case by hand as the Navier-Stokes equations are partial-differential equations

that cannot be solved analytically and must be solved numerically, by doing a domain discretization that allow us to integrate them. This is the reason why we are using *OpenFoam*, a very powerful open source CFD software, in order to solve the problem.

3.1.1 Turbulence

Turbulence in fluid mechanics is a very common phenomenon characterised for being the opposite of laminar flows, where all the fluid layers flow without disruption between them. When these well organized flows have excessive kinetic energy and it can overcome the viscosity of the fluid, which damps the flow, then turbulence appears. Every time we talk about turbulence we should also have in mind some words such as unsteady, vortexes, chaos, irregular, fluctuations, mixing, etc[28].

Despite of the physics of turbulence is completely understood, there are many characteristics that have made it a good focus for studies, for example: when talking about turbulence we have tot take into account spatial but also temporal scales as it is transient, vortexes generate non-linear interactions (making it impossible to solve turbulence statistically). For these and many other reasons, turbulence is still under development and from now on in this section we are just focusing on the relevant aspects to take into account for engineering simulations, which allow us to obtain information from the Navier-Stokes equations that govern this phenomenon[29].

Turbulence is irregular, disordered, random, non-stationary, three-dimensional, non-linear, irreversible... It generates high intensity vortexes creating an Eddy structure with a continuous spectrum of fluctuations. When talking about turbulence it is a fact its irregular and intermittent nature , but it has been shown that many turbulent flows follow some patterns of repetition[30].
A very commonly used concept is the *Energy cascade* which is studied by the vortexes' dynamics and is described in *Figure 3.1* . It states that large-scales vortexes, which are created by the main direction of the flow, broke-up and generate smaller vortexes. This phenomenon moves the energy from large scales to the smaller ones at the same time it dissipates. The smaller the turbulent scale is the larger energy dissipation, as it increases with the velocity gradient (higher in smaller scales). Once the energy arrives to the smallest scales, such as the *Kolmogorov micro-scales*, there is the known viscous dissipation that transform it to thermal energy. All the complexity that surrounds turbulence is governed

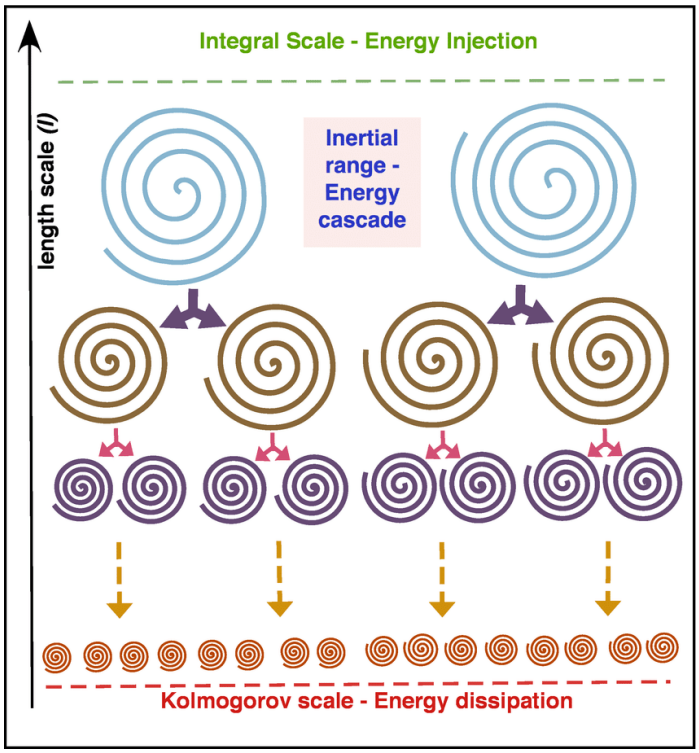

Figure 3.1: Visual representation of the energy cascade [6]

by the Navier-Stokes equations and as it is explained in the following section *Computational Fluid Dynamics (CFD)*, where this powerful tool, widely used for finding approximate solutions to the mentioned governing equations and for describing turbulence, is deeply explained.

3.1.2 Computational Fluid Dynamics (CFD)

Computational fluid mechanics can be defined as the "branch of fluid mechanics that uses numerical analysis and data structures to solve and analyse problems that involve fluid flows"[31].

CFD can be applied to a wide variety of engineering problems and consists on using computers in order to find the solution of the governing laws of fluid dynamics numerically. This can be done by doing a discretization of the domain we want to study, which will allow us to solve the partial differential equations in every small domain, called cell. By using the discretization we can move from algebraic partial derivative equations to linear numerical equations that can be integrated. Among the different methods available, finite difference,

finite elements and FVM, each one with its pros and cons, we have chosen the *Finite Volume Method (FVM)*. It allows us evaluate the PDEs in the form of algebraic equations using the divergence theorem, which allows us to convert volume integral to surface integrals[32]. After it, we can evaluate every surface integral as fluxes at every surface of the finite volume element, taking into account that conservation must be fulfilled.

Every CFD study has a basic workflow and in this study has the following structure:

1. **Pre-processing:**
   (a) **Make a geometry:** can be done by using different software.
   (b) **Meshing:** in this study the mesh creation has been done with Ansa v21.0.1.
   (c) **Set-up of initial and boundary conditions:** in this study *OpenFoam v7* has been used for implementing all the conditions and case setup (and for running the simulation afterwards).
2. **Processing:** the solver must be set up, the schemes, solvers... defined and then we can run the simulation.
3. **Post-processing:** in this part the physics knowledge must be applied in order to evaluate and analyse all the visualization results such as contours, plots, streamlines... For this thesis *ParaView* is the open-source software chosen; additionally *Matlab* has been also used.

After every CFD simulation verification and validation should be carried out, as what we have obtained is a result from a numerical solution and many aspects need to be checked: uncertainty, the model, the grid, convergence, dimensions, flow conditions, etc.

- **Verification** is about making sure that the programming and computational implementation of the model is correct (mathematical comparison in between models and analytical data): ”solving governing equations right”.
- **Validation** compares the computational simulation with the physical reality (scientific comparison in between models and experiments) what is the same as “solving the right governing equations” by taking into account discretization errors[33].

In general, a CFD simulation can be described as follows: we start from a really complex real problem (reality) that needs to be solved. Then we have to qualify the physical and mathematical models in order to do predictions and obtain a physical model, which is a set of equations (usually PDEs) that implement the physical laws. Once we have the physical model implemented, verification allows us to check that the numerical solution of the equations is correct. Once verified, we implement a numerical model writing a computer code (or implementing the equations in a commercial software) in order to solve the equations, choose a mesh, a time step, appropriate residuals and solve numerically the equations. The results of these equations must be checked in order to validate if the physical model is accurate enough[31].

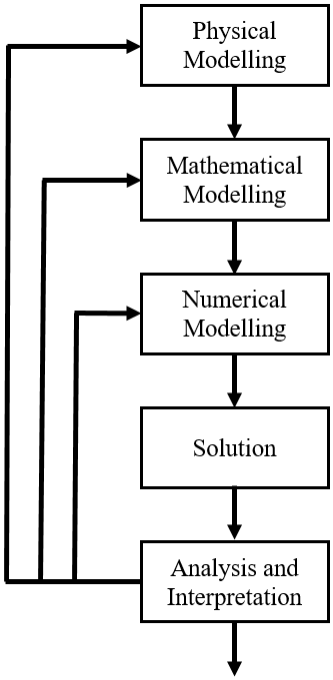

Figure 3.2: Graphic representation of a general CFD process

3.1.3 Mathematical models and equations

As we have explained, CFD is the powerful tool that we are using in order to conduct this study. By solving the Navier-Stokes equations using computational tools we can simulate the flow around buildings and, in this case, the pollutant transport and diffusion in street canyons. The pollutant dispersion, as many other phenomena, it is turbulent and for this

reason we need to solve the Navier-Stokes equations and all the fluid scales. As the fluid scales cannot be solved, we apply simplifications and models, which model a part or the whole turbulent kinetic energy spectrum. In this thesis we are using the RANS model, which models the kinetic turbulent energy spectrum and among all the turbulence models we have chosen *RNG k-epsilon model*, as this model has been shown to properly work with pollutant dispersion [13].
For the study of pollutant dispersion and retention in street canyons a general procedure is followed:

1. Street canyons meshing using Ansa.
2. Simulation process using a *RNG k-epsilon* model in order to obtain converged velocity and pressure fields *(OpenFoam)*.
3. Particle transport simulation using a **passive scalar transport** equation *(OpenFoam)*[34].

Now let's start talking about the physics and mathematics behind the solution of CFD studies.

3.1.3.1 Generic scalar transport equation

We have previously explained what CFD consists on and how it works, understanding the key role that it has in solving partial differential equations. Differential equations express conservation principles, which are the basis for the derivation of differential equations. These express a certain quantity as a dependent variable and the balance between them that makes this quantity change. All the dependent variables obey a generalized conservation principle described by the following differential equation:

$$\frac{\partial \rho\phi}{\partial t} + \nabla \cdot (\rho\vec{u}\phi) = \nabla \cdot (\gamma \nabla\phi) + S_\phi \tag{3.1}$$

Where:

- ϕ: dependent variable (scalar or vector).
- ∇: diffusivity (diffusion coefficient).
- $\frac{\partial \rho\phi}{\partial t}$: transient term (accumulation in the control volume).
- $\nabla \cdot (\rho\vec{u}\phi)$: convection term (transport of the variable because of the velocity field).

- $\nabla \cdot (\gamma \nabla \phi)$: diffusion term (transport of the variable because of the gradients).
- S_ϕ: source term (anything that creates or destroys the variable and cannot be fitted in the convection or diffusion terms) [35].

Having a basic understanding about how a generic transport equation is built, we are moving on and now we can start talking about the Navier-Stokes equations.

3.1.3.2 Navier-Stokes Equations

During the discretization process explained in the previous section we have talked about the Navier-Stokes equations, the ones that can be integrated at every node, after the discretization of the domain in cells, in order to, as mentioned, go from partial differential equations to linear algebraic equations[36]. This section has the main purpose of having a general understanding of these equations and acquiring a solid theoretical basis before moving to the street canyons case implementation in *OpenFoam* and to the simulations realization.

As we mentioned before, because of the low velocities in street canyons we are assuming the air as an incompressible homogeneous fluid, which will simplify the following mathematical expressions that relate pressure, temperature and density of the moving fluid that we are describing. They also include the effects of viscosity and are time dependent, and in total we have five initial equations presented here:

- **Mass conservation equation:**

$$\frac{\partial \rho}{\partial t} + \frac{\partial u_i}{\partial x_i} = 0 \tag{3.2}$$

  If we apply the previously mentioned simplifications:

$$\frac{\partial u_i}{\partial x_i} = 0 \tag{3.3}$$

- **Momentum conservation equations:** as momentum is a vector quantity we have three momentum conservation equations, one for each component. Momentum is conserved in every direction at the same time and has a magnitude and a direction. In *Einstein's Notation*, the momentum equations are defined as:

$$\frac{\partial}{\partial t}(\rho u_i) + \frac{\partial}{\partial x_j}(\rho u_i u_j) = \frac{\partial p}{\partial x_i} + \rho g_i + \mu \left(\frac{\partial^2 u_i}{\partial x_j^2} \right) \tag{3.4}$$

All these equations are born from the *Newton's Second Law*:

$$\sum \vec{F} = m\vec{a} \tag{3.5}$$

Reordering and using a compact notation, the general momentum equation for a incompressible fluid (we can apply *Equation 3.3*) without taking into account gravitational effects, as in street canyons the study fluid is air, is:

$$\rho\left(\frac{\partial u_i}{\partial t} + u_j\frac{\partial u_i}{\partial x_j}\right) = -\frac{\partial p}{\partial x_i} + \frac{\partial \tau_{ij}}{\partial x_j} \tag{3.6}$$

Where $\tau_{ij} = 2\mu S_{ij} = viscous\ stress\ tensor$ and $S_{ij} = \frac{1}{2}(\frac{\partial u_i}{\partial x_j} + \frac{\partial u_j}{\partial x_i}) = strain - rate\ tensor$.

The strain-rate tensor is the velocity gradient (a measure of how the velocity of the fluid changes between different points). Later on, when talking about the turbulence model used, we will see that some more extra equations are needed and an averaging of all equations is done in order to approximate the stress tensor by using the turbulence model[37].

- **Energy conservation equation:** for modelling the pollutant transport equations in *OpenFoam* we will see that it has a fundamental role.

$$\frac{\partial E}{\partial t} + \frac{\partial (u_i E)}{\partial x_i} = -\frac{\partial (u_i p)}{\partial x_i} - \frac{1}{RePr}\left[\frac{\partial q_i}{\partial x_i}\right] + \frac{1}{Re}\left[\frac{\partial (u_i \tau_{ij})}{\partial x_j}\right] \tag{3.7}$$

Where E is the energy, q_i are the heat fluxes, τ_{ij} are components of the stress tensor (second derivatives of the velocity components), Re the *Reynolds Number* and Pr the *Prandtl Number*. These dimensionless numbers are defined as:

  - **Reynolds number:** is the relation in between the inertial and viscous forces of a fluid and it is used in order to define the regime of the flow, depending on the relative importance of these two forces.

$$Re = \frac{uL}{\nu} \tag{3.8}$$

Being u the reference flow speed in $[m/s]$, L the characteristic dimension in $[m]$ and ν the kinematic viscosity in $[m^2/s]$[38].

– **Prandtl Number:** is the ratio of momentum diffusivity to thermal diffusivity.

$$Pr = \frac{c_p \mu}{k} \tag{3.9}$$

Being c_p the specific heat in $[J/kg \cdot K]$, μ the dynamic viscosity in $[Pa \cdot s]$ and k the thermal conductivity in $[W/m \cdot K]$[39].

On the left side of the equation there are the convection components (properties transported by the motion of the flow) and on the right side we have the diffusion ones (properties transported by the molecules of the fluid).

In these partial derivative equations we have four time-independent variables (x, y, z, t) and four time-dependent variables: pressure and the three components of the velocity vector. The other thermophysical properties, density and temperature, have been assumed to be constant. If we take into account the energy equation, another time-dependent variable appears, h/T. Anyways, when applying the RANS the new extra variables appear. Additionally, it is needed to add the fact that this is a coupled system of equations, what means that if you want to solve a problem you need to solve all the equations at the same time.

3.1.4 CFD simulations

Once we have a solid mathematical basis, we have to go a little bit further and start talking about how these concepts are going to be applied, and here is where the CFD simulations appear. When solving a fluid mechanics problem we have to take into account that Navier-Stokes equations are the general description of the laws that govern the fluid, and that it is needed to adapt them to every problem. Depending on the flow or fluid type, the computational resources that we have, the knowledge or even the time that we want to spend during the processing step, we should decide to use one simulation type or another and then adapt to the study requirements.

In order to solve the Navier-Stokes equations we have different possibilities such as potential flow solvers, Direct Numerical Simulations (DNS), Large Eddy Simulations (LES), Reynolds-Averaged Navier-Stokes equations (RANS), among others, such as hybrid models[40]. As we want to obtain information about turbulence, we will just briefly explain the three last simulation types, which can resolve or model the turbulence in a wide range of time and length scales. On the other hand, potential flux solvers can just be used in zones

where vortexes, wakes and boundary layers are not important to be predicted as a potential flux solver is irrotational (the curl in the velocity field is always zero, $\nabla \times V = 0$)[41].

Turbulence is generated at large scales and starts dissipating while reducing the scale because of the turbulence energy transfer. We will see during the pollutant transport simulation that these concepts are quite important, as well as it is needed to keep in mind that turbulence is chaotic, unsteady, 3D but with coherent structures.
As during the validation chapter we will use LES simulations in order to validate the results obtained during our RANS simulations, we are going to have a look to the three most used and known CFD simulation types, which are represented in *Figure 3.3*.

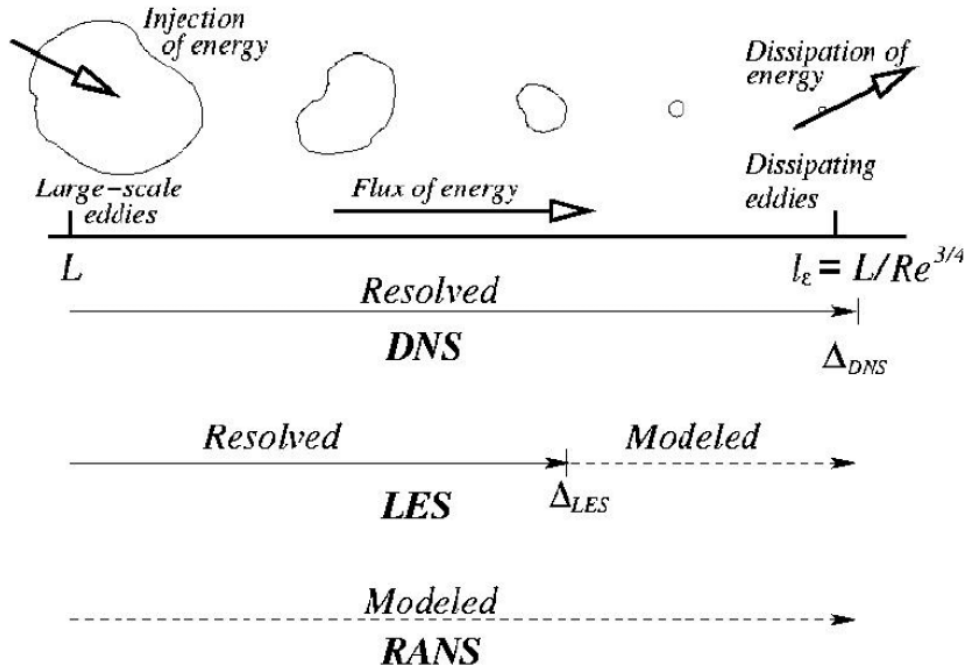

Figure 3.3: Main CFD simulation types depending on the turbulence length scale representation [7]

- **Direct Numerical Simulations (DNS):** using a DNS all the Navier-Stokes equations will be solved numerically without any turbulence model, from the largest scale eddies to the smallest ones (Kolmogorov scales). For our study it is not feasible to use this method as for solving all the spatial and temporal turbulence scales it is needed a huge amount of computational resources (the mesh and time step must be very fine)[42].

- **Large Eddy Simulations (LES):** as its name indicates it is a mathematical model that does a direct solution of large scales and models the smaller eddies. This kind of filter saves a lot of computational cost[43].
- **Reynolds-Averaged Navier-Stokes equations (RANS):** this models are based on introducing the Reynolds Averaging operators in the Navier-Stokes equations and applying mathematical models for turbulence. The averaging operation applied to the equations for obtaining the mean values creates some additional terms in the momentum equations that need to be modelled: the *Reynolds stress terms*[44].

With the turbulence models we can close the equations and solve the unknowns created by the Reynolds stress terms and turbulence models can be classified depending on the additional equations that add to the Averaged Navier-Stokes equations.
Despite of having different averaging methods, as what we want to solve is a transient and homogeneous turbulence of an incompressible and Newtonian fluid, we are focusing on the Reynolds time-averaging. By having the need to model transient turbulence, for computing the velocity fluctuations, the use of a RANS model will generate great error when computing second order terms, as seen in further chapters, among other reasons because fluctuations are transient and RANS models are the ones where modelling has more importance, see *Figure 3.4* .

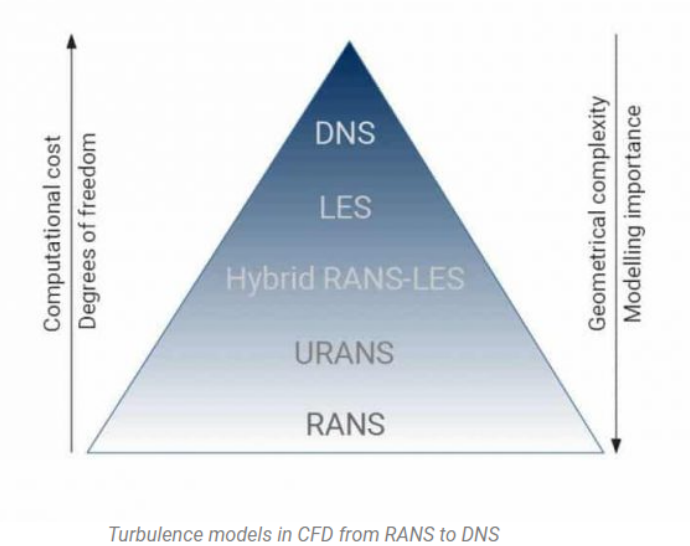

Figure 3.4: Turbulence models in CFD from RANS to DNS [8]

3.1.4.1 Reynolds-Averaged Navier-Stokes equations

When doing a Reynolds-averaging of a non-stationary value, with respect to time, we go from instantaneous values to the sum of the mean part plus the fluctuations. This can be appreciated in *Figure 3.5*, where the RANS model appears as a mean value while the other models represent with more detail the fluctuations.

Figure 3.5: Graphical representation of velocity in the difference CFD simulation types [9]

When averaging an instantaneous value we obtain $\phi = \bar{\phi} + \phi'$ and, as mentioned, we can appreciate the instantaneous value is composed by a mean part plus the fluctuations. If we average the velocity, the second order fluctuating term that appears is called the *Reynolds stress tensor* and the mean part is a Reynolds Operator (whose properties will help us obtain the final solution)[45]. Later we will see how these components can be modelled in order to solve the closure problem that has been generated. The Reynolds stress tensor represents the contributions of the turbulent motion generated by velocity fluctuations to the mean stress tensor in momentum equations, being the shear stresses $u'v'$, $v'w'$ and $u'w'$ the ones that play the most important role, compared to the normal stresses ($u'u'$, $v'v'$ and $w'w'$)[46].

If we apply this property for velocity and pressure:

$$u_i = \bar{u}_i + u_i' \tag{3.10}$$

$$p_i = \bar{p}_i + p_i' \tag{3.11}$$

Starting from the Navier-Stokes equations presented in a previous section and applying

the mentioned rules we obtain:

$$\frac{\partial \bar{u}_i}{\partial t} + \frac{\partial}{\partial x_j}(\overline{u_i u_j}) = -\frac{\partial \bar{p}}{\partial x_i} + \nu \frac{\partial^2 \bar{u}_i}{\partial x_j \partial x_j} \tag{3.12}$$

$$\frac{\partial \bar{u}_i}{\partial x_i} = 0 \tag{3.13}$$

As we can appreciate a non-linear term has appeared and the simplicity of the continuity equation reminds us that it is linear but the momentum one is not. By definition, the mean value of a fluctuation is zero and, taking into account the mean product of two variables, this term can be expanded as:

$$\overline{(u_i u_j)} = \overline{(\bar{u}_i + u_i')(\bar{u}_j + u_j')} = \overline{\bar{u}_i \bar{u}_j} + \overline{\bar{u}_i u_j'} + \overline{u_i{}' \bar{u}_j'} + \overline{u_i' u_j'} = \bar{u}_i \bar{u}_j + \overline{u_i' u_j'} \tag{3.14}$$

Applying this property and several mathematical manipulations to the *Equation (2.12)* we finally obtain the RANS equations:

$$\frac{\partial \bar{u}_i}{\partial t} + \frac{\partial}{\partial x_j}(\bar{u}_i \bar{u}_j) = -\frac{\partial \bar{p}}{\partial x_i} + \nu \frac{\partial^2 \bar{u}_i}{\partial x_j \partial x_j} - \frac{\partial}{\partial x_j}(\overline{u_i' u_j'}) \tag{3.15}$$

As we can see, the Reynolds stress tensor can be defined as: $\tau_{ij} = \overline{u_i' u_j'}$
This term includes the effects of turbulent motions on the mean stresses (normal and shear stresses). It is symmetric but by averaging we have just added six new independent unknowns, with a total of ten: $\langle u_1^2 \rangle, \langle u_2^2 \rangle, \langle u_3^2 \rangle, \langle u_1 u_2 \rangle, \langle u_1 u_3 \rangle$ *and* $\langle u_2 u_3 \rangle$. This las term of the RANS modelling momentum equation constitutes the closure problem and we can define the modelled tensor, R, as:

$$R_{ij} = -\overline{u_i' u_j'} \tag{3.16}$$

In order to obtain a solution we have to apply the *Boussinesq Hypothesis* and we finally obtain the approximation of the tensor that will be found after calculating the ν_t by using the equations given by the turbulent model chosen, which in this thesis is the two-equation model *RNG k-epsilon*.

$$R_{ij} = -\overline{u_i' u_j'} = 2\nu_t S_{ij} \tag{3.17}$$

Where $S_{ij} = \frac{1}{2}\left(\frac{\partial U_i}{\partial x_j} + \frac{\partial U_j}{\partial x_i}\right)$. All the concepts mentioned in here are explained in the following sections.

As we have just explained, now we have an unclosed equations system and we have to express the stress tensor in function of the other variables, but every step that we operate this equations for solving the Reynolds stress tensors (using the Reynolds-stress equations,

for example) the number of unknowns is increased. That shows us that turbulence cannot be solved by deriving new equations, instead we must obtain knowledge enough, about the turbulence in the actual study, for being able to apply the models that better fit. There are two main possible approaches: *Eddy Viscosity Models* and *Reynolds Stress Models*. Eddy-viscosity models (EVMs) allow us to model the Reynolds stresses and, as we will see, some of them will allow us to close the system. EVMs can be classified in linear and non-linear models but in this study we are just focusing on the linear ones, as after the first part of the study done by *Jordi Galí*, the turbulence model chosen is a two-equation linear model.

3.1.4.2 Linear Eddy Viscosity Models

Linear EVMs model the Reynolds stresses, previously obtained after averaging the Navier-Stokes equations, using the Boussinesq hypothesis as a linear relationship with the mean flow:

$$-\rho \left\langle u_i u_j \right\rangle = 2\mu_t S_{ij} - \frac{2}{3}\rho k \delta_{ij} \tag{3.18}$$

Where:

- μ_t: Eddy Viscosity
- $k = \frac{1}{2}(\langle u_1 u_1 \rangle + \langle u_2 u_2 \rangle + \langle u_3 u_3 \rangle)$ is the mean turbulent kinetic energy
- $S_{ij} = \frac{1}{2}[\frac{\partial U_i}{\partial x_j} + \frac{\partial U_j}{\partial x_i}] - \frac{1}{3}\frac{\partial U_k}{\partial x_k}\delta_{ij}$ is the main strain rate

As k is the mean turbulent kinetic energy, that term will only be significant when solving models that require this term (for example, two-equation models).
This hypothesis relates the turbulent stresses to the mean flow by implementing a new proportionally constant: the turbulent eddy viscosity, which is an effective modification of molecular viscosity.

3.1.4.2.1 EVMs classification

- **Zero-equation models:** as deduced from its name, this models do not include any additional equation to be solved as they are directly solved from the flow variables. The value of eddy viscosity is a simple algebraic equation. On the other hand, this simplicity makes them incomplete and not useful for many situations.

- **One-equation models:** these models just solve one turbulent transport equation (usually the turbulent kinetic energy, k). This make these models incomplete as the turbulence length scale is related to a flow parameter and it is not calculated using an equation. We can emphasize the *Spalart-Allmaras Model*, as it is widely used in aeronautics when the flow is attached[47].

- **Two-equation models:** these are the most used turbulence models and are constantly under development. As its name indicates, a two-equation turbulence model include two extra transport equations for modelling the turbulence, the first one usually represents the turbulent kinetic energy (k) and the second one tends to be more specific of the problem and represents the turbulence scale[48].
  As all the EVMs, the two-equation models include the Boussinesq assumptions defining the Reynolds-stress tensor as:

$$\tau_{ij} = 2\mu S_{ij} - \frac{2}{3}\rho k \delta_{ij} \tag{3.19}$$

  Where $k = \frac{\overline{u_i{}' u_i'}}{2}$

  This hypothesis simplifies a lot the Reynolds stress tensors resolution and allows to include more understandable variables for defining turbulence, such as turbulence intensity and turbulence length scale. On the other hand, this simplification cannot be applied in certain studies where the curvature is so strong or the flux is so complex. Among these models we can emphasise the *k-epsilon* and *k-omega* models, with all their variants. For this study, as investigated and validated during Jordi Galí thesis, we are using the *RNG k-epsilon model*.

3.1.5 RNG k-epsilon model

After many previously done studies, it has been concluded that Re-normalization-group k-epsilon model is the best fit for street canyons CFD simulations.

In the standard k-epsilon model the eddy viscosity is determined just for a turbulent length scale, committing great error in turbulent diffusion. Using the RNG model (re-normalization is a statistical technique) a new refined epsilon equation is derived and the different scales are taken into account for the production term. This model assumes that the flow is fully turbulent and neglects the molecular viscosity, but as the modified epsilon equation is implemented, this model can be used for a wider class of flows; with the new

included terms it is more accurate for strained (rotating) flows and for a wide range of Reynolds numbers[49].
The equations of this model can be directly derived from the Navier-Stokes equations using renormalization-group methods. Using this technique the model constants are different from the standard k-epsilon model and in k and $epsilon$ equations new terms appear.

The equations, terms and constants of this model are the following:

- **Turbulent kinetic energy:**

$$\frac{\partial}{\partial t}(\rho k) + \frac{\partial}{\partial x_i}(\rho k u_i) = \frac{\partial}{\partial x_j}\left[\alpha_k \mu_{eff} \frac{\partial k}{\partial x_j}\right] + G_k + G_b - \rho\varepsilon - Y_M + S_k \tag{3.20}$$

- **Dissipation rate:**

$$\frac{\partial}{\partial t}(\rho \varepsilon) + \frac{\partial}{\partial x_i}(\rho \varepsilon u_i) = \frac{\partial}{\partial x_j}\left[\alpha_\varepsilon \mu_{eff} \frac{\partial \varepsilon}{\partial x_j}\right] + C_{1\varepsilon}\frac{\varepsilon}{k}(G_k + C_{3\varepsilon}G_b) - C_{2\varepsilon}\rho\frac{\varepsilon^2}{k} - R_\varepsilon + S_\varepsilon \tag{3.21}$$

  Where:

  - G_k: turbulence kinetic energy generated due to mean velocity gradients
  - G_b: turbulence kinetic energy generated due to due to buoyancy
  - Y_M: contribution of the compressible turbulence in the dissipation rate
  - S_k and S_ε:user-defined source terms
  - $C_{1\varepsilon}$, $C_{2\varepsilon}$ and $C_{3\varepsilon}$: constants
  - α_k and α_ε: turbulent Prandtl numbers for k and ε, respectively.

- **Turbulent viscosity:**

  If we integrate the eddy viscosity differential equation

$$d\left(\frac{\rho 2k}{\sqrt{\varepsilon\mu}}\right) = 1.72\frac{\hat{\nu}}{\sqrt{\hat{\nu^3} - 1 + C_\nu}}d\hat{\nu} \tag{3.22}$$

  Where $\hat{\nu} = \frac{\mu_{eff}}{\mu}$ and $C_\nu \approx 100$

  in the high-Reynolds number limit ($\frac{\mu mol}{\mu_{eff}} = 1$) we obtain:

$$\mu_t = \rho C_\mu \frac{k^2}{\varepsilon} \tag{3.23}$$

Where $C_\mu = 0.0845$ is a constant directly obtained from the RNG, close to the 0.09 value chosen empirically for the standard k-epsilon model in order to obtain consistent results. As will be seen in further sections, $k = 0.19 m^2/s^2$ and $\varepsilon = 5.57 m^2/s^3$, being the kinetic turbulent energy and the energy dissipation rate, respectively.

Applying this formula we obtain the value of the turbulent kinematic viscosity $\nu_t = 0.000548 m^2/s$, which is used when calculating the diffusivity, important for the pollutant transport. The turbulent viscosity is a very important parameter to be calculated throughout the whole domain, but with this purpose before we need the values of k and ε using the constants and values mentioned, when using an *RNG k-epsilon* model.

- **Prandtl Numbers:** Prandtl number is a dimensionless number that relates momentum and thermal diffusivity. From the RNG theory the following expression is derived:

$$\left|\frac{\alpha - 1.3929}{\alpha_0 - 1.3929}\right|^{0.6321} \left|\frac{\alpha + 2.3929}{\alpha_0 + 2.3929}\right|^{0.3679} = \frac{\mu_{mol}}{\mu_{eff}} \tag{3.24}$$

Where $\alpha_0 = 1.0$ and $\alpha_k = \alpha_\varepsilon \approx 1.393$, in the high Reynolds Number limit. In our case definition these parameters are going to be explained and calculated as the value α_t is not taken as constant.

$$\alpha_t = \frac{\nu_t}{Pr_t} \tag{3.25}$$

The turbulent viscosity is a variable that depends on the turbulent kinetic energy and the energy dissipation rate and for this reason it is computed using *OpenFoam*. On the other hand the turbulent Prandtl number is taken as constant with a value of 0.72.

What makes this model different from the standard k-epsilon model is the R_ε term, which can make a positive or negative contribution to the equation, depending on the other terms related to this variable.

Because of the complexity of the calculation and comprehension of these terms, for a better understanding we can directly check the original paper[50].

3.1.6 Near-wall effects

When we talk about turbulence we cannot avoid talking about the *Energy cascade*, which has been mentioned in previous sections. This cascade is composed by vortexes of different sizes, from the largest ones directly influenced by the domain (main flow), to the smallest

vortexes which contain low proportion of the overall energy but are important for the dissipation *(Kolmogorov micro-scale)*[51] .

Modelling turbulence is not an easy task, but when we are near to a wall the difficulty is increased as we have an *inverted energy cascade*, because of the ejection created by the wall. In this cascade small vortexes create big ones, creating a new modelling need to be fulfilled. Additionally, the wall also orientates the flow, affecting to the turbulent length-scales, and creates steep gradients in certain variables[30].

Some Low-Re turbulent models are good for preventing the possible committed errors caused by the previously aspects, but today we are focusing on the *Wall functions*. These functions allow us to connect the near-wall regions with the ones with a coarse mesh (regions far from the wall where no much level of detail is needed).

The Law of the Wall defines the mean velocity of a turbulent flow at a certain point as:

$$U = u_\tau \left[\frac{1}{k} ln \frac{u_\tau y}{\nu} + C^+ \right] \tag{3.26}$$

Where:

- $y^+ = \frac{y u_\tau}{\nu}$: dimensionless distance to the wall
- $u^+ = \frac{u}{u_\tau}$: dimensionless velocity parallel to the wall
- $u_\tau = \sqrt{\frac{\tau_w}{\rho}}$: shear velocity
- τ_w: shear stress
- $C^+ \approx 5.0$: constant
- $k \approx 0.41$: Von Kármán constant

When analysing *Figure 3.6* we can appreciate the lack of precision in the approach of velocity near the wall, with $y^+ \leq 30$.In the *Buffer sub-layer*, a region in between the viscous and inertial sub-layer, the logarithmic treatment is not accurate enough and for this reason some *Law of the wall* recombination and variants may be applied.

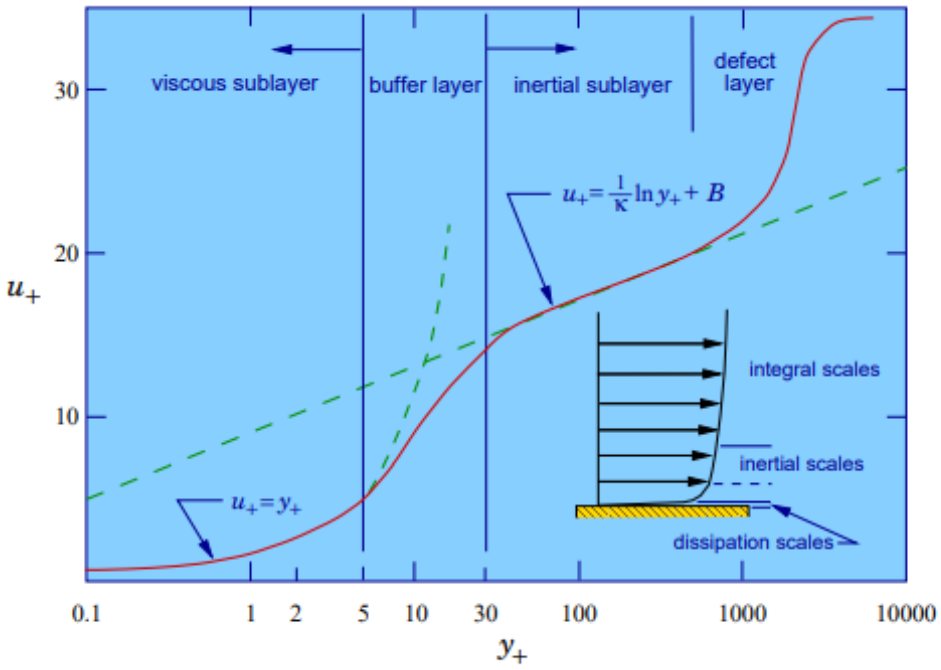

Figure 3.6: Boundary Layer division of sub-layers according to Law of the Wall [10]

3.2 Pollutant transport and dispersion in street canyons

Nowadays, in our fast-growing cities with tall buildings, narrow streets and thousands of cars driving down them, pollution problems are main issues as they have many impacts including health and environmental repercussions. This emissions are caused by motor vehicles (not only cars), industrial plants... Despite of not being the only source, cars are the main pollutants source in urban street canyons.

As this is a problem that concerns every single person of our society, many studies and technological improvements have been done during the last decades. Despite of this continuous effort, emissions in cities are an issue that must be eradicated as soon as possible. For this reason, this study is strongly focused on this phenomenon.

In order to study this phenomenon we will continue improving and implementing transport equations in the OpenFoam model used in order to validate the study using LES simulations and experimental results. During this study many factors will be taken into account, such as turbulence structure, pollutant transport characteristics, buildings and

street canyons geometry, pollutant source... One of the most important, and that affects the most, characteristics is the canyon's aspect ratio (AR), defined as the relation in between buildings' height (H) and street canyon's width (w). The initial study will be carried out by implementing and simulating in *OpenFoam* the pollutant generation in a street canyon of AR=1.00 with free-stream wind perpendicular to the street axis, with the possibility of moving on and implementing the 0.50 and 2.00 AR cases.

If possible, doing the comparison in between street canyons with different AR values will give us the possibility to compare and understand how this key factor affects to the pollutant circulation and retention in canyons (a direct result of the rotating and counter-rotating recirculations generated, and the flow regimes obtained depending on the AR).

After validating the simulation results obtained running the 2D case without pollutant transport and making sure that the velocity, pressure, etc. values are correct, we have a solid basis and can implement the pollutant transport equation on the basis of the results previously mentioned, as it has been shown that $k - \varepsilon$ models can give us realistic information, despite of the lack of precision in some parts such as the secondary recirculations; it is also important to mention the information that is lost by conducting a 2D simulation instead of computing the spanwise data, only available in 3D flows . Many simulations using this model have been carried out during the years and for an AR=1.00, just a primary recirculation has been computed. This turbulence model used is appropriate for our computational resources but we must take into account that many studies show that it underpredicts turbulent intensity, leading to weaker recirculations.

When the AR changes, the number and characteristics of recirculations is modified too, and for this reason street canyons with an aspect ratio in between 0.10 and 3.50 have been studied in many occasions. This phenomenon is really important to have in mind as it will completely affect the turbulent transport, leading to a change in pollutants retention in street canyons. This can be directly translated to air quality changes.

3.2.1 Mathematical model for pollutant transport

For understanding the mathematical model that describes the pollutant transport we have to move to the previous chapter and use the explained general transport equation (3.1). If we apply the mentioned simplifications and transform this equation, we obtain the equation

that describes the transport of a scalar through an incompressible turbulent flow:

$$\frac{\partial \phi}{\partial t} + \frac{\partial}{\partial x_i}(u_i \phi) = \frac{\partial}{\partial x_i}\left(D \frac{\partial \phi}{\partial x_i}\right) + S_\phi \tag{3.27}$$

Where:

- D: diffusivity $[m^2/s]$. After averaging it can be calculated in two parts: the turbulent diffusivity $D_t = \frac{\nu_t}{Sc_t}$, being Sc_t the turbulent Schmidt number and ν_t the turbulent Eddy Viscosity previously explained, and the molecular diffusivity $D_{mol} = \frac{\nu}{Sc}$. In this thesis both Schmidt numbers are considered equal, despite of a value check will be done. Sc is a dimensionless number that compares the momentum diffusivity and the mass diffusivity[52]. The first one is directly related to the viscosity of the fluid and for this reason it can be defined as $Sc = \frac{\nu}{D}$.
- ϕ: passive scalar
- S_ϕ: source term

If we take the scalar as the pollutant concentration, c, with a passive concentration transport, we can rewrite the general time-averaged governing equation for the concentration transport in an incompressible turbulent flow:

$$\frac{\partial c}{\partial t} + \frac{\partial}{\partial x_i}(u_i c) = \frac{\partial}{\partial x_i}\left(D \frac{\partial c}{\partial x_i}\right) + S_\phi \tag{3.28}$$

If we apply the Reynolds-averaging to this equation we obtain the transport equation that needs to be solved:

$$\frac{D\overline{c}}{Dt} = \frac{\partial}{\partial x_j}\left(D \frac{\partial \overline{c}}{\partial x_j}\right) - \frac{\partial}{\partial x_j}(\overline{c'u'}) + \overline{S}_\phi \tag{3.29}$$

Where, after averaging, the diffusivity is composed by the two different mentioned parts: the molecular diffusivity directly obtained from the kinematic viscosity and the Schmidt number, and the turbulent part which is completely modelled as explained for an *RNG k-epsilon* turbulent model.

$$D = D_{mol} + D_t \tag{3.30}$$

In this study Re=12000 and Sc=0.72, two important values to take into account as are necessary for lately implementing the passive scalar pollutant transport equation in *OpenFoam*[53]. For these conditions and taking into account the turbulent diffusivity, that appears after the averaging process, the total diffusivity obtained is 0.000877 m^2/s.

In *Equation 3.27* we can appreciate two important terms that need to be commented because of the repercussion that they have when conducting the CFD simulations. The first one is that despite of having chosen a transient solver, in this study case where no transient phenomena, such as pollutant sources depending on the time, are taken into account, using a stationary solver would be appropriate too, as in a RANS model everything is modelled and there is no part directly solved.

Additionally, for computing the turbulent fluxes ($\overline{c'u'}$) it is necessary to use the *Simple Gradient Diffusion Hypothesis (SGDH)* adapted to the pollutant concentration flux. This is necessary to be applied as the traditional equations included when solving the CFD problem, do not include the scalar fluctuations.

The equation that will allow us to obtain the mean pollutant concentration fluxes is:

$$\overline{u_i'c'} = -\frac{\nu_t}{Pr_t}\frac{\partial c}{\partial x_i} \tag{3.31}$$

3.2.2 Pollutant source modelling

As vehicles exhaust emissions take place so close to the street surface, the pollutants generation will be modelled as a thin surface (which can be taken as a line) in the center of the street canyon ($x_s = w/2$) in the spanwise direction and parallel to the z axis. In the 2D simulations this will be taken as a point where the pollutant, modelled as a passive scalar, will be generated and from here, dispersed because of the wind and turbulence generated in the canyon.

This pollutant will be mixed and trapped in the recirculations but with the turbulent transport and diffusion some of it will finally arrive to the roof-level and flow to the main stream. For this phenomenon it is important to take into account that our geometry generates an skimming flow regime, which produces a minimum air exchange and almost all the pollutant (in between the 95-99%, depending on the AR) gets trapped in the street canyon.

The flow regime will vary depending on the aspect ratio simulated and a further study will be done, analysing where are the highest concentration of pollutant parts in the street canyons, how many aspects of the flow can affect to the pollutant retention and which is the importance of the number of recirculations existing in a canyon.

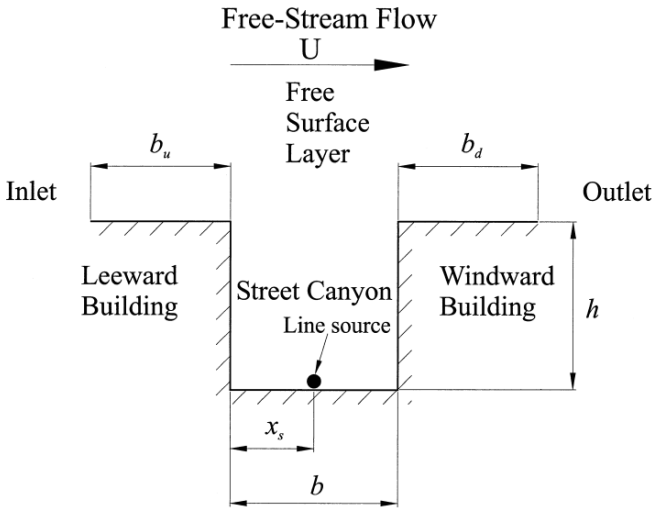

Figure 3.7: Computational domain and boundary conditions for the flow and pollutant transport [11]

Related to the boundary conditions we can emphasise the use of an open boundary condition for the pollutant for the outlet:

$$\frac{\partial \overline{c}}{\partial t} + \overline{u}\frac{\partial \overline{c}}{\partial x} = 0 \tag{3.32}$$

And the use of *Von Neumann* zero normal derivative conditions for the solid boundaries. As the pollutant source has been included in the model as a part of the boundary conditions, with a direct adimensionalization and with an uniform fixed value of 1.00, the results obtained from the simulations of this thesis will differ from the literature, where the pollutant modelling has been done in a different way. Additionally, the grid refinement is also an important factor to taking into account as is a major source of the error commited.

3.2.3 General overview

After having explained all the mathematical models and equations, the principles and hypothesis applied, a general overview of the solution process can be done, emphasising the most important parts.

The study of the airflow and pollutant transport in street canyons is a fluid mechanics problem that can not be solved analytically, for this reason we have chosen to solve it by using CFD. The physical laws governing the problem are the Navier-Stokes equations and

among the different ways how CFD can be applied in order to find a solution, we have chosen to use RANS equations. This decision has been made because of the amount of computational resources, time and knowledge that we have.

The main difficulty source of the Navier-Stokes equations, and the main reason why they cannot be solved analytically, is because of the existence of a second-order term: the Reynolds stress tensor, the origin of the closure problem. When applying the averaging to the equations, the Reynolds stress tensor needs to be modeled and with this purpose we have applied an Eddy Viscosity Model. When applying the Boussinesq Hypothesis to the equations the modelled stress tensor is "redefined" and now depends on a new term: the turbulent viscosity, ν_t.

As a new term has been included and we have an open system of equations we need more equations in order to close the problem and, for this reason, a turbulence model needs to be implemented. In this thesis the two-equation turbulence model *RNG k-epsilon* has been chosen. The two new equations that this model adds, the k and ε ones, allow us to obtain the turbulent viscosity. Apart from the turbulent kinetic energy and energy dissipation rate values, some other constants and dimensionless numbers are needed, which have been previously explained and defined. Once we have the approximation or estimation of the turbulent viscosity, the Reynolds stresses can be calculated and then all the other parameters of the case, such as the velocity and pressure, can be obtained too.

The presented workflow is the essence of the chosen CFD simulations, the information that is behind the code that we introduce in *OpenFoam*, but we can not forget that apart from having the knowledge to precisely conduct a CFD simulation, it is also needed to know how to properly extract the information from it. In the following chapters all the post-processing steps will be explained, such as the function used for the obtaining of the R modelled tensor.

Once we understand which is the presented problem, which are the physical fundamentals that govern, the basic workflow of a CFD simulation and all the not as obvious information behind the simulations, we can move one and present all the work done, from the geometry and mesh creation to the validation.

Chapter 4

Validation of numerical results. No pollutant transport

Once all the theoretical fundamentals, necessary for running a CFD simulation, are clear it is time to do the initial validation of numerical results. Before implementing the transport equation of a passive scalar pollutant and studying its distribution in street canyons, it is necessary to correctly implement the case in the software chosen.

For validating the velocity and pressure (as having good converged results is crucial before implementing passive scalar pollutant) some existing information in going to be used, such as the experiment that we will explain and the LES simulations that appear in some of the papers mentioned in the *State of the art* section. In order to do this, the RNG k-epsilon model used in the simulation is carried out by reproducing the geometry and boundary conditions to lately obtain the necessary data from the same street canyon (the 4th out of seven with AR=1.00) as in the reference literature, for performing the validation. It is important to mention the fact that some error and variances are expected during this process, mainly in the second order terms (Reynolds stress tensor terms), as for this thesis a RANS simulation is used, with all the pros and cons that it has.

In this section many crucial information is covered, from the geometry and mesh generation, done with *Ansa*, to the processing step running a simulation with *OpenFoam v7* and finishing with the post-processing step in *ParaView*; in this last section some validation is done by using *Matlab* and some other post-processing tools necessary for properly validating the study.

4.1 Experimental study

The experimental study used for the validation of this case was carried out in 2007 by *Xian-Xiang Li, Dennis Y.C. Leung, Chun-Ho Liu and K.M. Lam*[12]. In this experiment a water channel was used for studying the flow in street canyons with an AR of 0.50, 1.00 and 2.00; for the validation just the AR=1.00 is used and for this reason we are just focusing on the explanation of this particular configuration.

This physical modeling has been carried out by using a water channel, as it can obtain data about the flow and pollutant transport inside urban street canyons. This channel of 10m long, 0.30m wide and 0.50m high maintains the flow rate at $28 L/s$ by using and pump and some other devices such as a flow-meter.

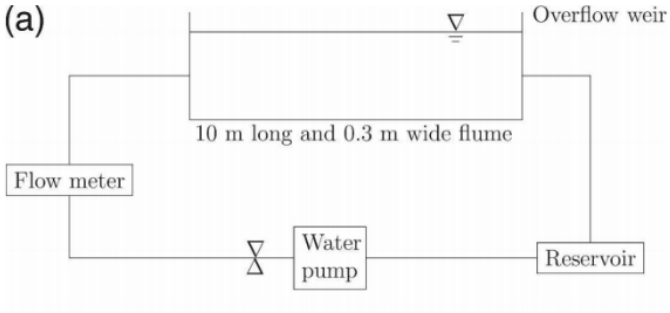

Figure 4.1: Schematic representation of the experiment[12]

For measuring all the data, without interfering in the values, a non-intrusive device was used, the Laser Doppler Anemometer (LDA), a fiber-optic system which uses a 4-W argon ion laser and can measure the velocity in the X and Y direction. This technique improves substantially the quality of the measurements as any other physical device would interfere in the flow. Despite of being non-intrusive, for obtaining the measurements some seeding particles were added. This particles were polycristalline powders of a nominal diameter of 30 μm, whose properties are quite good when using laser devices.

The geometry used for this experiment is composed by eight identical buildings of *0.298 m x 0.100 m x 0.100 m*, being squared buildings with a total width that perfectly fits in the flume. The height of the buildings (H) is fixed and for varying the flow, the width of the canyon (b) is modified. As mentioned before, the validation process in this thesis will just focus on the street canyons with AR=1.00, the reason why are just explaining this configuration.

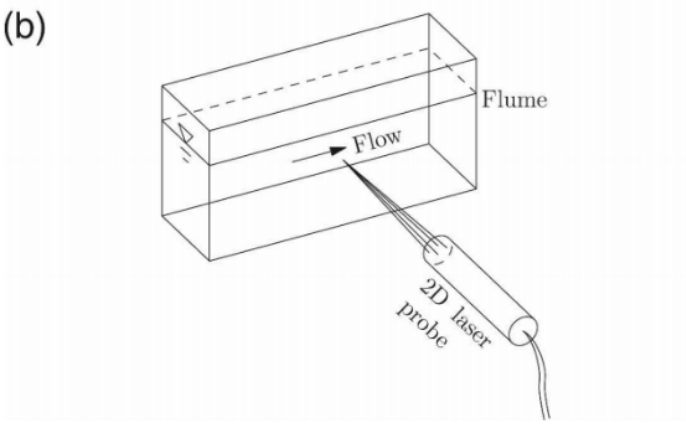

Figure 4.2: LDA experiment setup[12]

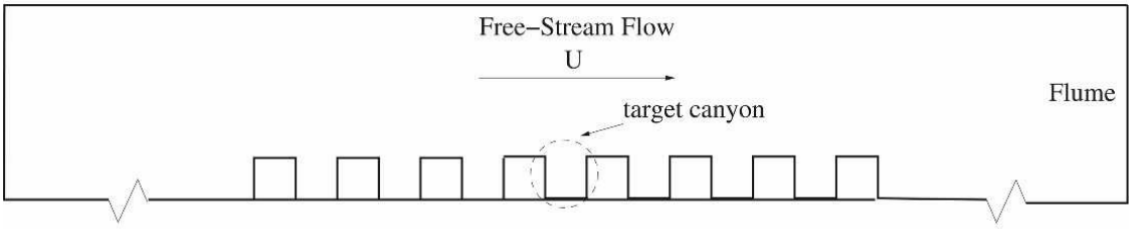

Figure 4.3: Full model schematic representation[12]

In *Figure 4.3* and *Figure 4.4* we can visualize the geometry used. During the simulation the axis used can be defined being X the longitudinal direction (perpendicular to the inlet), Y the parallel direction to the buildings and Z the axis that represents the length of the canyons. Despite of it, in the experimental study a different configuration was chosen.

This geometry, with a free-stream velocity and parameters that make the Reynolds Number equal to 12000, is the one used for performing the experiments whose are shown for a street canyon of AR=1.00. It is important to take into account that the measurements have been done in three different vertical locations *(x/H=0.25, x/H=0.50 and x/H=0.75)* and two horizontal ones *(y/H=0.50 and y/H=1.00)*. These lines, in which data is obtained, are the same used during the CFD simulations post-processing steps to obtain results, and are presented in *Figure 4.5*. As will be seen in following section, the data obtained from the horizontal line at roof-level is one of the most important parts of the pollutant transport modelling.

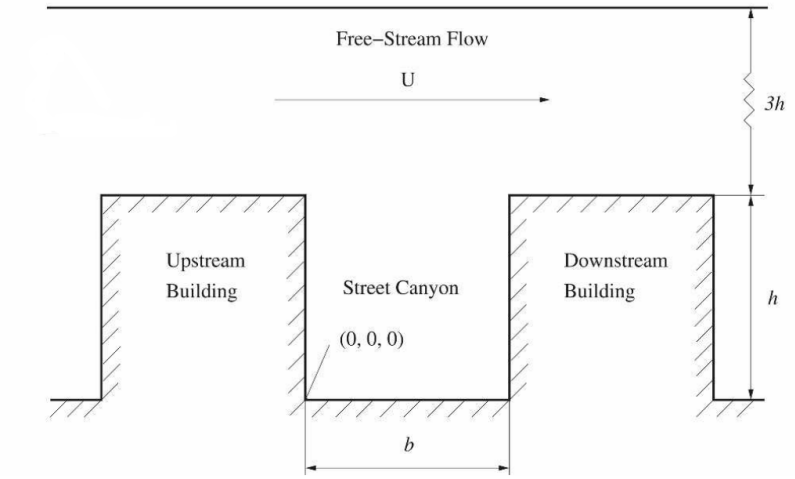

Figure 4.4: Detail view of an experimental street canyon[12]

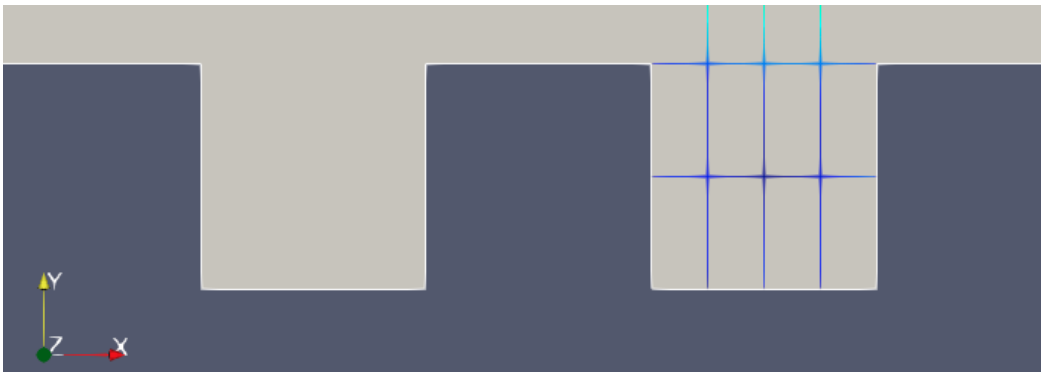

Figure 4.5: Detail view of the lines used for obtaining data in the 4th canyon

It has been done in this way in order to obtain the mean velocities and Reynolds stress tensor components in X but also in Y direction at different locations among all the street canyon. All the presented results have been made non-dimensional by using the free-stream velocity, U_{inlet}, and the buildings' height, H. When doing experiments with models, which are not in real dimensions, it is so important to work with dimensionless terms as it will allow us to scale them if needed and be able to adapt to different situations and requirements.

4.2 Geometry definition

Following the geometry guidelines previously mentioned for the experimental study, the design of the street canyons control volume has been done using *Ansa 21.0.1*. The configuration consists of eight buildings with a height and width of 1 meter located in a row. The distance between them (street canyon's width) is also 1m, as we want to validate the results of canyons with an aspect ratio equal to the unit.

The presented geometry has eight buildings and seven street canyons in order to ensure that the flow has been completely developed and stabilized in the 4th canyon (the one chosen for our study). The simulation domain has a total length of 35m, leaving 5m free at the beginning (from the inlet to the windward of the first building) and 10m at the end of it. All these distances have been chosen for ensuring the complete development of the flow and for being able to observe all the phenomena such as the wake generated by the buildings at the end of the domain and, in further sections, how the pollutant is transported downstream. Regarding to the height, the domain is 4m tall and, as *OpenFoam* needs a 3D geometry for running the simulation, has a width (Z direction) of 3m. This extrusion, as shown during the meshing section, will just have a cell for ensuring a 2D simulation, as it is the aim of this thesis.

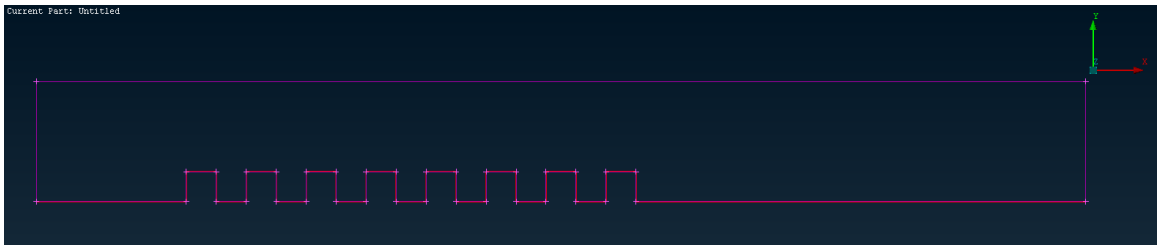

Figure 4.6: Front view of the street canyons geometry

Finally, it is important to mention that the geometry has been created using *Ansa* instead of a CAD (Computer-Aided Design) software because of the simplicity of the domain and the wide variety of tools that *Ansa* offers are sufficient for this study.

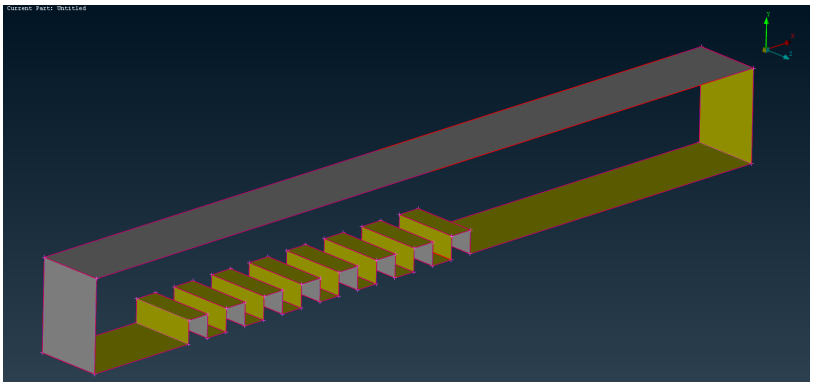

Figure 4.7: Isometric view of the street canyons geometry

4.3 Mesh generation

Meshing is one of the most important and time demanding procedures among the pre-processing steps of a CFD simulation. This is because having an appropriate mesh is very important for a good results obtaining as if the mesh is too coarse, the software used for running the simulation will not be able to capture the values good enough. On the other hand, excessively refined meshes can cause an over-computational cost and can turn to long simulation times without an obvious improvement of the obtained results, corresponding to the refinement.

Taking into account all these concepts and using *Ansa*, an structured mesh has been created. Structured meshes can be defined as the ones with regular connectivity by using quadrilateral 2D elements and hexahedral 3D ones. This type of mesh has been chosen as it ensures a better convergence and resolution than the unstructured grids.

The mesh creation process has had two different phases: the first one with a minimum element length of 0.025m and a maximum of 0.200m, see *Figure 4.8*, *Figure 4.9* and *Figure 4.10*, and a second one with a major refinement, obtaining a minimum element length of 0.015m and a maximum of 0.150m, see *Figure 4.11*, *Figure 4.12* and *Figure 4.13*. This refinement has been done because, as will be shown during the *Simulation results*, the first mesh, despite of including wall functions, did not model correctly the velocity near the wall. This refinement, with more computational resources than a personal computer, could have been greater and the results obtained would have improved; during the presentation

of the results, having this in mind can help us understand one of the causes of the possible error committed, when comparing to the LES and experimental results.

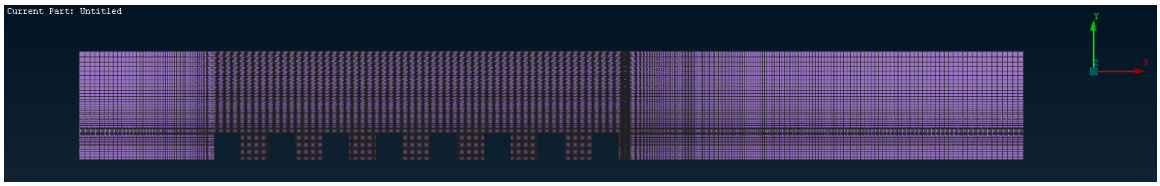

Figure 4.8: Top view: coarse mesh

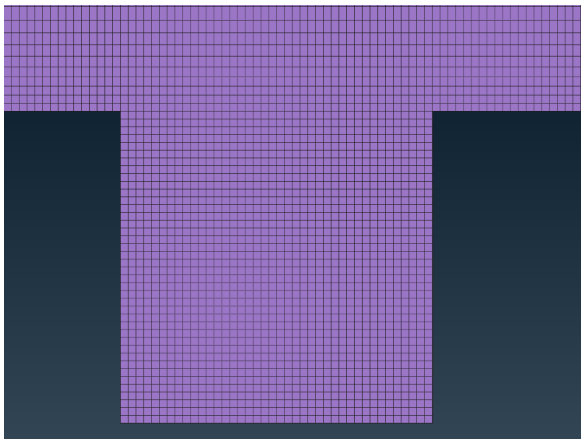

Figure 4.9: Detail view 1: coarse mesh

For improving the mesh quality and refinement, street canyons' grid size has been fixed to the minimum element length, and out from them a progressive spacing has been done. This has been possible because the resolution needed for this study far from the wall and out of the canyons is less important than the regions where the flow affected by the presence of the buildings.

Mesh	**Number of elements**	**Minimum element area**
Coarse	91 898	$6.25 \cdot 10^{-4} H^2$
Fine	195 750	$2.25 \cdot 10^{-4} H^2$

Table 4.1: Meshes comparison

After the generation of the mesh shown from *Figure 4.8* to *Figure 4.13*, a mesh check has been performed by using *Ansa* and, later on, with the *checkMesh* command in *Open-*

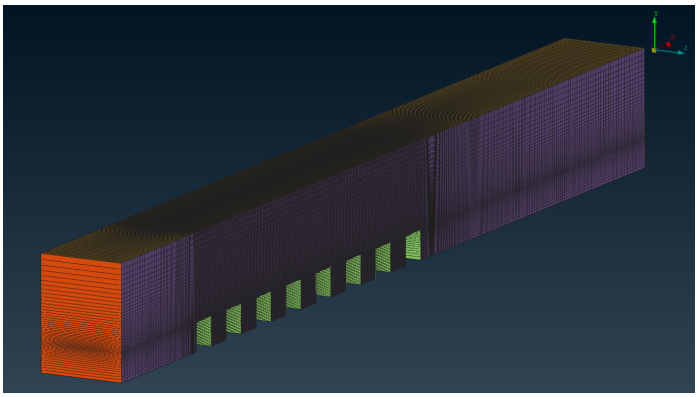

Figure 4.10: Isometric view: coarse mesh

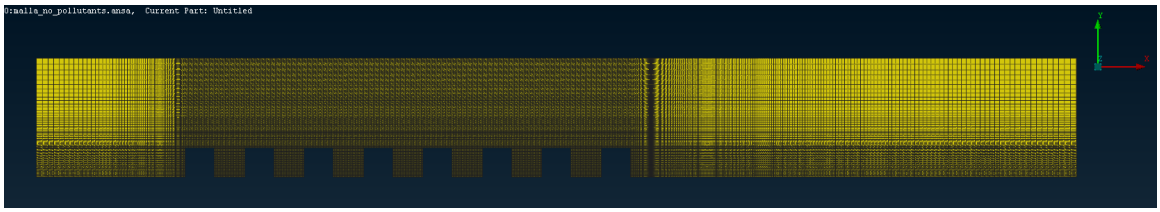

Figure 4.11: Top view: fine mesh

Foam. These checks have been done for finding out some typical problems such as: non-orthogonality (cell centers are not arranged and it turns to lack of accuracy and robustness of the solution), skewness (it is the difference in between the shape of a cell and the shape of an equilateral cell of equivalent volume, turning out to simulation destabilization), etc [54].

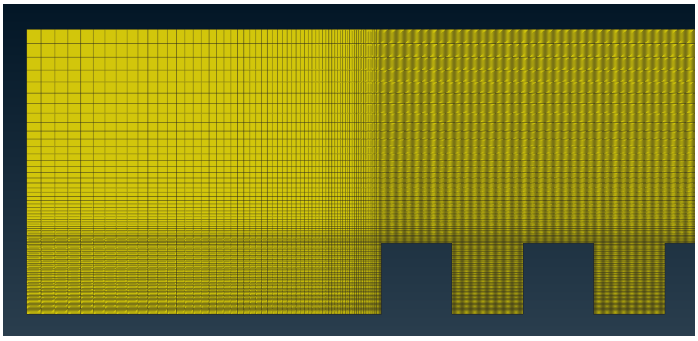

Figure 4.13: Detail view: fine mesh

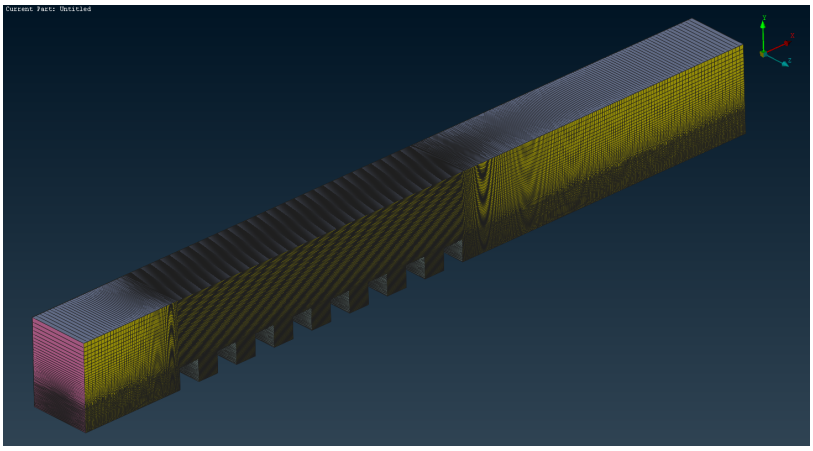

Figure 4.12: Isometric view: fine mesh

4.4 Case setup

4.4.1 Study parameters

Once the geometry and mesh are defined, it is time to prepare the *OpenFoam* setup, what means: implementing all the necessary parameters for running the simulation using the previously mentioned RNG k-epsilon model. Some of these parameters are: the turbulent kinetic energy (k), energy dissipation rate (ε), the inlet velocity, time-step, etc. All this data is obtained from the first part of this study done by *Jordi Galí*, which consisted on performing simulations with six different models in order to obtain the best results possible comparing to the experimental and LES existent studies[14].

All these parameters have been obtained using a validation process and a turbulence intensity (I) of just the 25%, as it is an urban street canyons study. By using the turbulence intensity and the reference speed, the turbulent kinetic energy can be obtained. From here, finding the turbulent length scale appropriate for the study can be found and, applying the corresponding formulas, ε can be calculated. This process is not explained in this thesis as it is part of the previous study cited in this section.

Regarding to the time step chosen, it has been proved that with a minimum grid dimensionless length $(\Delta x/H)$ of 0.015 and a reference velocity of 1 m/s, applying:

$$Co = \frac{v\Delta t}{\Delta x} \leq 1 \tag{4.1}$$

We ensure that while running the transient simulation we have stability in the numerical schemes. If Co>1, it means that the information propagates more than one grid cell in a

time step, leading to some problems such as divergence, inaccuracy and the obtaining of non-physical results.

The Reynolds number is 12000, as it is the value used in the experimental study used for the validation and it ensures the desired flow conditions. Once the Re and reference velocity are known, if we use as reference values, for making the variables non-dimensional, the $U_{inlet} = 1m/s$ and the height of the buildings, $H = 1m$, we obtain a simplified way to obtain the kinematic viscosity in function of the Reynolds number:

$$\nu = \frac{1}{Re} \tag{4.2}$$

By using this expression we obtain the used viscosity value of $8.33 \cdot 10^{-5} m^2/s$. The velocity, ρ and buildings height which are equal to 1, are assumptions frequently used for easing the process of making the simulation variables dimensionless; by using these values, when moving from one case to another changing the geometry, the post-processing step is quite simpler than when these values are not the unit.

On the other hand, some other processes could be followed to obtain the parameters, such as using the hydraulic diameter of the domain, defined as follows, we can apply the Reynolds number formula and obtain the kinematic viscosity.

$$d_h = 2\frac{ab}{a+a} \tag{4.3}$$

Where a and b are the canyon's width and height, respectively.

$$Re = \frac{d_h U_{inlet}}{\nu} \tag{4.4}$$

Schmidt number is directly obtained from the literature of previously mentioned CFD simulations as we want to have the same diffusion conditions and we apply the hypotheses that it is the same as the turbulent Schmidt and Prandtl numbers.

Once we have applied the FVM method for the discretization, in order to go from the PDEs to the linear numerical equations, the mesh is created and we have all these parameters clear, we can build the numerical model by writing the computer code (setup), in *OpenFoam*, which solves the equations, note before having applied the necessary boundary conditions. This implementation in the open source software will be explained in the next section.[31]

Parameter	Value
k	$0.19 m^2/s^2$
ε	$5.57 m^2/s^3$
U_{inlet}	$1.00 m/s$
Re	12000
Sc	0.72
Sc_t	0.72
Pr_t	0.72
ν	$8.33 \cdot 10^{-5} m^2/s$
Δt	$5 \cdot 10^{-3} s$

Table 4.2: Case setup parameters

4.4.2 OpenFoam implementation

For closing the conceptual model, which includes the mathematical equations mentioned (which solve the physical system proposed), we need the initial and boundary conditions; all of them are explained while presenting the implementation in *OpenFoam*, which is the computational model that includes the conceptual one and is composed by all the necessary code for performing the CFD simulations.

As *OpenFoam* is a software whose structure is build by using directories, the most important files in each of the three main directories are explained: *0, constant and system*. As you will see, in these files the case setup parameters that have been explained are included[55].

4.4.2.1 *0* directory

This is the time directory that contains files of data for particular fields. If our simulation does not start at time 0, as happens when simulating the pollutant, we may have other initial time directories. In our simulation, the most important files in here to mention are the pressure, velocity, epsilon and k, and additionally the fluctuations obtained using some post-processing functions. In each one the initial conditions, units and boundary conditions for each field are defined. The *property IDs (PIDs)* have been defined using *Ansa* and for the validation simulation we have: *INLET, OUTLET, TOP, SYMMETRY and CANYON*, being considered each one as a wall except from the symmetry one that is empty because we want to perform a 2D simulation, as if canyons' length (z direction) was infinite. *PIDs*

store geometrical information (such as the number and distribution of cells) and in them the boundary conditions can be applied when implementing the CFD model. Symmetry boundaries are not explained because for every field, the boundary condition is *empty*.

- **Pressure:** in every surface it has the *zeroGradient* boundary condition, as we do not want the value to be changed in there, just to extrapolate it from one cell to another. The *Outlet* has a *uniform value* of 0 m^2/s^2(as pressure is a scalar) for ensuring the flow moves out the control volume properly. We initialize the pressure at 0 m^2/s^2 in all the domain

- **Velocity:** velocity is also initialized at an uniform value, 0 m/s, in all the domain (internal field). The top surface has the *slip* condition because we do not want it to create a boundary layer (affecting the flow) but we want the flow to not leave the domain. In the inlet, the velocity is set at (1 0 0) m/s because it is a vector and only has X component, perpendicular to the inlet surface. The outlet is also considered as a *zeroGradient* boundary field and, as the buildings are not moving walls, the canyon surface has a fixed value of (0 0 0) m/s *(no-slip condition)*.

- **k:** the internal field has been set at an uniform value of 0.19 m^2/s^2. Outlet and top have a *zeroGradient* boundary condition. In the canyon a wall function, *kqRWallFUnction*, has been applied for ensuring a good modelling near the wall with an uniform value of 0.19 m^2/s^2. In the inlet, for improving the second order terms, it has been applied a *Turbulent Intensity Kinetic Energy* boundary condition of the 5% .

- **Epsilon:** it is so similar to the k field but with an uniform internal value of 5.57 m^2/s^3 and with no *Turbulent Intensity Kinetic Energy* boundary condition for the inlet. The wall function is the appropriate *epsilonWallFUnction* with an uniform value of 5.57 m^2/s^3.

Apart from these main files, we also have the *nut* and *nuTilda* ones which are related to the turbulent viscosity; in this study are set to an uniform initial value of 0. Finally, as we have already mentioned, once the simulations are finished we can apply the R post-processing function in order to obtain the modelled Reynolds Stress tensor components. Other ways to obtain the fluctuating components, as using the $Uprime2mean$ function, are not adequate for this study as we need the modelled part of the tensor because a RANS simulation has no directly solved part.

4.4.2.2 *constant* directory

This directory contains the *polyMesh* folder, where all the mesh files imported from *Ansa* are stored. Additionally, there are also the *transportProperties* and *turbulenceProperties* files.

- **transportProperties:** in here the transport model is set to Newtonian and the kinematic viscosity is established at a value of $\nu = 0.000083 m^2/s$, after having done the calculation mentioned in the *Setup* section.

- **turbulenceProperties:** the simulation type can be chosen in here. As mentioned in the *Theoretical framework*, the simulation type chosen is a RANS model and the implemented turbulence model is the RNG k-epsilon. As the model variables, turbulent kinetic energy (k) and turbulent energy dissipation rate (ε), are defined in the time directory, anything else has to be defined in here.

4.4.2.3 *system* directory

Finally we have to talk about the *system* directory, where all the parameters related to the solution procedure are defined. At least, this folder must contain these three files:

- ***controlDict:*** in here the case controls are defined, such as the initial and final time, the time step, the precision , among others[56]. Additionally, in here is also defined the solver used for the study. As we want to perform a turbulent, incompressible and transient simulation the best choice is using the *pisoFoam* solver[57]. Despite of it, as a RANS simulations is completely modeled and our study case has no transient phenomena, a steady solver such as *simpleFoam* could be tested in order to reduce the computational cost.
  It is important to mention that some functions have been also added to this file in order to compute the *fieldAveradge* values, the *yplus1* and, for the pollutant transport study, the *scalar* used for modelling the passive pollutant.

- ***fvSchemes & fvSolution:*** in these files the numerical schemes (for time, gradient...) and the solvers, tolerances and algorithm are respectively defined.

As will be seen after the simulation is done, some other files such as the *residuals* can appear in here. For the post-processing step this will be used for studying the convergence of simulations.

4.5 Post-processing

Post-processing is the last step of many CFD simulations and the one where all the physical knowledge has to be applied. Without this knowledge, all the maps, plots, streamlines... have no sense, as they can not be interpreted nor analysed.

In this section all the results obtained using *paraView* and the post-processing work done by using *Matlab* are presented, interpreted and afterwards discussed. All these data will be used for obtaining the conclusions of this airflow and pollutant distribution in urban street canyons.

4.5.1 Simulation results

In this initial simulation, as the scalar pollutant transport equation has not been added, we will present all the results needed for validating the velocity and pressure fields, as well as the residuals used for ensuring the simulation has completely converged.

4.5.1.1 Residuals

As seen in the *Theoretical framework*, CFD simulations solve the Navier-Stokes equations using an iterative process. We must be sure that our solution has reached the stationary state before collecting all the data for the analysis.

When we talk about residuals we are referring to the error or imbalance of a variable in every control volume, after solving the equations that define the problem. As the residuals plot shows the difference between successive solutions of the equations, when the lower the value at which the residuals converge, the better the variable has converged[58].

In *Figure 4.14*, the residuals are plotted in a logarithmic scale (Y axis) versus the simulation time (X axis) and using a different line for each studied parameter.

It is clear that, despite of having reached a stable value of $1 \cdot 10^{-2}$ after approximately 20s of simulation, pressure convergence is not as good as could be desired. These results on pressure convergence could be directly related to the fact that a pressure outlet boundary condition is used. On the other hand, velocity in the x and y direction have passed the *transition* after approximately 60s, reaching stationary residual values of almost $1 \cdot 10^{-5}$ and $1 \cdot 10^{-6}$, respectively. That means that velocity has converged properly.

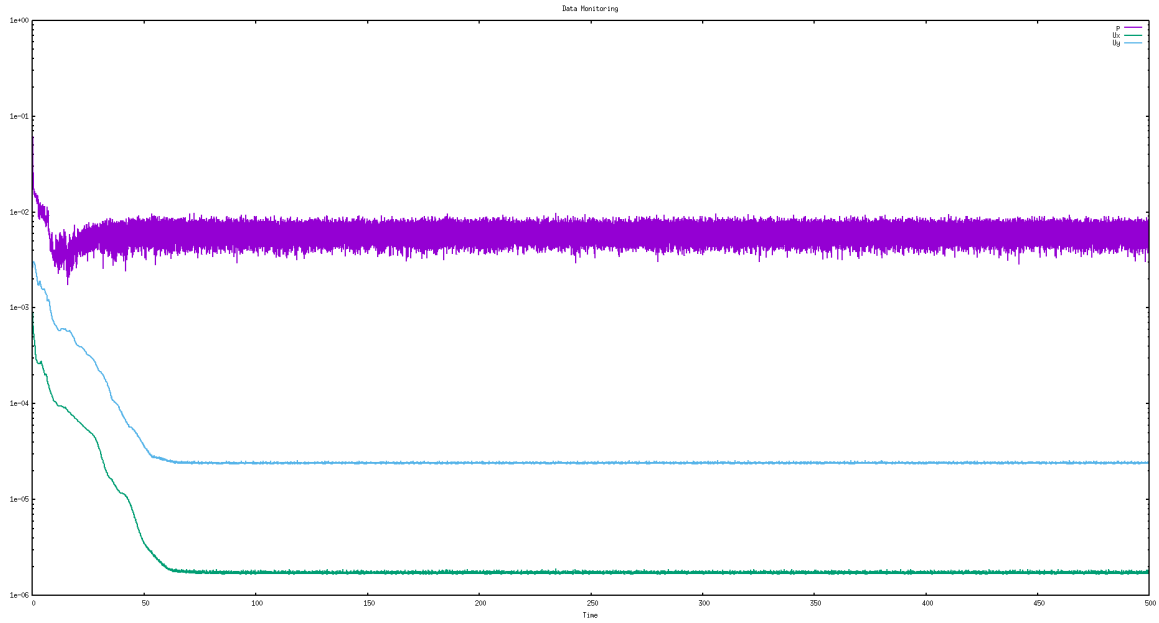

Figure 4.14: Velocity and pressure residuals plotted using *gnuplot*

4.5.1.2 Velocity maps

The average velocity maps are going to be shown in this section in order to do a further study and discussion in the following sections. It is not only going to be presented the magnitude mean velocity, but also the vertical component, as for the pollutant transport and removal in street canyons is one of the most important indicators.

In order to have a clear vision and good understanding of how airflow is in a street canyon of AR=1.00, we have focused on the 4th one. The reason why it has been chosen is because as there are 7 street canyons in the domain, after a fast analysis it is easy to appreciate that it is the first one with an stabilized flow and in the down-stream canyons there is a clear repetition pattern of the maps.

The average velocity in magnitude is a clear representation of how buildings disturb the airflow generating the different flow regions studied during the *Theoretical framework* section. The first building creates a massive flow disturbance by accelerating it to the maximum speed of the domain, close to 1.9m/s. As *Bernoulli Principle* states for an in-compressible flow, where the velocity is maximum pressure must be minimum. As will be seen in the pressure maps, it generates a suction zone and after that the flow starts stabilizing.

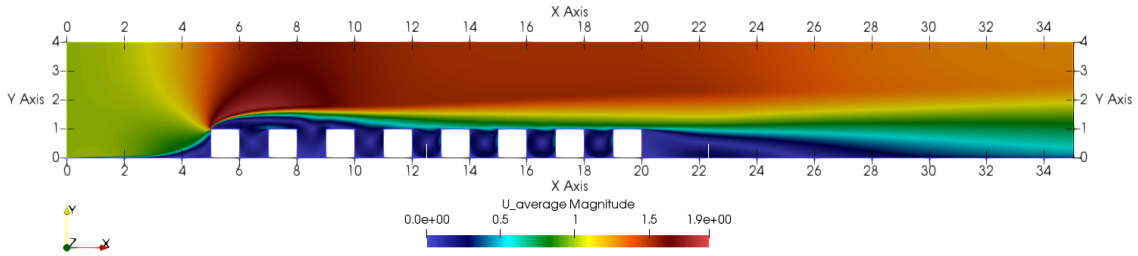

Figure 4.15: 2D average velocity map of the complete studied domain

In *Figure 4.16* it can be better appreciated the airflow in the studied canyon. Using this detail view, more phenomena can be appreciated, such as the high speed parts which will be directly translated to important zones for the pollutant study.

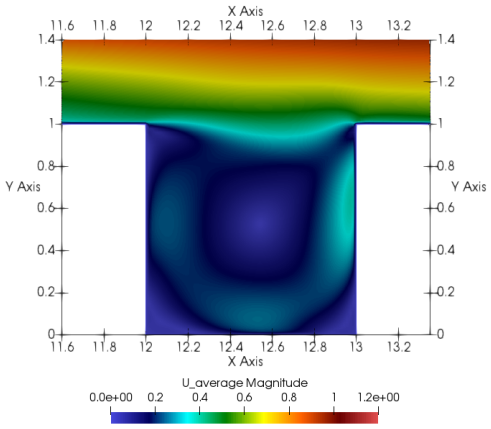

Figure 4.16: 2D average velocity map of the 4th canyon

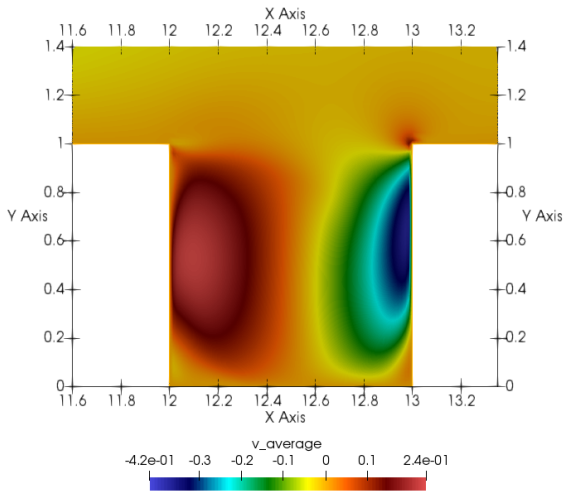

Figure 4.17: 2D average velocity in Y direction map, 4th canyon

If we just focus on the velocity map in the Y direction, shown in *Figure* 4.18, we obtain valuable information to be discussed.

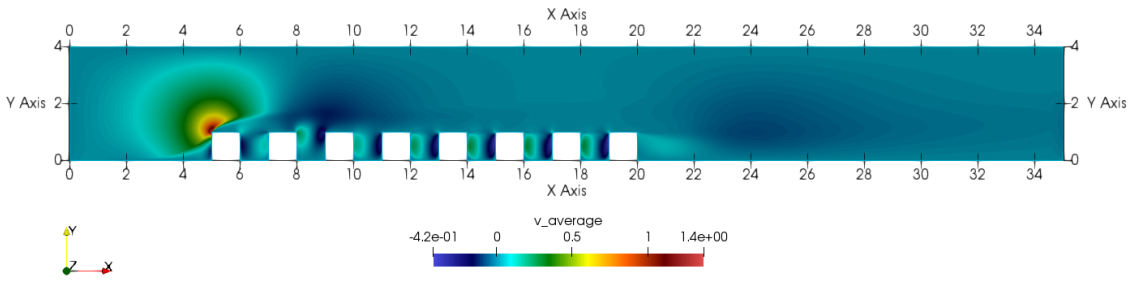

Figure 4.18: 2D average velocity in Y direction map, complete domain

4.5.1.3 Pressure maps

In the presented pressure map of the complete domain it can be appreciated the suction zone created by the first building. After the stagnation point, coinciding with the top of the windward side of the firs building, the pressure drops drastically in the first canyon reaching a peak value of approximately -1.1 m^2/s^2. After this zone, the pressure increases gradually and achieves an outlet constant value of $0m^2/s^2$, as the boundary condition imposes.

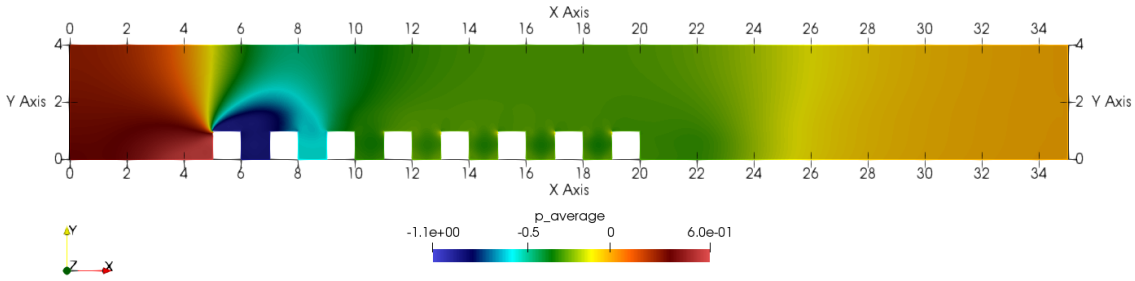

Figure 4.19: 2D average pressure map, complete domain

In the 4th street canyon, the pressure is uniform with the following distribution. It is important to notice the very close data range used in the *Figure 4.20* map for appreciating the different pressure zones.

4.5.1.4 Streamlines

Streamlines are a powerful post-processing tool that can perfectly describe the airflow in street canyons. As the pollutants tend to follow the airflow, streamlines will be used

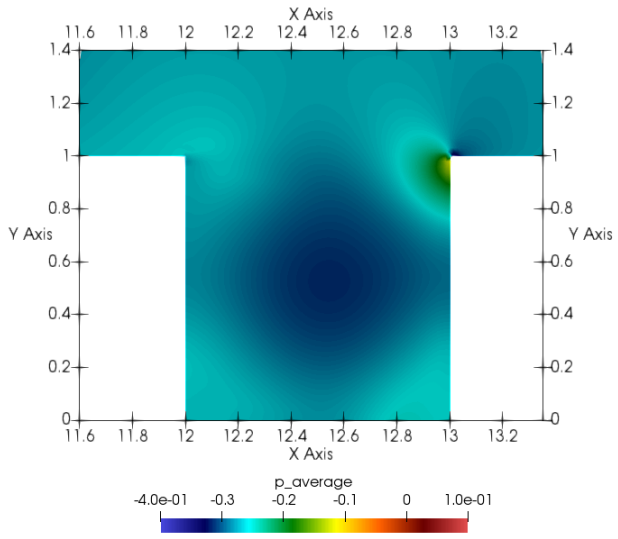

Figure 4.20: 2D average pressure map, 4th canyon

lately when talking about the pollutant transport and the recirculations generated in street canyons, which make it difficult to remove these harmful substances from our cities.

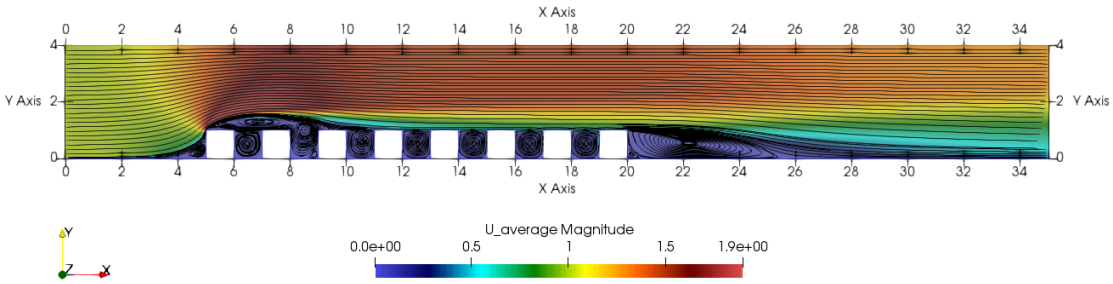

Figure 4.21: 2D velocity streamlines, complete domain

In this general view of the domain, *Figure* 4.21, it is so easy to identify the zones where the flow is undisturbed, where it is completely turbulent and the wake that leave the buildings, generating a massive recirculation at the end of the domain.

When doing a detail view of the studied canyon we can clearly appreciate the main recirculation and the two small vortexes in the windward and leeward corners of the canyon. This is so important to take into account when doing the discussion about pollutant transport, as well as the fact the main recirculation is completely isolated from the free-

stream.

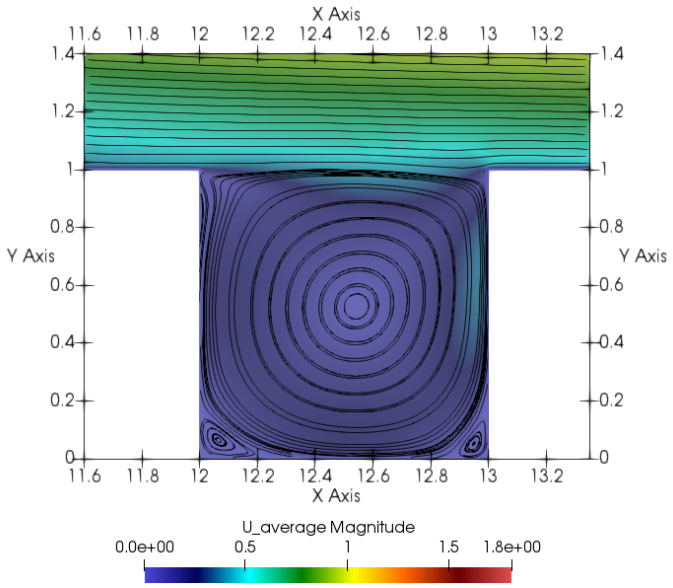

Figure 4.22: 2D velocity streamlines, 4th street canyon

4.5.1.5 Contours

Finally we are presenting the contours plotted for visualizing the vertical velocity, see *Figure 4.23* and *Figure 4.24*. This post-processing tool will allow us to clearly identify the areas of the street canyon where the air comes in and comes out, values directly related to the pollutant removal. This maps are just presented in this section and will be deeply discussed in *Chapter 5*.

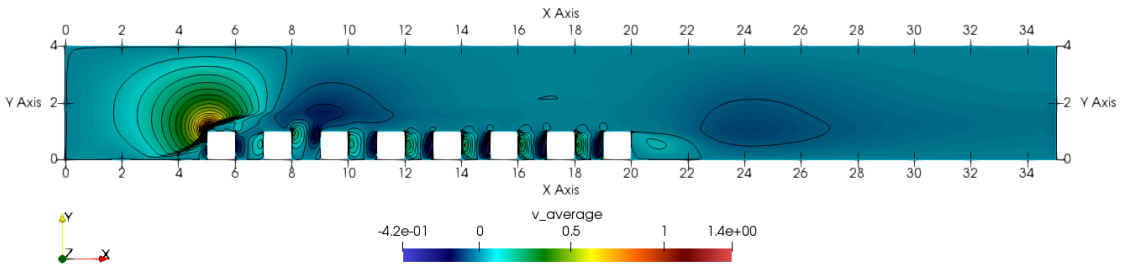

Figure 4.23: Vertical velocity contour, complete domain

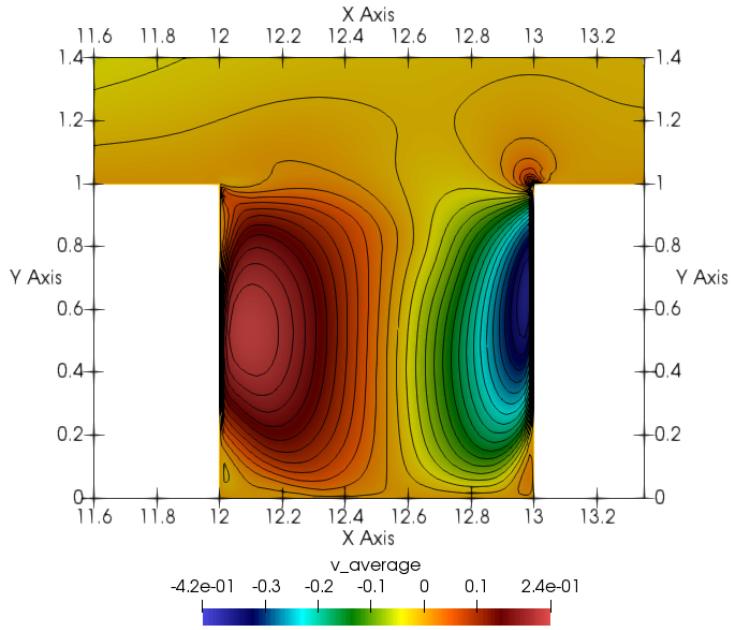

Figure 4.24: Vertical velocity contour, 4th canyon

4.5.2 Validation

Once all the results of the 2D simulation with no pollutant modelling are presented, it is time to start the validation process, one of the most important ones in order to know if all the computational results obtained from the simulation coincide with the physical reality and with some other numerical results, which are already validated.

In order to do the validation of the obtained *RNG K-epsilon* simulation results we are using the experimental and LES results from [12], another LES simulation provided by this thesis director, *Ivette María Rodríguez*, and the RNG k-epsilon values from the first part of this study performed by *Jordi Galí*[14].

The presented graphics represent the velocities in X and Y direction ($\overline{u}$ and $\overline{v}$, respectively) and the fluctuating velocities in the same directions (expressed as $\overline{u''u''}^{\frac{1}{2}}$ and $\overline{v''v''}^{\frac{1}{2}}$). These data is made dimensionless by using the reference speed, U_{inlet} and is represented in function of the X or Y dimensionless distance (using the buildings' height, H), depending on if the data is collected from a vertical or horizontal line.

The values of velocity and fluctuations are collected from the four different lines de-

scribed: three vertical and one horizontal; the last one will give us priceless information when doing the pollutant transport simulations as it is collected at roof level *(y/H=1.00)*. The vertical data collection is from $x/H = 0.25$, $x/H = 0.50$ and $x/H = 0.75$, being x the distance from the leeward in the 4th street canyon, where all the information is collected. If we refer to absolute distances, this lines are at 12.25m, 12.50m and 12.75m from the inlet, respectively.

It is important to mention that as the buildings' height is taken as H=1.00m and the reference velocity as U_{inlet}=1.00m/s, we will have no problem for the adimensionalization of the studied variables.

Before presenting the previously mentioned graphics it is important to concisely define the colours legend for having no trouble during the graphics analysis.

- **Red circles:** experimental data from [12].
- **Discontinuous black line:** LES simulation from [12].
- **Continuous black line:** LES simulation provided by *Ivette María Rodríguez*.
- **Discontinuous green line:** RANS simulation from [14].
- **Discontinuous blue line:** RANS initial simulation performed with no wall function nor mesh refinement.
- **Discontinuous red line:** final RANS simulation performed for this thesis using RNG k-epsilon model with $\varepsilon = 5.57 m^2/s^3$, $k = 0.19 m^2/s^2$, wall functions and mesh refinement near the wall and in street canyons.
- **Continuous magenta line**: in the fluctuations plots, an additional line called "RANS4" is presented, being the average fluctuations calculated using the R function, instead of the Uprime2mean one. This plot represents the modeled part of the velocity fluctuations in this study case with the same configuration as "RANS3".

As can be appreciated in the graphics of y/H=1.00 (horizontal line data collection), it is only used one LES simulation, from [12], for performing the validation.

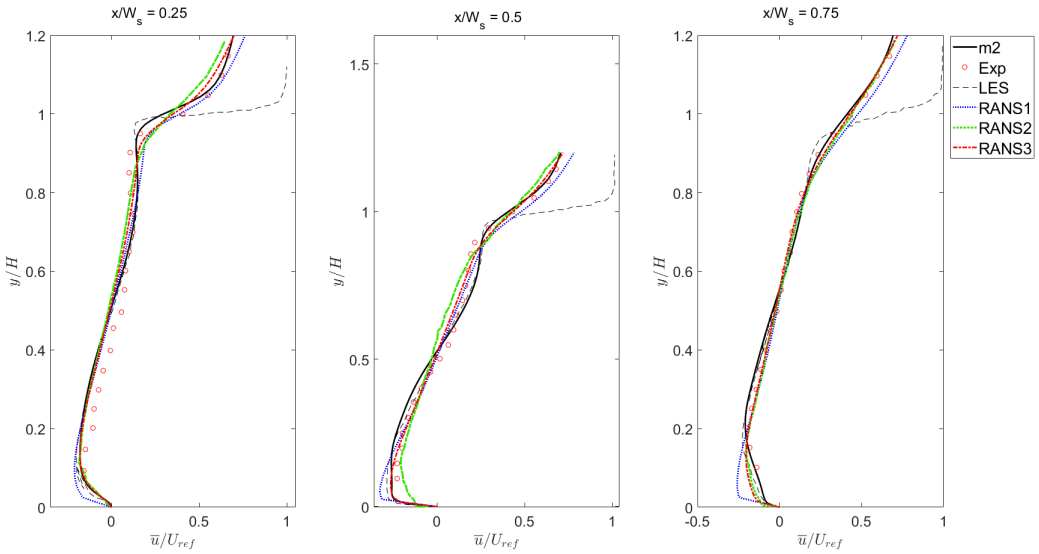

Figure 4.25: X direction velocity comparison

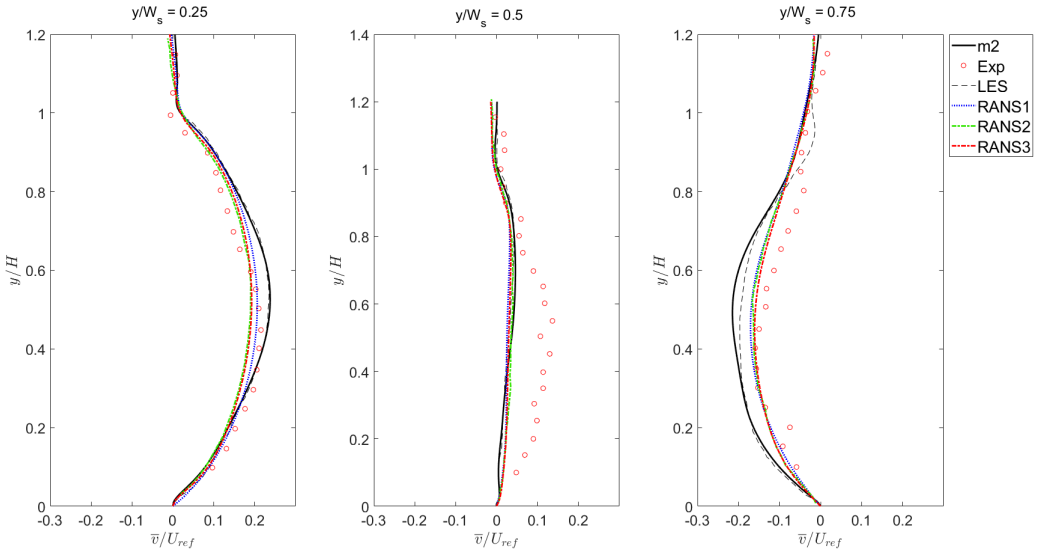

Figure 4.26: Y direction velocity comparison

In *Figure 4.25* and *Figure 4.26* the comparison in between all the velocities data is done, for the X and Y direction along the three chosen lines for the study.

As can be appreciated, the final CFD simulation performed using the RNG k-epsilon model (the discontinuous red lines tagged as "RANS 3") follows with high precision the other RANS simulations, the LES ones and the experimental results. Regarding to the U velocity (X direction) in *Figure 4.25*, from y/H=1.00 on a noticeable deviation from the LES simulation can be appreciated despite of the accuracy compared to the experimental results. This deviation can be attributed to the fact that this point is where the join in between the free-stream and the main vortex of the canyon is found.

If we focus on the initial performed simulation, tagged as "RANS 1", it is obvious the error committed near the wall compared tot the other values, as a result of the lack of mesh refinement and wall functions.

If we move on to the *Reynolds stress tensor* components, we present the second order terms: the fluctuating velocities. This is one of the most difficult parts to properly simulate using a Reynolds-Average Navier-Stokes model, as it solves the governing equations by averaging the velocity and pressure fields. When we apply the averaged terms to the equations, the Reynolds Stress Tensor appears, generating higher order terms and a closure problem. For this reason the RNG k-epsilon turbulence model has been applied, in order to close the system and find a solution by creating a relation in between the stresses and the mean flow velocities. The Reynolds Stresses are not strictly stresses but momentum fluxes created by the unsteady turbulence. Despite of being able to estimate the turbulence, as we are using a RANS model, it is expected to obtain not a good enough approach for the Reynolds stresses[59].

In this section we are just presenting the Reynolds normal stress terms of a 2D simulation, which can be made dimensionless by u''^2/U_{inlet}^2 and v''^2/U_{inlet}^2. This is because we are not studying the effect of the turbulent boundary layer, if not, we should focus on the Reynolds shear stresses and neglect the normal components. In the presented plots, see *Figure 4.27, Figure 4.28, Figure 4.31 and Figure 4.32*, the square root of the fluctuations has been done for obtaining the fluctuating velocities as are the measures available in the literature for doing the validation.

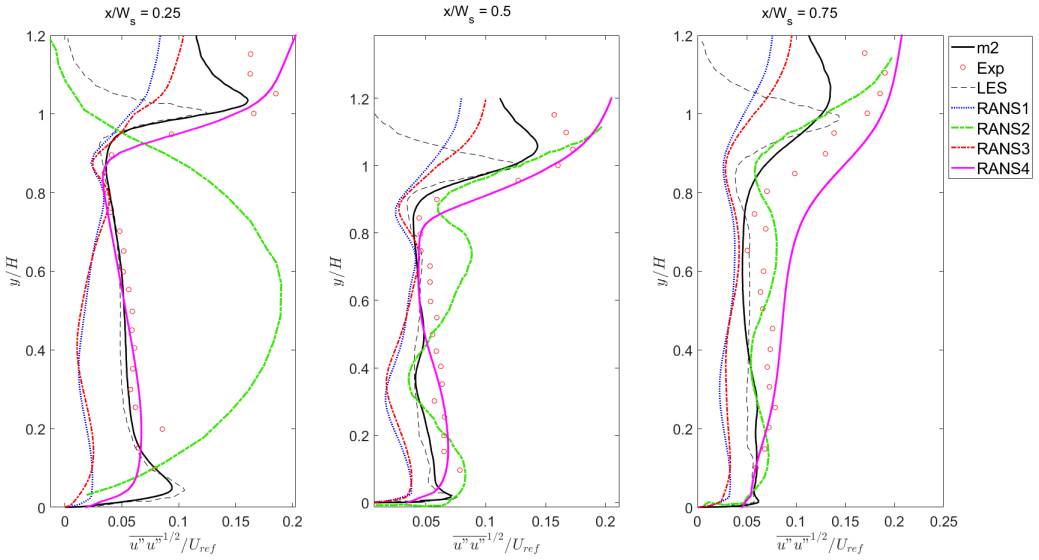

Figure 4.27: X direction velocity fluctuations comparison

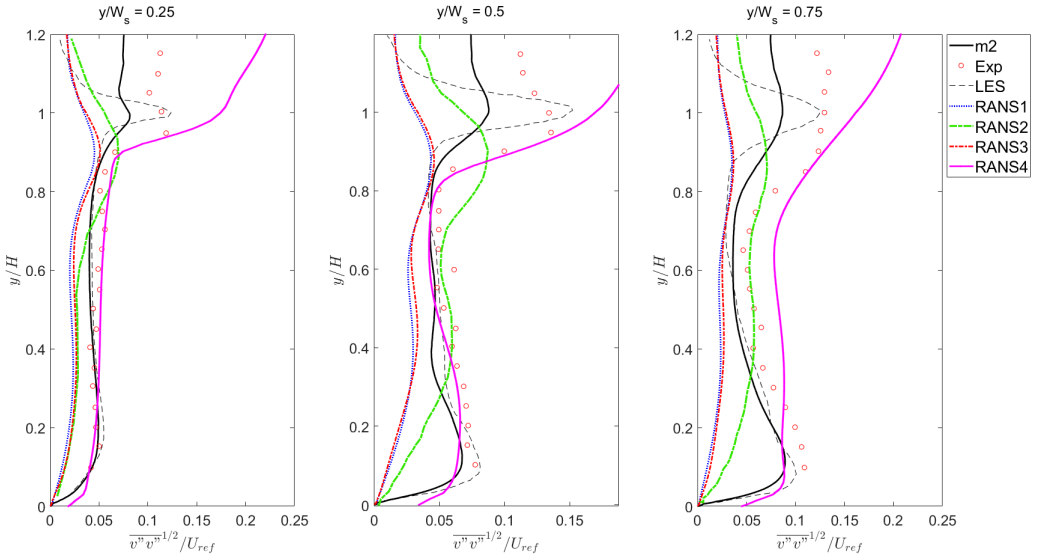

Figure 4.28: Y direction velocity fluctuations comparison

When analysing the momentum fluxes we can appreciate the clear under-prediction of the RANS simulations compared to the experimental results and LES simulations when

using the function *Uprime2mean* in *OpenFoam* for obtaining the tensor's components. Despite of having included and inlet boundary condition of turbulent kinetic energy of 5% the obtained results have considerable error in the results tagged as *RANS1, RANS2* and *RANS3*. Nevertheless, the stresses profiles are quite similar to the expected and when moving far from the wall the precision increases. In the Y direction the fluctuations have a clear divergence and maximum error near $y/H = 0.00$ and $y/H = 1.00$. On the other hand, if we analyse the *RANS4* results, we can appreciate the improvement, regarding to the profile's similarity in magnitude and distribution. This has been achieved using the post-processing function *R*, the one that allows us to acquire just the modeled part of the tensor, which is the 100% as we are performing RANS simulations. In these results, for the vertical and horizontal fluctuating velocities, *Figure 4.27* and *Figure 4.28*, it is appreciated the clear precision of the result until we reach the roof-level of the street canyon. Once y/H=1.00 is reached there is a deviation that can be caused by the lack of accuracy at modelling results at the junction of the canyon's recirculation and the free-stream.

Even though the RANS accuracy when approaching fluctuating terms could be improved, in RANS4 the improvement is clear. In further studies some changes could be done in order to improve the results by including other wall functions, other turbulence intensities at the inlet, improve the mesh quality, etc.

Once we have presented all the results obtained from the vertical lines located at an absolute distance of 12.25m, 12.50m and 12.75m, respectively, from the inlet, we can talk about the data obtained in the horizontal line at $y/H = 1.00$ in the 4th street canyon. This is an important and valuable analysis as in the next section, the values at this zone will be crucial when performing the pollutant transport analysis and the Air Exchange Rate calculation.

When looking at the velocity profiles in the X and Y direction, see *Figure 4.29* and *Figure 4.30*, the most remarkable aspect to talk about is the velocity peak found near the windward of the next building in the 4th street canyon. As all the results, for different types of data obtaining, are around the same values, we can predict that this zone, in between $x/H = 0.90$ and $x/H = 1.00$, there is a velocity and peak because of the airflow deviation caused by the building, which increases vertical velocity and generates a turbulent kinetic energy peak. Despite of it, as will be seen later, is not in here where the major part of the pollutant is

removed from the canyon. This will be studied later using the *Air exchange rate* and the mean pollutant concentration fluxes.

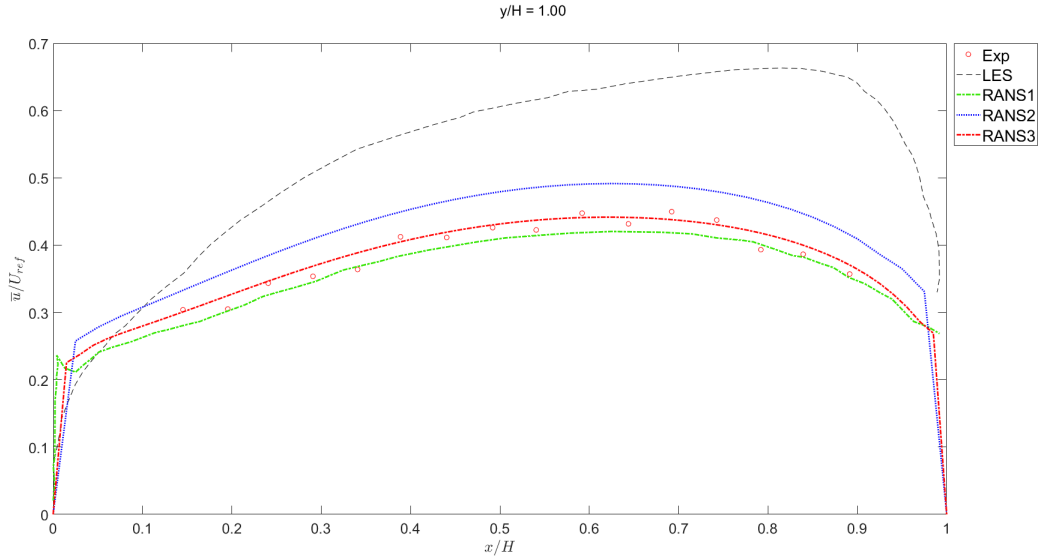

Figure 4.29: X direction velocities comparison

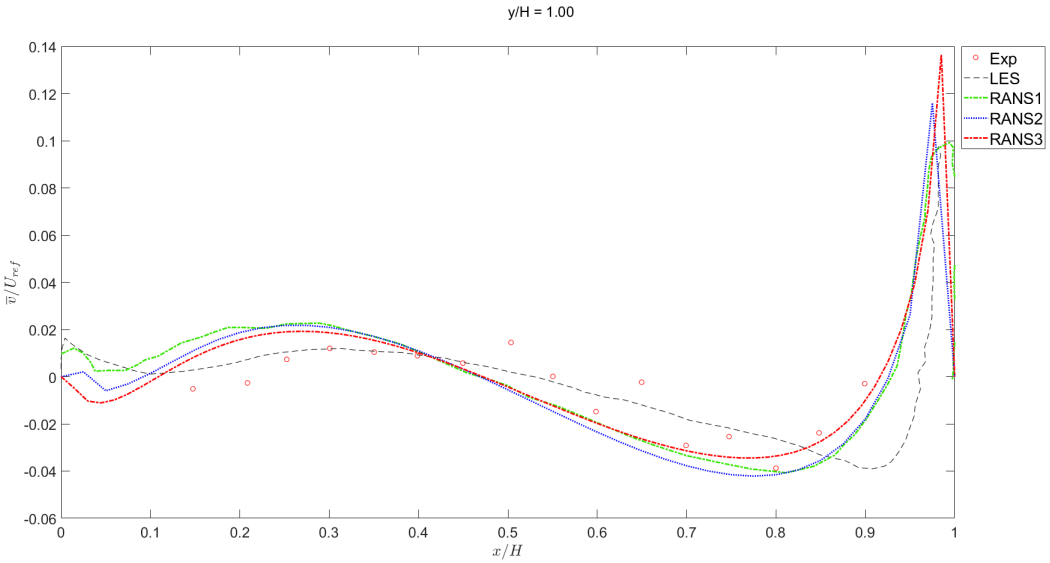

Figure 4.30: Y direction velocities comparison

Finally we can present the Reynolds stresses obtained in this line in *Figure 4.31* and *Figure 4.32*. As expected, for *RANS1*, *RANS2* and *RANS3* simulations there is a clear under-prediction of the fluctuating velocities. On the other hand, when analysing the *RANS4* results, in *Figure 4.31* and *Figure 4.32*, the precision is highly increased. Regarding to the X direction fluctuating velocity our results are so similar to the experimental results until the windward side of the building is reached. When talking about the Y direction fluctuating velocity there is an over-prediction of the results that could be caused by the case configuration or the mesh quality, among other factors. This over-prediction will be appreciated when computing the ACH in the *Discussion* section, as for the AR=1.00 street canyon the results will be also over-predicted.

In this part of the study it is shown the importance that choosing the right way to obtain data has as well as to know how properly prepare the physical setup. The next presented results that involve the velocity fluctuations, as the turbulent kinetic energy and mean pollutant concentration fluxes maps, are calculated using the *R* post-processing function, as it is the adequate for a RANS study and it has been shown that offers better results.

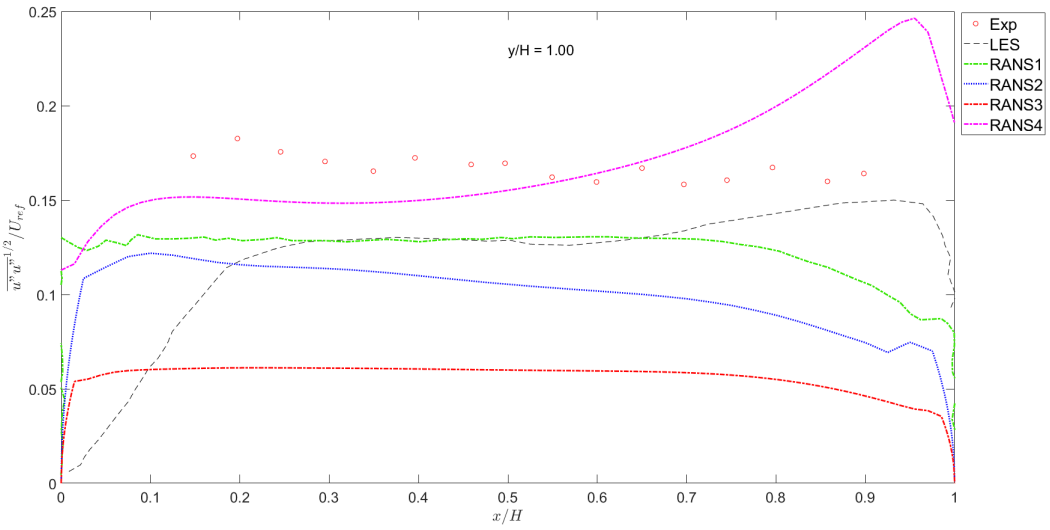

Figure 4.31: X direction velocity fluctuations comparison

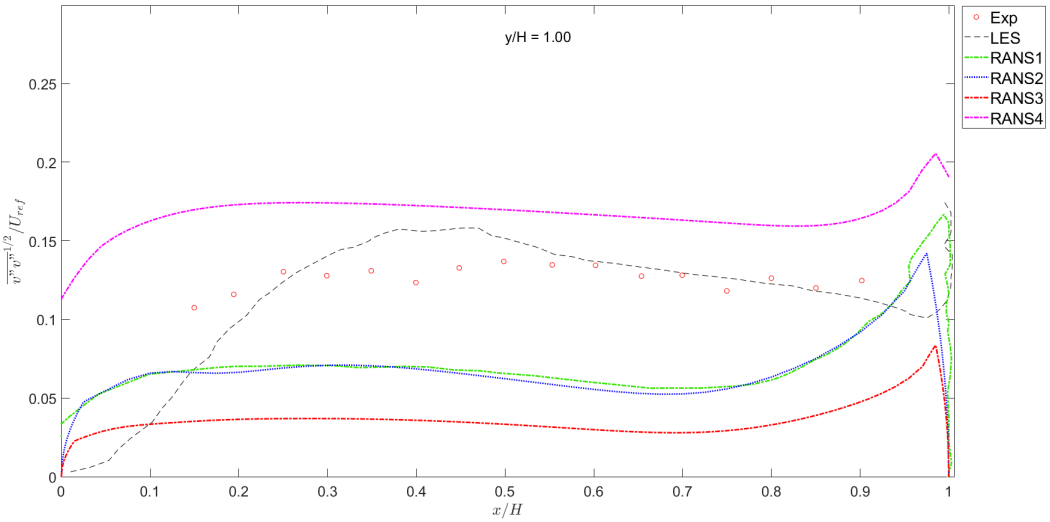

Figure 4.32: Y direction velocity fluctuations comparison

Chapter 5

Pollutant transport numerical results

Nowadays, in our fast-growing cities with tall buildings, narrow streets and thousands of cars driving down them, pollution problems are main issues as they have many impacts including health and environmental impacts.

In order to study this phenomenon we will start from the case setup explained in *Chapter 4* and implement the passive scalar pollutant transport equation in the OpenFoam model used in order to validate the study using LES simulations and experimental results. As one of the most important characteristics, referring to pollutant transport and airflow, is canyon's aspect ratio (AR), defined as the relation in between buildings height (H) and street width (W), the initial study has been carried out by implementing and simulating in OpenFoam the pollutant generation in a street canyon of AR=1.00 with free-stream wind perpendicular to the street axis. Later on we have done a comparison with 0.50 and 2.00 AR cases. This gives us the possibility to compare and understand how this key factor affects to the pollutant circulation and retention in canyons (a direct result of the rotating and counter-rotating recirculations generated and the flow regimes obtained depending on the AR).

After validating the simulation results obtained running the 2D case without pollutant transport and making sure that the velocity, pressure... values are correct in the previous sections, we have a solid basis and can implement the pollutant transport equation on the basis of the results previously mentioned, as it has been shown that $k-\varepsilon$ models can give us realistic information, despite of the lack of precision in some parts such as the secondary recirculations, and the information that is lost by conducting a 2D simulation instead of computing the span-wise data, only available in 3D flows . Many simulations, using this model, have been carried out during the years and for an AR=1.00 just a primary

recirculation has been computed. This turbulence model used is the appropriate for our computational resources but we must take into account that many studies show that it under-predicts turbulent intensity, leading to weaker recirculations and directly affecting to the pollutant transport throughout the canyon[11].

When the AR changes, the number and characteristics of recirculations is modified too, and for this reason street canyons with an aspect ratio in between 0.10 and 3.50 have been studied in many occasions. This phenomenon is really important to have in mind as it will completely affect the turbulent transport, leading to a change in pollutants retention in street canyons, which can be directly translated to air quality changes.

5.1 Case definition

The pollutant transport has been implemented by using the theoretical basis and the lineal source explained in section *3.2.2 Pollutant source modelling*. The main goal of this thesis' part is to implement a passive scalar pollutant in *OpenFoam* and study the transport and diffusion that it has in the street canyon and throughout all the computed domain, in order to obtain solid conclusions about the effects that AR and *diffusivity* have.

A comparison in between street canyons with three different aspect ratios (0.50, 1.00 and 2.00) has been done; the AR=1.00 case has been carried out by using the same geometry and fine mesh as in the simulation run with no pollutant source. For the AR=0.50 and AR=2.00 simulations the following geometries have been chosen. It is important to mention that the buildings' height (H) has remained constant at H=1.00m, as the process to make the variables dimensionless is simpler; for this reason, the street canyons' width has been changed from 1.00m, in the AR=1.00 case, to 0.50m for the AR=2.00, and 2.00m for AR=0.50. As the simulations are 2D, the domain is 3.00m wide and has just one cell in the Z direction. The inlet distance to the first building has remained constant at 5m and the number of street canyons in the domain varies depending on the AR, but a study has been done in order to make sure the flow in the studied canyon is stable with fully developed turbulence and flow and that the distance from the last building to the outlet is sufficient to capture the wake created by the buildings' airflow disturbance.

In the AR=0.50 case we have a total of 5 street canyons and the study and pollutant modelling has been done in the 3rd one. The distance from the 6th building's leeward to the outlet is 14.00m with a building's width of 1.00m and a total domain length of 35.00m.

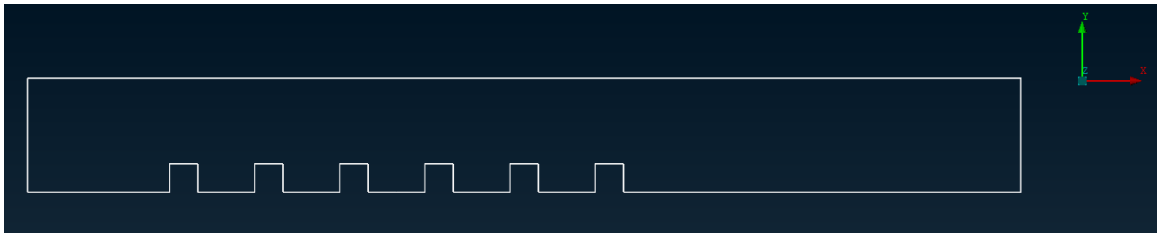

Figure 5.1: AR=0.50 geometry, front view

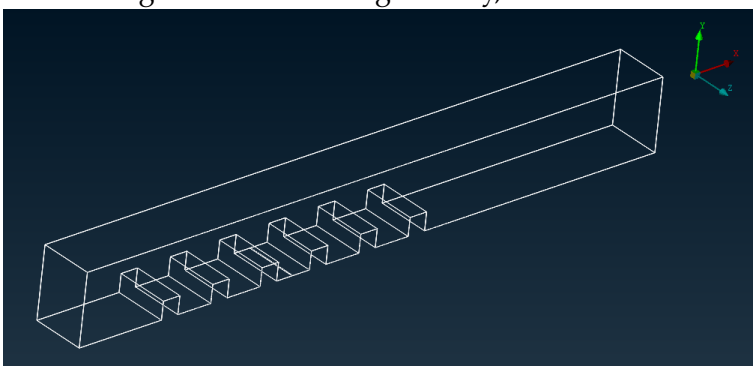

Figure 5.2: AR=0.50 geometry, isometric view

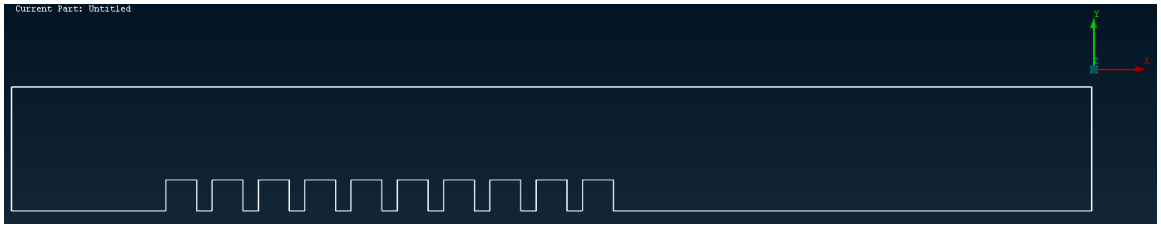

Figure 5.3: AR=2.00 geometry, front view

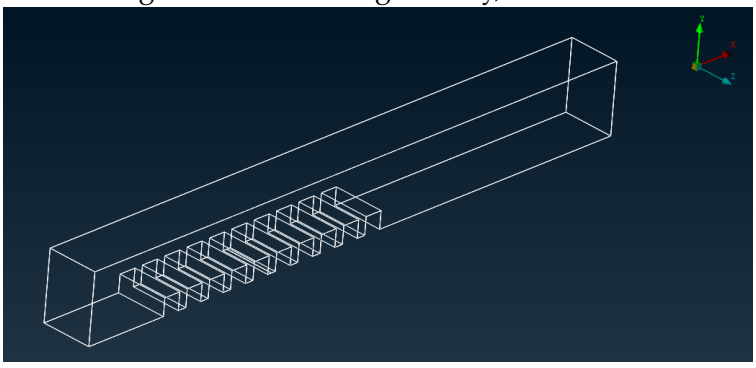

Figure 5.4: AR=2.00 geometry, isometric view

In the AR=2.00 domain there are 9 street canyons 0.50m wide and the study and pollutant modelling has been carried out on in the 5th one. The final distance to the outlet is 15.50m with a buildings' width of 1.00m and a total domain length of 35.00m, too.

Regarding to the mesh creation, the same procedure as for the validation with no pollutant transport setup has been followed, with a minimum cell length of 0.015m, a maximum of 0.20m in a structured grid. The only difference that can be appreciated in all three pollutant modelling cases is the existence of a new *PID* surface called "POLLUTANT". This models the lineal pollutant source and it is a rectangular surface of 0.015m wide per 3.00m long. As the relation in between the width and length of this surfaces is 0.005, there is not a big error committed in considering it as a lineal source located in the middle of the studied street canyon.

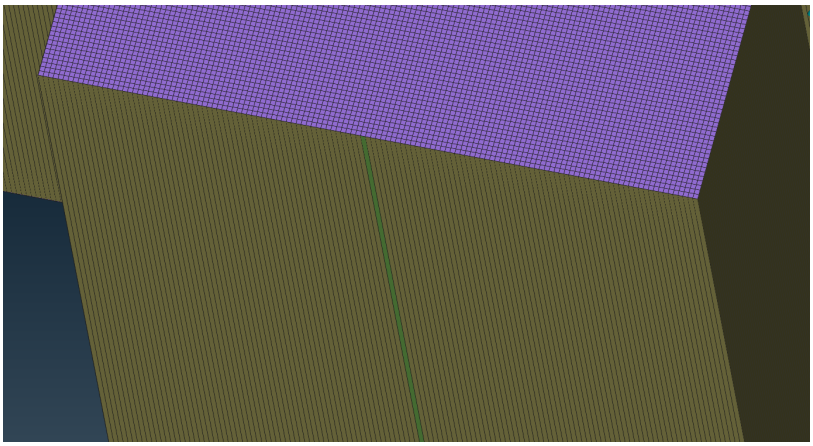

Figure 5.5: Detail view of the pollutant source

5.2 Case setup

5.2.1 Study parameters

After defining the geometry and mesh used for the different cases including pollutant transport in the middle of the chosen street canyon, we are defining the parameters that are implemented in *OpenFoam* for running the simulations. For all aspect ratios the values will be the same, as the buildings' height and the reference velocity remain constant with a value of the unity. As in the first part of this thesis we have already obtained converged velocity and pressure values, the parameters will be the same as defined in *Table 4.2*.

Diffusivity type	**Value** $[m^2/s]$
Molecular	$1.16 \cdot 10^{-4}$
Turbulent	$7.61 \cdot 10^{-4}$
Total	$8.77 \cdot 10^{-4}$

Table 5.1: Diffusion coefficient values

It is only necessary to define the diffusion coefficients that are necessary for implementing the transport equation for a passive scalar pollutant in a incompressible turbulent flow. In this thesis we are just focusing on gaseous inert pollutants, not in particles or pollutants with fast chemical reactions in the presence of light and O_2 such as NO and NO_2[25].

Taking into account that the diffusion coefficient in a turbulent flow after applying the averaging process according to an *RNG k-epsilon model* can be defined as:

$$D = D_{mol} + D_t \tag{5.1}$$

Where D_{mol} is the molecular diffusion coefficient that depends on the pollutant as well as in the flow conditions, and D_t is the turbulent diffusion coefficient modelled and defined as:

$$D_t = \frac{\nu_t}{Sc_t} \tag{5.2}$$

As calculated before $D_t = 7.61 \cdot 10^{-4} m^2/s$. To this value the molecular diffusion contribution is added which only depends on the Reynolds Number and the Schmidt Number, as stated, and has a value of $D_{mol} = 1.16 \cdot 10^{-4} m^2/s$.

A comparison has been performed in order to see how the turbulent diffusivity affects to the pollutant diffusion by performing two simulations for AR=1.00: one taking into account the turbulent diffusion and another without it.

5.2.2 OpenFoam implementation

The implementation in *OpenFoam* is the same as mentioned in *Chapter 4* but with some variances regarding to the passive scalar pollutant transport implementation. In this section we are are talking about the key aspects in every folder that make the difference in between this configuration and the previously explained.

5.2.2.1 *0* directory (time directory)

The initial time directory, when including the pollutant transport, changes depending on the aspect ratio: for AR=1.00, as we have the velocity and pressure fields already converged from the validation section, we do not use the *0* folder. Instead we have the folder of time 500, as it is the latest time from the previous simulation. In the other aspect ratios the setup for the time directory will be the same as explained in *Chapter 4*.

In here, the most important aspects to emphasise are the fact that in the boundary conditions of every field (U, p, k, epsilon) must be included the cell defined as "POLLUTANT", the PID that allows us to implement the polutant source in the boundary conditions. This is the pollutant source and for every field it works as a static wall (the same as the canyon). For AR=1.00, as we do not start the simulation from zero, we will have initial values in every file except in the new one: the **s file**.

- **pollutant concentration (s):** it is defined with no dimensions as we have set a fixed uniform value of 1.00 in the pollutant source. This have been done with the purpose of having the pollutant concentration already adimensionalized without the need of using the volumetric flux, as it has been done in some previous studies. In the "symmetry" surfaces the boundary condition used is *empty* and for all the other boundary fields it has been used a *Von Neumann* condition (*zeroGradient*).
  Despite of defining the pollutant source with a *Dirichlet* boundary condition, the obtained results will allow us to compare them to the literature ad obtain conclusions about pollutant transport and distribution in street canyons[60] .

As happened before, the *nut* and *nuTilda* files are set at an uniform initial value of 0.00, including at the new boundary condition set for the gaseous source. The modeled tensor,*R*, file is obtained for every time-step after applying the appropriate post-processing function.

5.2.2.2 *constant* directory

The *polyMesh* included in here varies depending on the AR chosen but in the *boundary* file it includes the pollutant source as a wall in all of them.
Regarding to the *transportProperties* and *turbulenceProperties*, there are no differences compared to the already explained case setup.

5.2.2.3 *system* directory

- **controlDict:** for running the simulations including pollutants, the *pisoFoam* solver is still used and the temporal parameters used are also the same as mentioned. On the other hand, a new function has been included: *scalar1*. This function is set for including the scalar transport of the previously defined field, s. It is also defined the diffusion coefficient of the gaseous pollutant in air, which can vary depending on if we take into account the turbulent diffusion or just just the molecular.
- **fvSchemes & fvSolution:** the solution schemes, algorithms, solvers... are the same as in the first part of the study but including some special solvers and schemes for the pollutant concentration.

5.3 Post-processing

5.3.1 Simulation results

In previous sections we have already presented and commented the results obtained from the first simulation run without pollutant source. Now we are focusing on the pollutant transport and distribution in street canyons and for this reason some post-processing results are presented, such as: average pollutant concentration maps and contours, Y direction velocity maps and contours, streamlines, etc.

Additionally, as we are presenting two new geometries, AR=0.50 and AR=2.00, the pressure and velocity maps for this study cases are going to be shown, too.

5.3.1.1 AR=0.5

The first new study case is the street canyons with an AR=0.50. As the aspect ratio is one of the most important factors, regarding to the pollutant transport and removal, it is important to present the values obtained in order to do a further study and comparison during the *Discussion* section.

5.3.1.1.1 Residuals

As can be appreciated in *Figure 5.6* the residuals of this simulations show a very good convergence of the results, as all the residuals are stabilized in the values of $1 \cdot 10^{-6}$, $1 \cdot 10^{-10}$ and$1 \cdot 10^{-11}$, respectively.

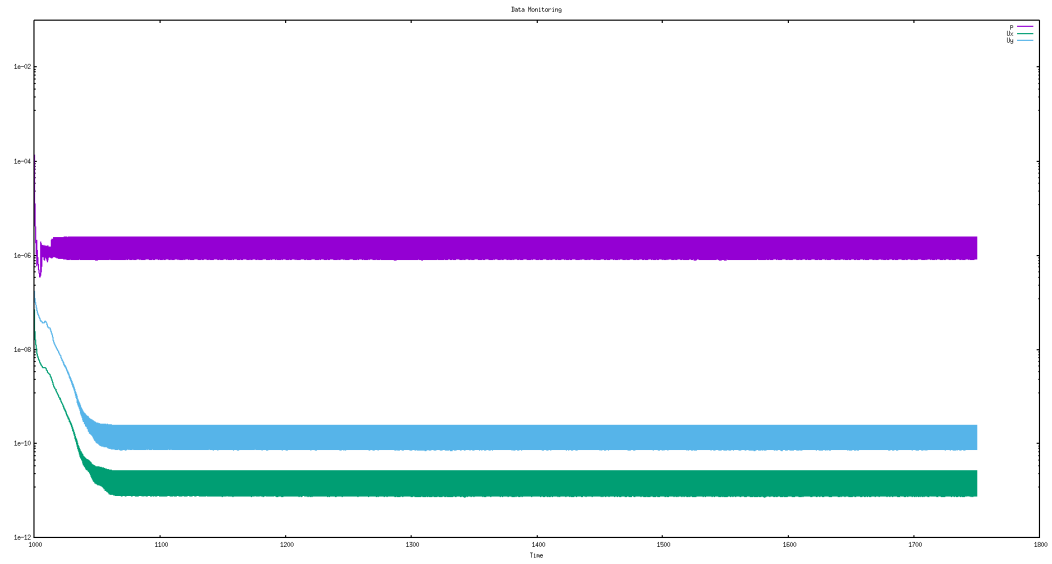

Figure 5.6: Residuals of AR=0.50 simulation

It is important to mention that the simulation, whose residuals are shown, is the second one performed after applying some changes to the initial configuration; for this reason the time starts at 1000s and finishes at 1750s and the convergence is fast.

5.3.1.1.2 Velocity maps

The velocity maps shown are from the complete domain and the 3rd street canyon. The detailed study of a street canyon has been done in the 3rd one as, because of the change in geometry for adapting to the new AR, the flow characteristics and the spatial requirements indicate that this is the appropriate and in there is where the pollutant source has been modeled.

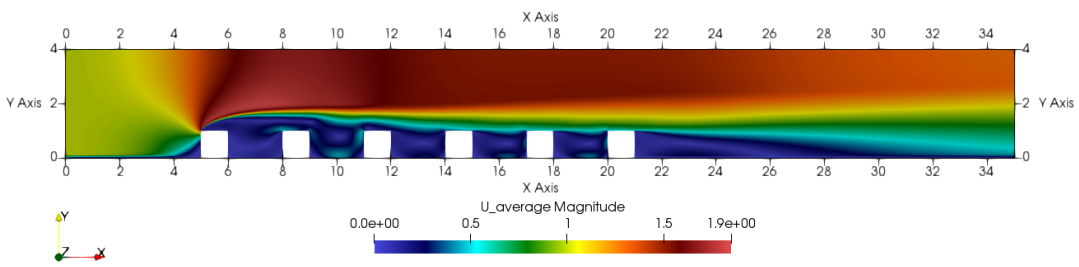

Figure 5.7: 2D average velocity map, complete domain AR=0.50

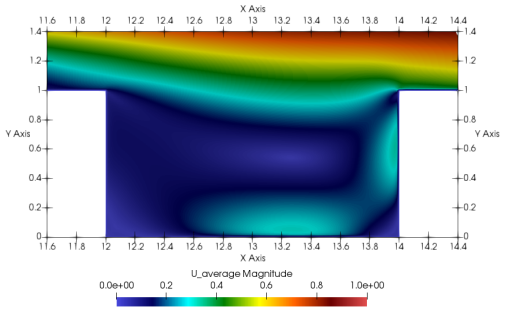

Figure 5.8: 2D average velocity map of the 3rd canyon, AR=0.50

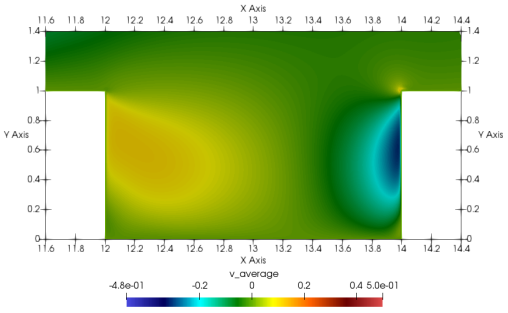

Figure 5.9: 2D average velocity in Y direction map of the 3rd canyon, AR=0.50

We can move to the most significant velocity maps regarding to the pollutant removal from the canyons. The Y direction velocity maps allow us to identify the zones zones of the street canyon with the highest and lowest average and in *Figure 5.10* the repetition pattern followed from the 3rd canyon on can be perfectly appreciated.

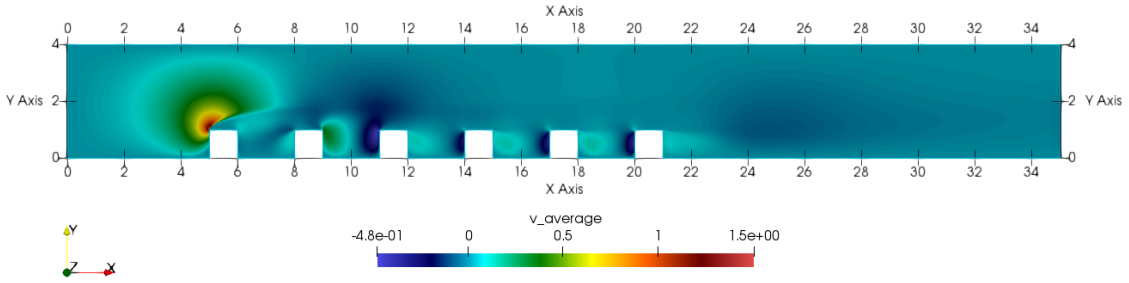

Figure 5.10: 2D average vertical velocity map, complete domain AR=0.50

5.3.1.1.3 Pressure maps

As we have been talking about pressure maps in *Chapter 4*, and the gaseous pollutants follow quite precisely the airflow in the street canyons, we are just presenting the maps obtained. The interpretation from this images is the same as the one which has been already done.

In the pressure distribution in this street canyon the low pressure zone found in the middle of the canyon for AR=1.00 is not substantial, and the high-pressure point at roof-level

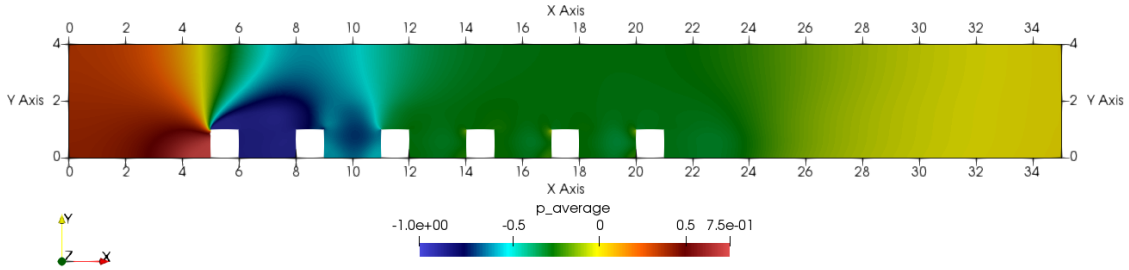

Figure 5.11: 2D average pressure map, complete domain AR=0.50

is less noticeable. This phenomenon is given because of the change in airflow distribution because of the increase of the street canyon width.

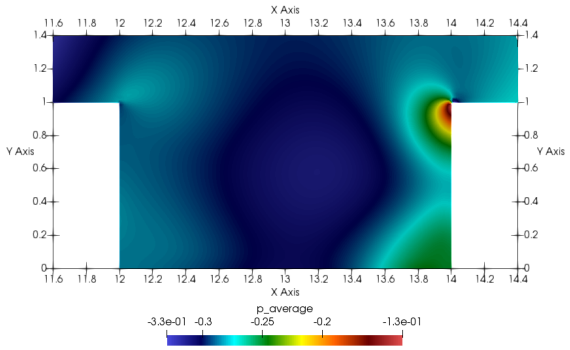

Figure 5.12: 2D average pressure map in the 3rd canyon, AR=0.50

5.3.1.1.4 Streamlines

Now that we have an initial idea about how the air distribution in a street canyon is, we can focus on the streamlines, which give us a clear and visual representation of it. It is a very important part of the post-processing process as represents in a reliable way the path that the pollutant follows throughout the canyon.

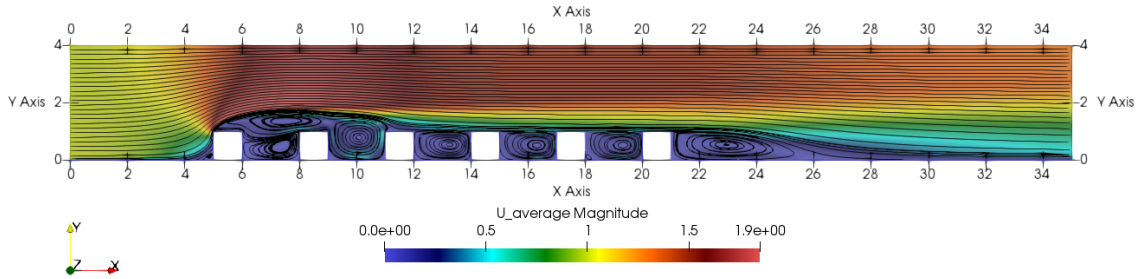

Figure 5.13: Streamlines complete domain, AR=0.50

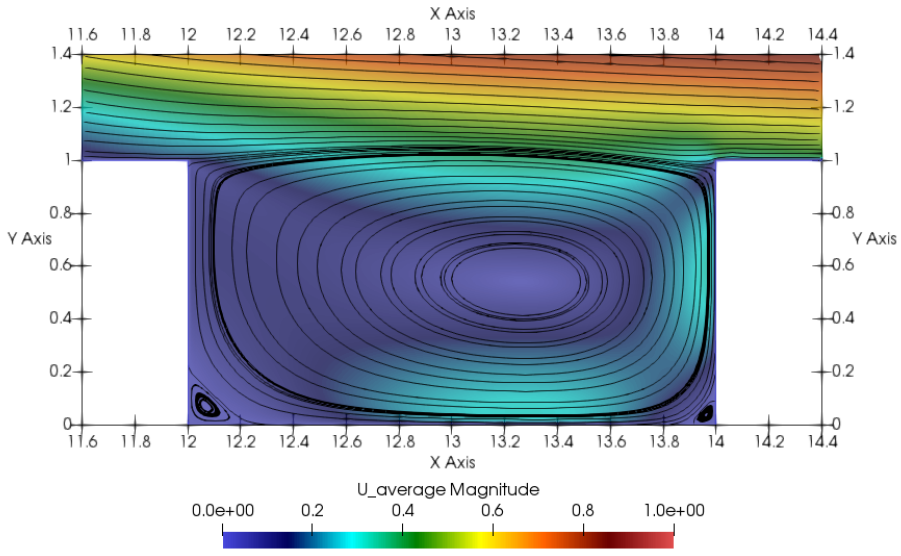

Figure 5.14: Streamlines in 3rd canyon, AR=0.50

When analysing the streamlines present in all the domain it is easy to notice the high vorticity zone generated in the first canyon and the clear flow stabilisation that starts at the 3rd one. At the end of the domain, after all the successive buildings the wake generated

shows a massive recirculation that will also be present when talking about the pollutant dispersion from its source in the 3rd street canyon.

In the detail view of the 3rd street canyon, see *Figure 5.14*, the two secondary counter-rotating recirculations can be observed. The *RNG K-epsilon* model used has enough precision for capturing this phenomenon which has a direct effect to the pollutant retention. As will be commented during the discussion of these results, the center of the primary recirculation is not at the center of the street canyon and there are no secondary recirculations generated at roof-level.

5.3.1.1.5 Mean pollutant concentration maps

Now we can talk about the pollutant concentration in street canyons in order to study how is it transported, the level of pollutant removed from the canyon and how is it dispersed once out of it. We are taking the average pollutant concentration.

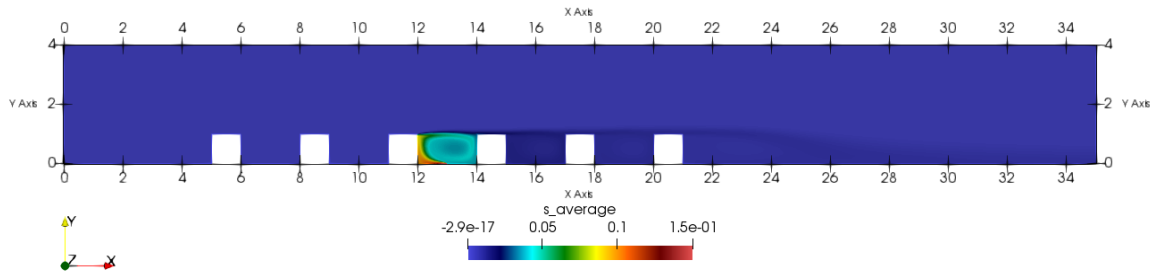

Figure 5.15: Pollutant concentration map of complete domain, AR=0.50

In here, after having reduced the scale to a maximum concentration of 0.15, we can appreciate how the pollutant follows the airflow and , with a very low concentration, leaves the canyon in the leeward side. What is also important to emphasise is the low level of pollutant concentration that arrives at the end of the street canyons, and that with the chosen levels of diffusion and flow parameters the pollutant gradually enters in the following street canyons, but with lower concentration levels. On the other hand, in *Figure 5.17* we can appreciate how the pollutant is distributed in the canyon and which are the zones with higher concentration levels and where is the zone where it leaves the canyon.

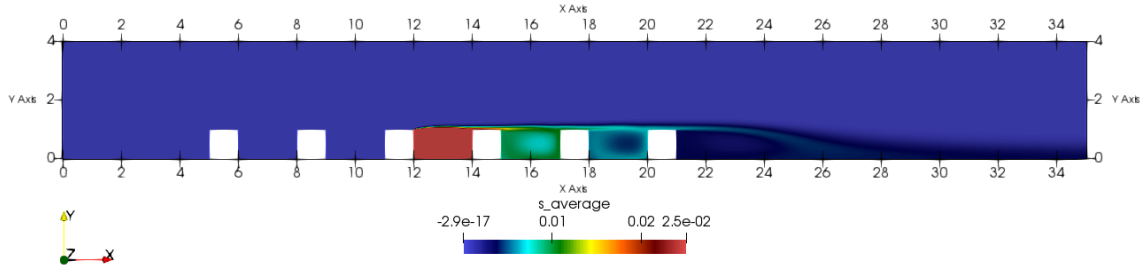

Figure 5.16: Scaled pollutant concentration map of complete domain, AR=0.50

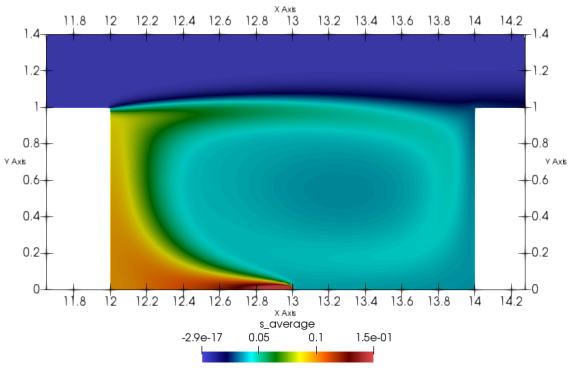

Figure 5.17: Pollutant concentration map of the third street canyon, AR=0.50

The detail view of the street canyon, where the pollutant source has been set, clearly shows how the pollutant follows the primary clock-wise rotating primary recirculation and at the leeward roof-level is the point where the pollutant, via turbulent transport, moves out the canyon and enters the free-stream (this is clearly seen with the contours). What can also be appreciated is the massive pollutant concentration given at the leeward, with a concentration variance coinciding with the secondary recirculation found at ground-level, which seems to act as a bubble which prevents the pollutant to affect in the same magnitude this region.

The effect of the diffusion, taking into account the molecular and turbulent part, is clear, despite of following the primary recirculation the pollutants ends to occupy the whole canyon with different mean concentration levels. As will be seen when analysing the pollutant transport in AR=1.00, when the diffusion coefficient increases the range of pollutant dispersion is also increased significantly, compared to a study where the turbulent

diffusion coefficient is not taken into account, for example.

5.3.1.1.6 Contours

Contours, when analysing the pollutant transport and removal in street canyons, play an important role as they allow us to clearly visualize the zones where the pollutant concentration is higher, the ones with more vertical and horizontal velocity levels... in conclusion, contours are a popular tool used for appreciating the flow structures and scalars distribution as they show us lines with constant values and depending on the density and separation of them we can visualize the magnitude of it.

In this section we are presenting the contours of X and Y direction velocities, as well as the pollutant concentration ones. These last results, combined with the vertical component of the velocity and the turbulent kinetic energy (all made dimensionless), are so helpful for performing a good analysis and discussion about the main subject of this thesis.

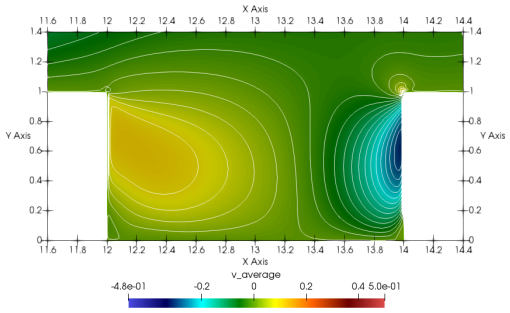

Figure 5.18: Y direction velocity contour, AR=0.50

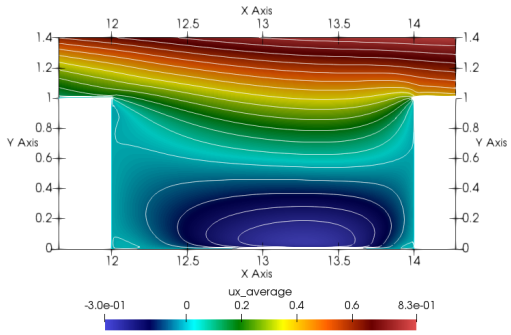

Figure 5.19: X direction velocity contours, AR=0.50

In *Figure 5.18* we can clearly appreciate the two main zones with vertical velocity, near the leeward side the flow is upward and at windward, downward. The flow structure depicted by the X direction velocity spatial contours is also interesting to be presented, as well as the pollutant concentration and turbulent kinetic energy ones.

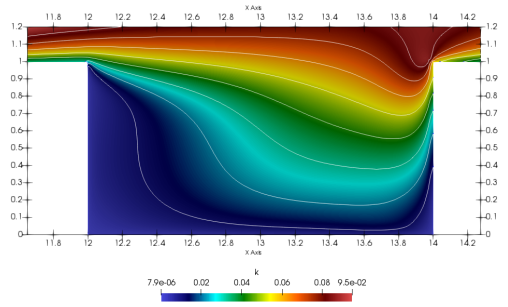

Figure 5.20: Turbulent kinetic energy contour, AR=0.50

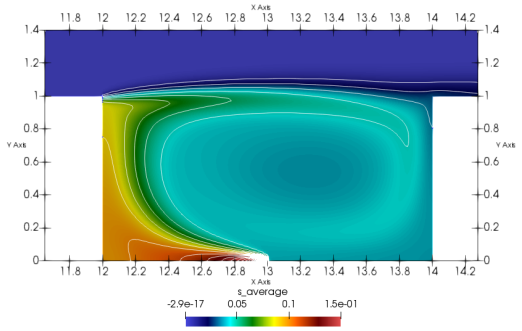

Figure 5.21: Pollutant concentration contour, AR=0.50

From the analysis of the spatial contours of dimensionless turbulent kinetic energy (k/U^2_{inlet}) where $k = 0.5 * (\overline{u''u''} + \overline{v''v''} + \overline{w''w''})$, being $\overline{u''u''}$, $\overline{v''v''}$ and $\overline{w''w''}$ the three normal mean velocity fluctuations, we can see that there is a quite uniform distribution of turbulent kinetic energy with some distortion or value increase at roof level, generally attributed to the generation of k by the mechanical wind shear[13].

5.3.1.1.7 Mean pollutant concentration fluxes

When studying the pollutant transport in street canyons, the turbulent pollutant fluxes defined as $\overline{u''s''}/U_{inlet}$ and $\overline{v''s''}/U_{inlet}$, for the stream-wise and vertical directions respectively, are an interesting tool for visualizing the removal of inert gaseous substances. As the Reynolds Number chosen for this thesis has a value of 12000 and the diffusion coefficients are low, the molecular transport can be neglected because it is proportional to the D (diffusivity) and the pollutant concentration gradient [61]. As seen in the expressions, these parameters just depend on the fluctuating velocities and the pollutant concentration. The fluctuating velocities are calculated as the square root of the velocity fluctuations, and as the pollutant concentration is dimensionless, the only thing needed for making the pollutant fluxes dimensionless is the reference velocity.

When the governing equations were presented in the *Theoretical framework* section, we appreciated that in *Equation (3.26)* the fluctuating component of the pollutant concentration was not solved. As for the calculation of the mean pollutant concentration fluxes this component is needed, it has been necessary to use the previously explained *Simple Gradient*

Diffusion Hypothesis (SGDH). By using this hypothesis, as we have computed using *OpenFoam* the turbulent viscosity, the turbulent Prandtl Number is know and imposed at a value of 0.72 and the pollutant concentration gradients can be computed using post-processing tools, we have obtained the mean pollutant concentration fluxes shown in *Figure 5.22* and *Figure 5.23*.

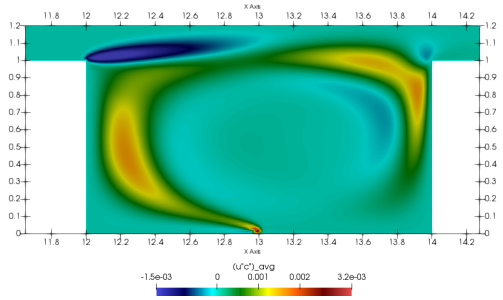

Figure 5.22: Dimensionless mean stream-wise pollutant flux, AR=0.50

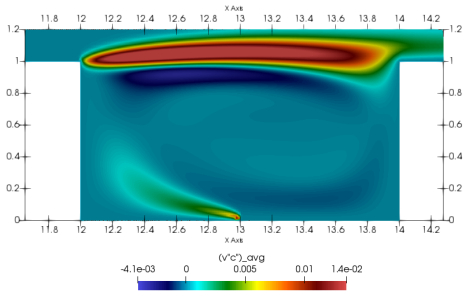

Figure 5.23: Dimensionless mean vertical pollutant flux, AR=0.50

It is of particular interest the mean vertical pollutant flux as it is a direct representation of the pollutant removal in the street canyon. We can appreciate how the maximum detected is at leeward roof-level of the canyon, which coincides with the previously seen data in mean pollutant concentration maps and contours. It is clear that the highest pollutant fluxes are at roof-level, where the pollutant via turbulent transport moves from the canyon's recirculation to the free-stream.

Among the roof-level both, stream-wise and vertical pollutant fluxes, have not maximum but substantial values, as expected, because when the pollutant joins the free-stream at the leeward wall it moves down-stream. On the other hand, at ground-level there is something interesting to mention: it is so clear that the secondary recirculations prevent the pollutant from entering these zones; this phenomenon has also been seen during the mean pollutant concentration maps analysis.

Regarding to the horizontal pollutant flux, the maximum is found at ground-level when the pollutant flows out the source and joins the clock-wise rotating primary recirculation.

Both images, *Figure 5.22* and *Figure 5.23* show how the pollutant fluxes and distribution are governed by the flow, following the recirculation generated and then joining the flow

free of pollutants. The secondary recirculations and the flow disturbance generated by the next building's corner also affect to the fluxes and it can be appreciated in the shown maps.

5.3.1.2 AR=1.0

Once the obtained results of the AR=0.50 study case are presented and explained, as well as the discussion done in the previous chapter for canyons of AR=1.00, in this part of the study and in the following with AR=2.00, we are presenting results just by emphasising and explaining the most relevant aspects of each geometry and the key aspects that differentiate one from each other. In the *Discussion*, a deep comparison of the three different studies will be presented in order to obtain relevant conclusions about the effect of this main characteristic.

As the velocity and pressure maps, streamlines and general contours have been already explained before for this study case, we are just talking about the pollutant related aspects after implementing the lineal pollutant source.

5.3.1.2.1 Mean pollutant concentration maps

In order to appreciate the importance of the gaseous pollutant diffusion coefficients in the dispersion and transport of them, we are presenting two complete domains with different diffusion coefficients. The first one, see *Figure 5.24*, only takes into account the molecular diffusion and in the second one, see *Figure 5.25*, the turbulent diffusion is also included (this second standard configuration is the one applied for the AR=0.50 and AR=2.00 studies). The values of the coefficients are both for a Reynolds Number of 12000 and a Schmidt Number of 0.72, but in the first one the turbulent part of diffusion obtained after applying the averaging has not been taken into account.

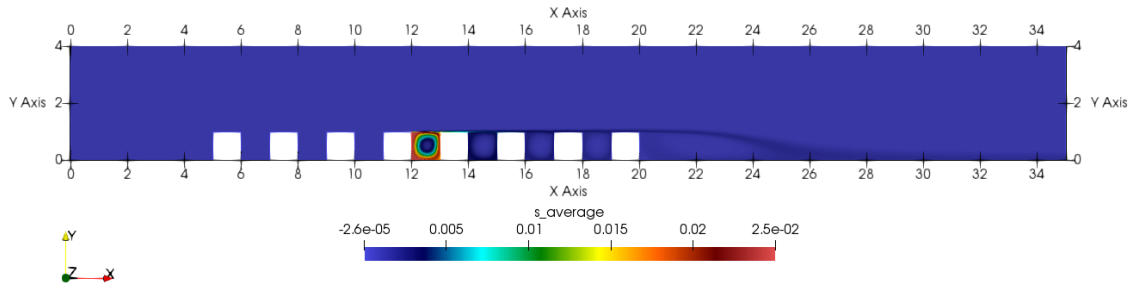

Figure 5.24: Pollutant concentration map without turbulent diffusion, AR=1.00

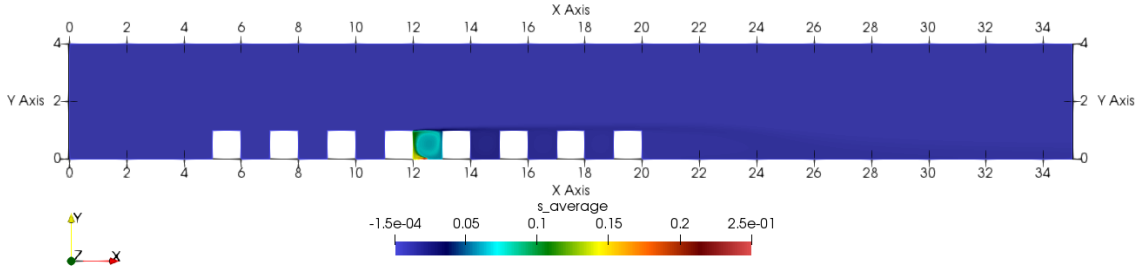

Figure 5.25: Pollutant concentration map with turbulent diffusion, AR=1.00

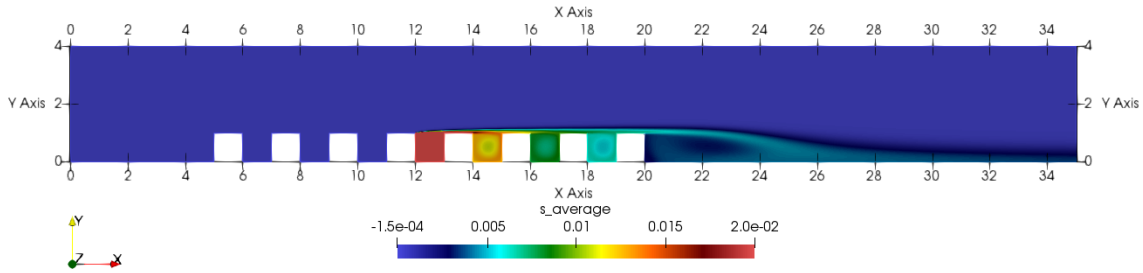

Figure 5.26: Scaled pollutant concentration map with turbulent diffusion, AR=1.00

Using the same color map scale it is absolutely obvious the difference in pollutant diffusion when the turbulent diffusion is included. Following the values shown in *Table 5.1* and the obtained by using *Formula 5.2*, the presented images are obtained with values of $D = 1.16 \cdot 10^{-4} m^2/s$ and $D = 8.77 \cdot 10^{-4} m^2/s$, respectively. If the mean pollutant concentration is scaled, *Figure 5.26*, it is obvious how the pollutant is gradually transported to the downstream street canyons, going from an approximately concentration greater than 0.02, in the fourth canyon, to 0.005 in the last one.

We can appreciate how with higher diffusivity values the pollutant diffusion, in the canyon with the pollutant source, is complete and the gaseous substance is expanded around the whole canyon. It is also important to notice how the turbulent transport and diffusion at roof-levels is increased and the pollutant that is transferred to the following street canyons is more relevant.

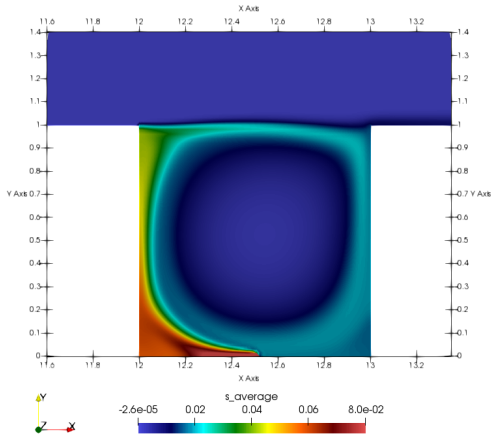

Figure 5.27: Pollutant concentration map in the 4th street canyon without turbulent diffusion, AR=1.00

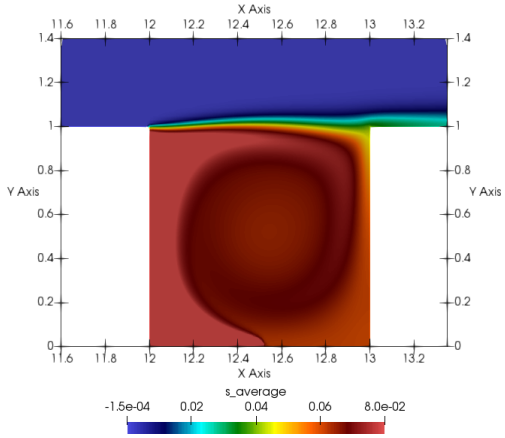

Figure 5.28: Pollutant concentration map in the 4th street canyon with turbulent diffusion, AR=1.00

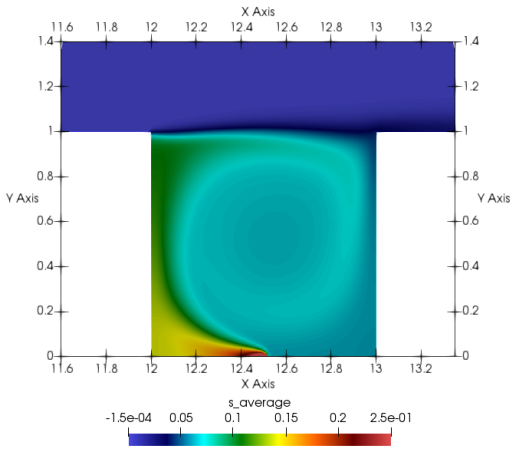

Figure 5.29: Pollutant concentration scaled map in the 4th street canyon with turbulent diffusion, AR=1.00

Figure 5.27 and *Figure 5.28* are a good way to visualize how pollutant follows the main flow recirculation, but at the same time, when the diffusivity is higher, the diffusion makes the pollutant gradually covers the whole canyon. If we change the color bar in order to better appreciate the pollutant distribution when $D = 8.77 \cdot 10^{-4} m^2/s$, we obtain the map shown in *Figure 5.29*.

When comparing it with *Figure 5.27* it is clear how the increase in diffusivity makes the two "low concentration" bubbles, that coincide with the secondary recirculations at ground-level, almost disappear. In this, as in the other two studies performed, the mean concentration values are made dimensionless directly by applying a fixed uniform value of 1.00 at the central linear source, what means that the values are all referenced to the maximum mentioned value of the unit at the source.

5.3.1.2.2 Turbulent kinetic energy contours

The turbulent kinetic energy contours have a direct relation with the velocity fluctuations. For this case, the obtained results have different distributions compared to the first aspect ratio street canyons, but the information that can be extracted is so similar. For obtaining a wider vision of the fluid mechanics that surrounds the turbulent kinetic energy, we are presenting three four different versions: two contour plots with a turbulent kinetic energy of the 5% at the inlet, one considering isotropy and another without it; additionally, the same plots but with 20% TKE at the inlet are shown.

The isotropy assumption is usually used when working with high Reynolds numbers [13] and in these simulations it can be appreciated the similarity in between results. When the turbulence intensity at the inlet is of the 5%, there is similarity in the two results obtained and, surprisingly, when using a 20% the results are so similar and even the isotropy consideration case is a little under-predicted, compared to *Figure 5.31*. The contours show how the TKE follows the flow, as the highest levels are detected at roof-level windward corner, where the flow is disturbed and a part comes into the street canyon, generating decreasing turbulent kinetic energy levels along the windward side.

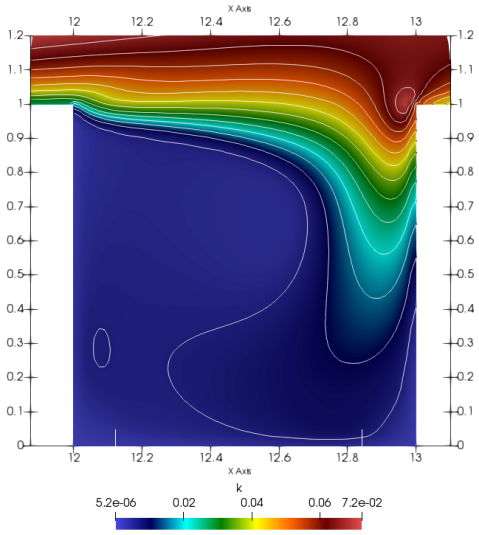

Figure 5.32: TKE contour with 20% turbulence intensity at the inlet, AR=1.00

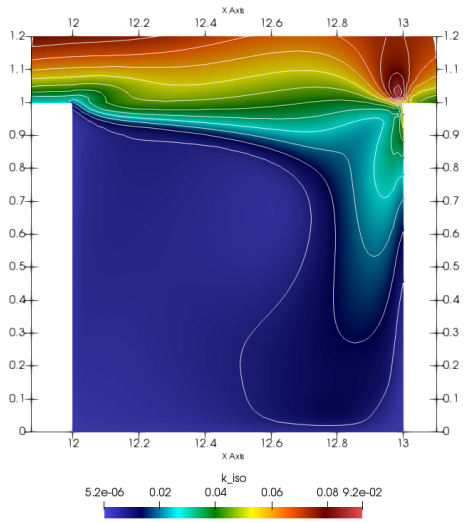

Figure 5.33: TKE contour with 20% turbulence intensity at the inlet considering isotropy, AR=1.00

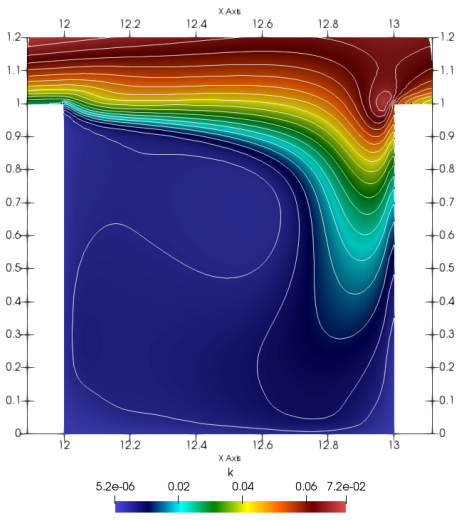

Figure 5.30: TKE contour with 5% turbulence intensity at the inlet, AR=1.00

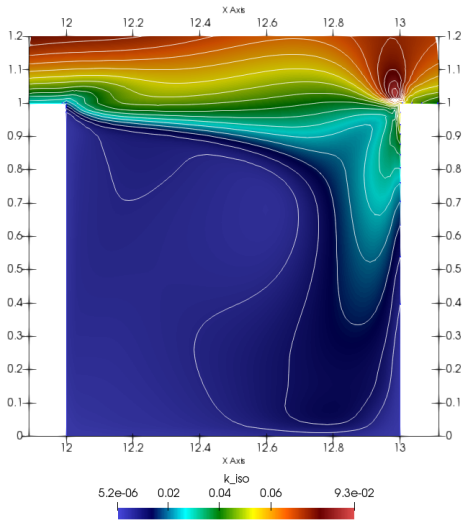

Figure 5.31: TKE contour with 5% turbulence intensity at the inlet considering isotropy, AR=1.00

5.3.1.2.3 Mean pollutant concentration fluxes

As stated during the AR=0.50 pollutant fluxes study, with the next maps and contours presented we can visualize which are the zones of this street canyon's configuration with highest pollutant fluxes, depending on the concentration of the gaseous substance and the fluctuating velocities in X and Y directions.

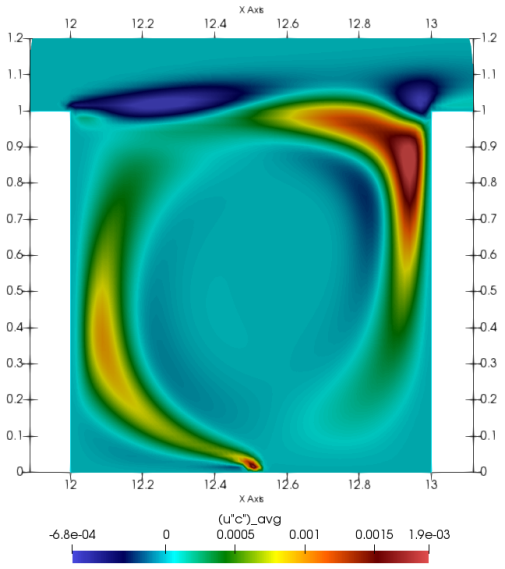

Figure 5.34: Dimensionless mean streamwise pollutant flux, AR=1.00

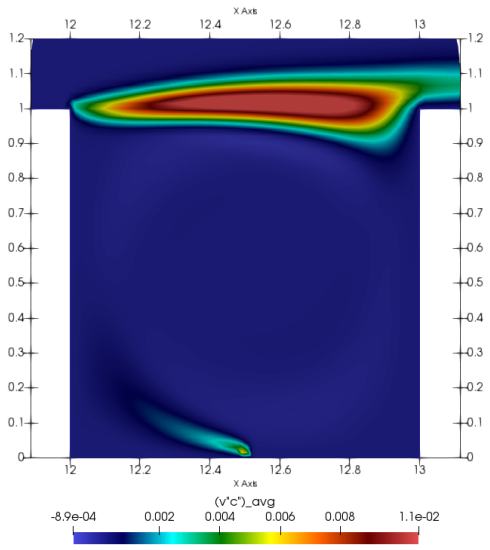

Figure 5.35: Dimensionless mean vertical pollutant flux, AR=1.00

Different from the 0.50 aspect ratio street canyon, when AR=1.00 the pollutant fluxes among all the leeward wall are quite weak until roof-level. In there, as happened before, the maximum fluxes occur having the highest value of vertical pollutant flux at leeward roof-level. This peak shows us the point that governs the pollutant removal of these street canyons. On the other hand, the pollutant fluxes far from the free-stream are almost unnoticeable.

5.3.1.3 AR=2.0

Finally it is time to talk about one of the worst study cases regarding to pollutant removal in street canyons. With high aspect ratios, where the height of buildings is larger than the street canyon width, the pollutant's highest part is trapped inside the canyon because of

the flow structure. As we will see in the presented maps and streamlines, the two primary recirculations generated in the vertical direction, one clock wise and another counter-clock wise rotating, generate a completely different airflow, compared to the previously seen. During the analysis of the obtained post-processing material it is easy to appreciate the higher level complexity of this flow structure.

5.3.1.3.1 Residuals

As we have done in previous chapters, the residuals of the simulation carried out for the AR=2.00 study are presented. This is important to take into account as it indicates if the solution has converged or not.

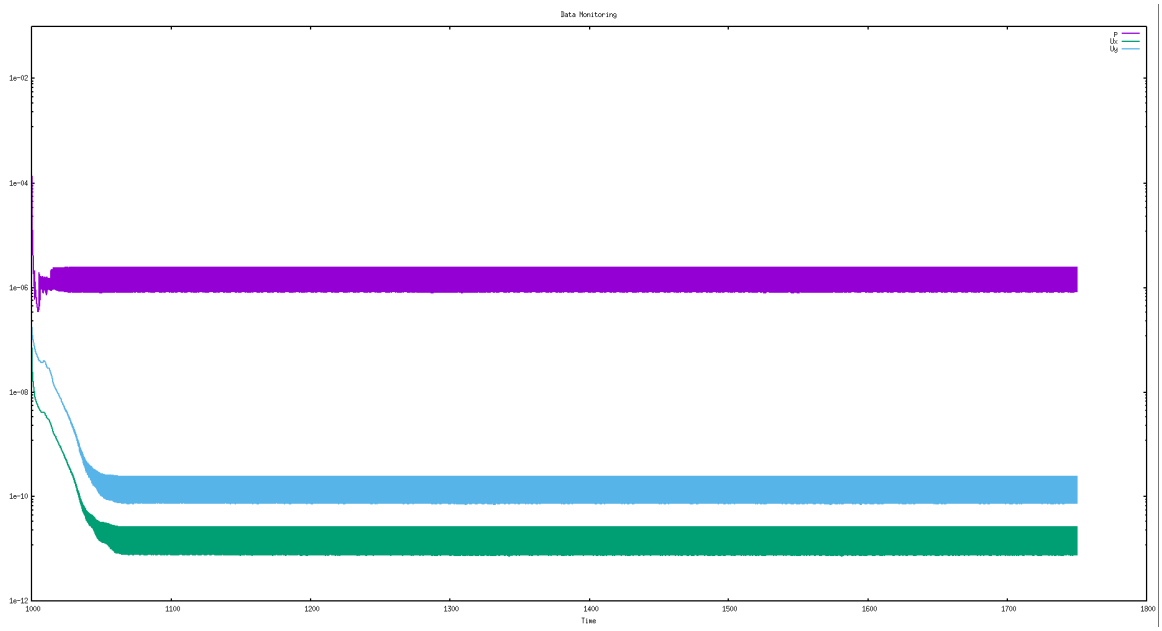

Figure 5.36: Residuals, AR=2.00

The pressure has converged at a value of $1 \cdot 10^{-6}$, while the velocity in X and Y direction components have done it at a value around $1 \cdot 10^{-10}$. All these results show a really good convergence in all the variables computed and the convergence has been reached after about 50s of simulation, what means that by using a time-step of 0.005s it is after 10000 iterations. It is also important to notice that the simulation run-time starts at 1000s seconds because we have used previously converged values of pressure and velocity.

Moreover, the *CourantNumber* of the simulation has a maximum and mean value of 0.68 and 0.20, respectively. This mean value is really good for performing a simulation as by being under the unit we ensure that there will be no instabilities.

5.3.1.3.2 Velocity maps

As the AR=2.00 velocity maps have not been already shown, we are doing it now. In order to maintain the buildings' height at 1.00m, to obtain the desired aspect ratio we have reduced the street canyon width to the half. By using this configuration we have nine consecutive street canyons whose height doubles the width. As after the suction bubble, generated by the free-stream airflow's collision with the first building, the flow starts to stabilize after the third street canyon, we have chosen the fifth one to perform our study.

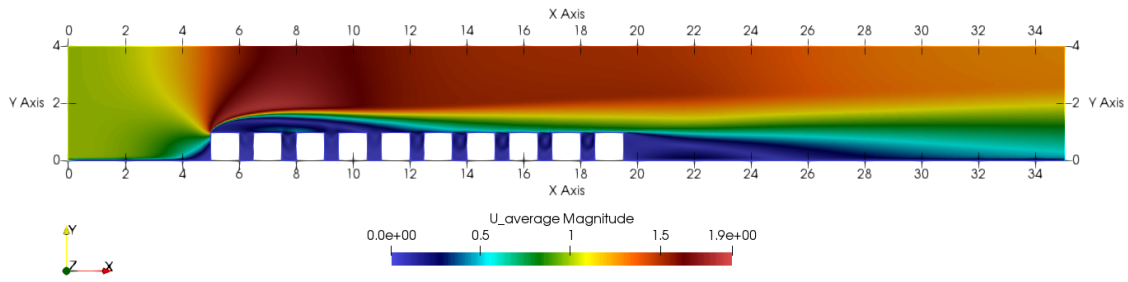

Figure 5.37: 2D average velocity map of the complete domain, AR=2.00

The general flow structure has no much difference compared to the previous maps, for this reason we are just moving on and presenting the detail views of the fifth street canyon.

As expected, because of the narrow street canyon, the average magnitude of vertical velocity and its horizontal component have very low values. The most useful maps to be analysed are the ones that show the vertical component of velocity. As will be seen when studying the streamlines of this flow, two primary recirculations are generated, which are counter-rotating. This creates a flow reversal in the mid-level of the canyon, approximately at y/H=0.50. For this reason we can clearly appreciate, see *Figure 5.41*, a positive vertical velocity region at the leeward and a negative one at windward sides of the canyon, respectively.

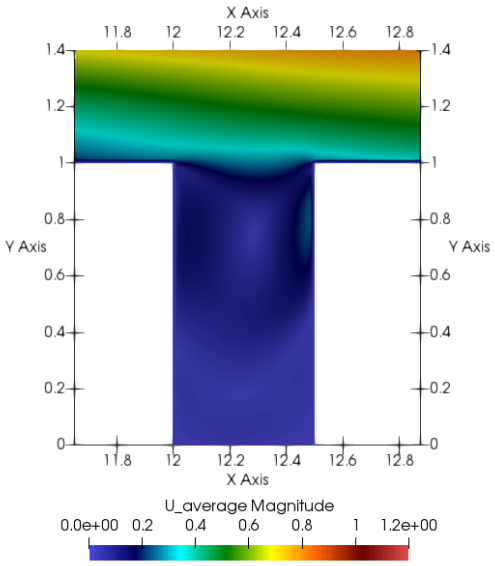

Figure 5.38: 2D average velocity map of the fifth street canyon, AR=2.00

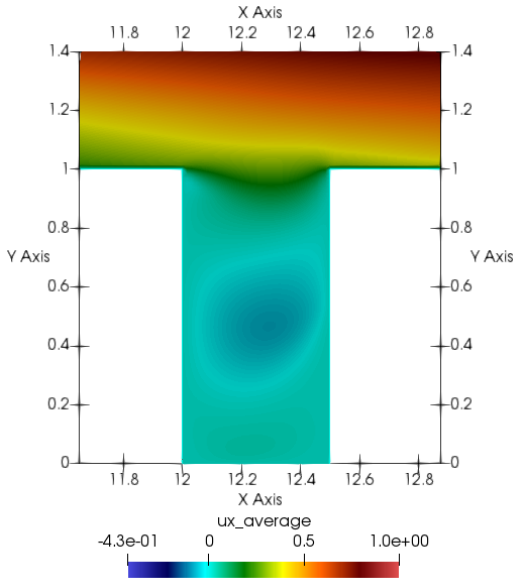

Figure 5.39: 2D average X direction velocity map of the fifth street canyon, AR=2.00

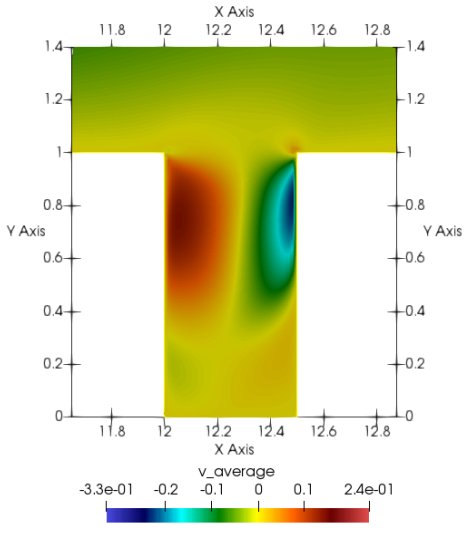

Figure 5.41: 2D average vertical velocity map of the fifth street canyon, AR=2.00

Having a look at the complete domain, *Figure 5.40*, the repetition pattern from the fifth canyon on is clear.

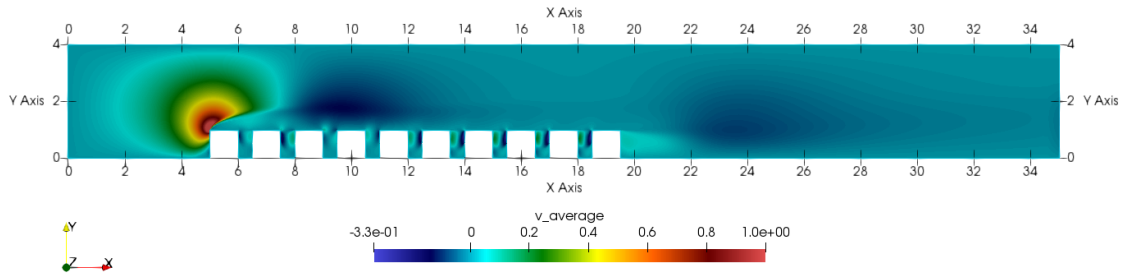

Figure 5.40: 2D average vertical velocity map of the complete domain, AR=2.00

5.3.1.3.3 Pressure maps

Regarding to the pressure distribution, we can appreciate the suction bubble after the stagnation point at the top of the first building. This generates the mentioned flow disturbance that starts to be stabilized after the third street canyon and at the fifth we can consider it stable.

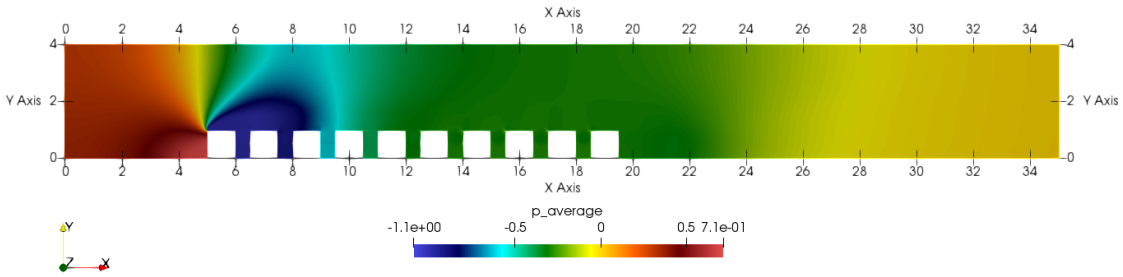

Figure 5.42: 2D average pressure map, AR=2.00

5.3.1.3.4 Streamliens

The most complicated flow structures, previously mentioned, can be visualized by using the dimensionless stream-functions calculated from the mean velocities. As the stream-functions of the complete domain have no much difference compared to the previous studies with other aspect ratios, we are just presenting the recirculation patterns generated in the fifth street canyon.

The two vertical aligned primary counter-rotating recirculations are exhibited. The

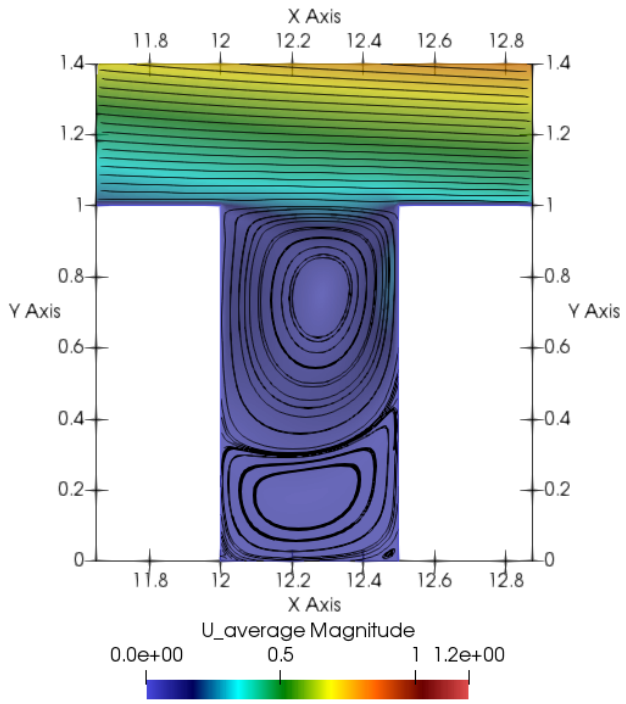

Figure 5.43: Dimensionless stream-functions in the fifth street canyon, AR=2.00

first one is generated at roof-level and, as the free-stream flow suggests, is clock-wise rotating. This vortex is the biggest one of the canyon and takes up almost the 70% of the street canyon's surface. At the same time, this forms a lower counter clock-wise rotating recirculation.

At ground-level, as happened for AR=0.50 and AR=1.00, two secondary counter clock-wise rotating recirculations are generated at leeward and windward, respectively. It would be expected, from previous LES simulations performed [62], to have a secondary recirculation at windward roof-level, but using this RNG k-epsilon model we have not been able to capture it. The reason of it may be the near-wall treatment chosen or the length scale limitation of these turbulence models, adding the possible mesh refinement need.
As happened in all the previous configurations, the flow structure inside the street canyon is isolated from the free-stream flow, as at roof-level we can see that the recirculation is not mixed with the main flow.

5.3.1.3.5 Mean pollutant concentration maps

It is important to have one thing in mind, the pollutant distribution and transport for AR=2.00 is completely different from the previously seen cases. As there are two primary recirculations and the pollutant source is located in the center of the street canyon at ground-level, firstly pollutant follows the lower primary recirculation and then it is transported toward the windward of the building. When the reversal flow point is reached (the point where the two primary vortexes coincide), a part of the pollutant moves to the upper recirculation and the other keeps in the lower one and reaches the leeward side of the building. As the two primary recirculations are isolated one from the other, the turbulent pollutant transport is not only important in between the upper recirculation and the free-stream, but also in between the lower and upper recirculations. As the turbulent velocity fluctuations are not high and the turbulent transport depends on them, as expected, the pollutant removal in this configuration is the lowest among all the studies. As it can be appreciated in *Figure 5.44*, the pollution levels at ground level are high and the pollutant removal is almost unnoticeable.

In order to appreciate the evolution of pollutant diffusion and transport throughout the street canyon, we present a sequence of mean pollutant concentration maps with gradually lower scales. By doing it we can see the different regions where pollutant is present and at which magnitude, clearly appreciating the mentioned "S" path that follows the inert gaseous substance.

Focusing on the very low scales used to obtain from *Figure 5.44* to *Figure 5.47*, we can clearly visualize and understand the low levels of pollutant removal and ventilation that the flow in street canyons of an AR=2.00 generates. As there has been used a boundary condition which defines a maximum pollutant concentration of 1.00 (dimensionless) at the pollutant source, we can conclude that the pollutant concentration that arrives to the roof-level of the canyon is two magnitude orders inferior.

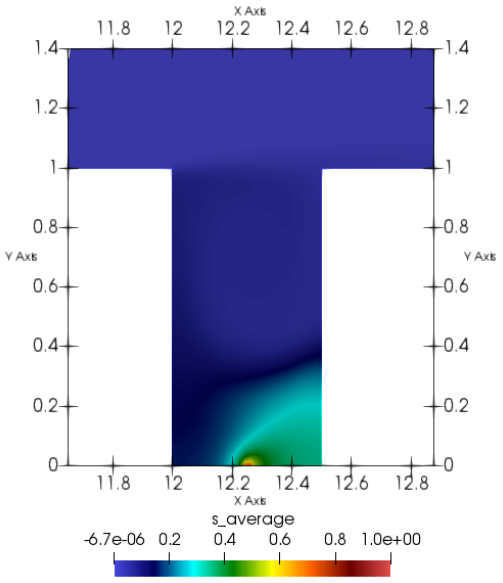

Figure 5.44: 2D mean pollutant concentration map of the fifth street canyon, AR=2.00. Scale 1

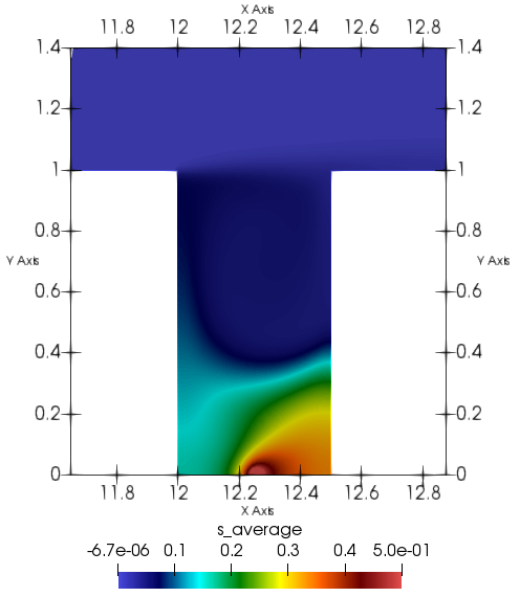

Figure 5.45: 2D mean pollutant concentration map of the fifth street canyon, AR=2.00. Scale 2

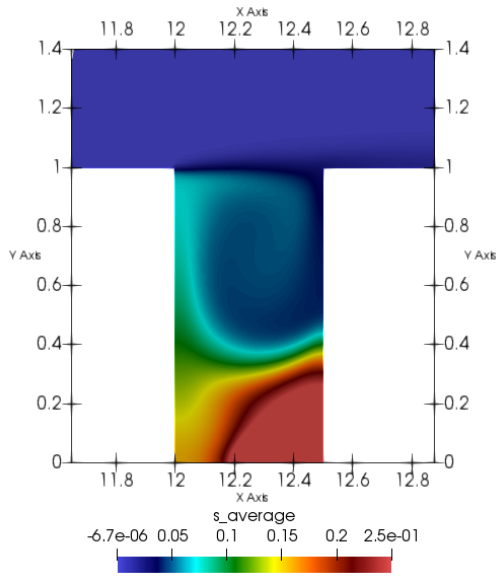

Figure 5.46: 2D mean pollutant concentration map of the fifth street canyon, AR=2.00. Scale 3

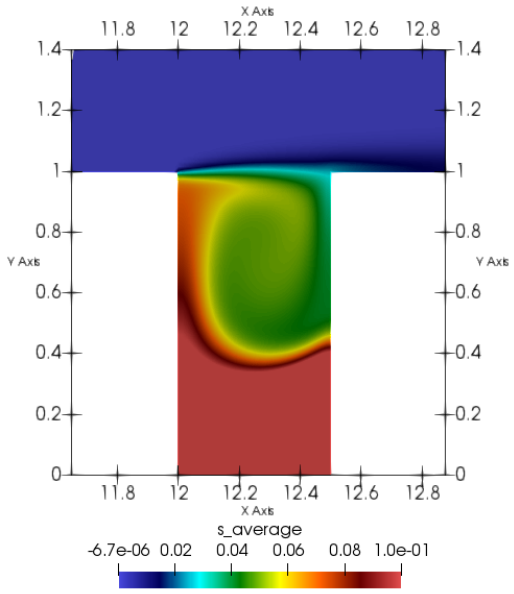

Figure 5.47: 2D mean pollutant concentration map of the fifth street canyon, AR=2.00. Scale 4

Finally we can present the pollutant distribution in the complete domain, information that will be used during the discussion in order to study the pollutant transmission of pollutant from one canyon to the other which are down-stream.

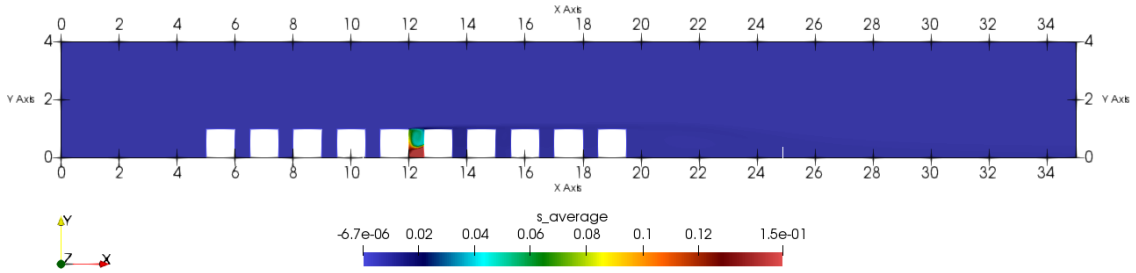

Figure 5.48: Dimensionless pollutant concentration of the complete domain, AR=2.00

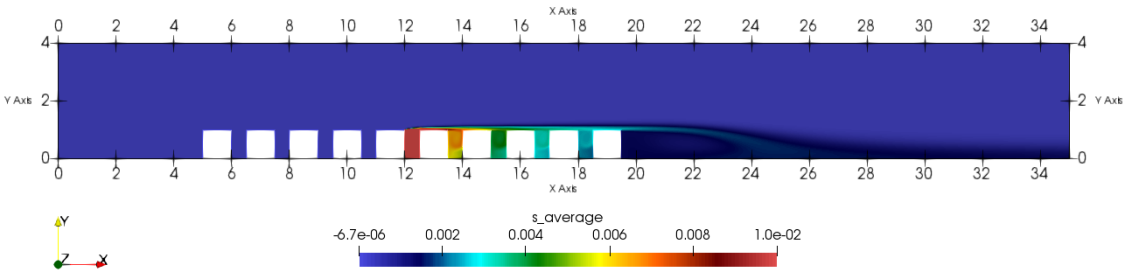

Figure 5.49: Scaled dimensionless pollutant concentration of the complete domain, AR=2.00

In *Figure 5.48* and *Figure 5.49* it is clearly shown how the pollutant retention in AR=2.00 street canyons is almost total. It has been necessary to scale the pollutant color bar for appreciating the pollutant transmission from the source canyon to the others.

5.3.1.3.6 Contours

The vertical velocity, the mean pollutant concentration and the turbulent kinetic energy are three key parameters to be studied using contours, as we obtain isosurfaces that give us a good understanding about the pollutant distribution, the parts where it is more likely to be removed and the strength of the velocity fluctuations, which are the main way of pollutant transport with the isolated flow found in these street canyons.

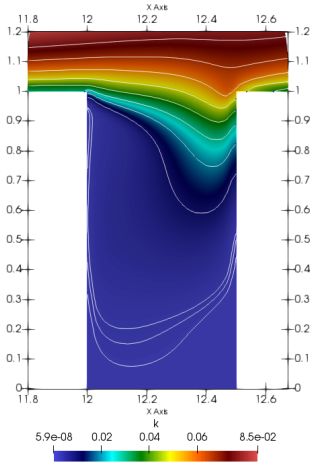

Figure 5.50: Turbulent kinetic energy contour, AR=2.00

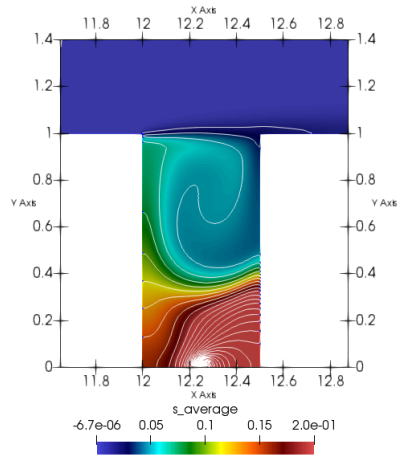

Figure 5.51: Mean pollutant concentration contour, AR=2.00

The turbulent kinetic energy contour map gives us the same information as mentioned for the other aspect ratios. On the other hand, the vertical velocity and mean pollutant concentration contours are quite different compared to the others. Both of them describe the exact situation that we commented when analysing the maps.

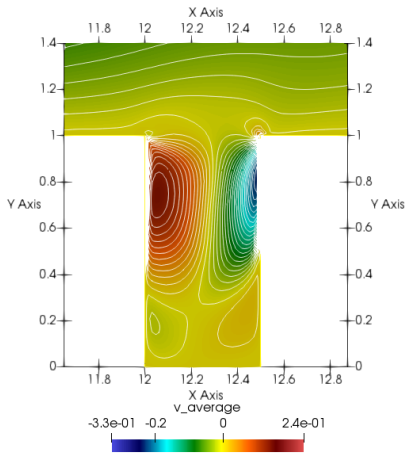

Figure 5.52: Vertical velocity contour, AR=2.00

Figure 5.51 depicts how the pollutant starts at ground-level, it is driven to the windward

side of the buildings and then a part keeps in the lower recirculation and another is transferred to the upper one. It can be appreciated how the point where more pollutant is removed is the leeward roof-level.

5.3.1.3.7 Mean pollutant concentration fluxes

This post-processing section ends with the analysis of mean pollutant fluxes for the AR=2.00 street canyons.

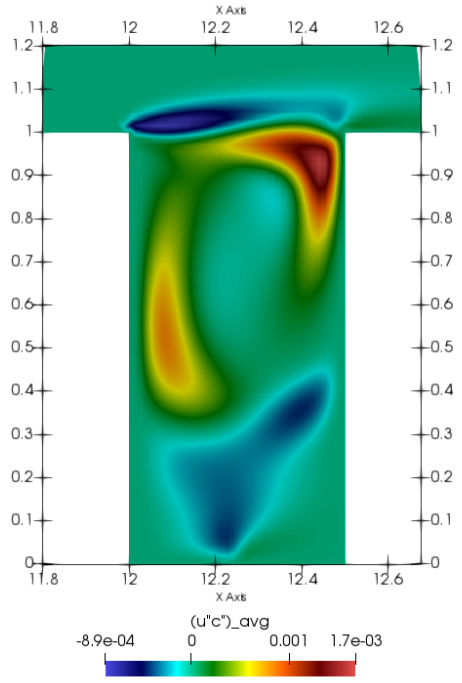

Figure 5.53: Dimensionless mean streamwise pollutant flux, AR=2.00

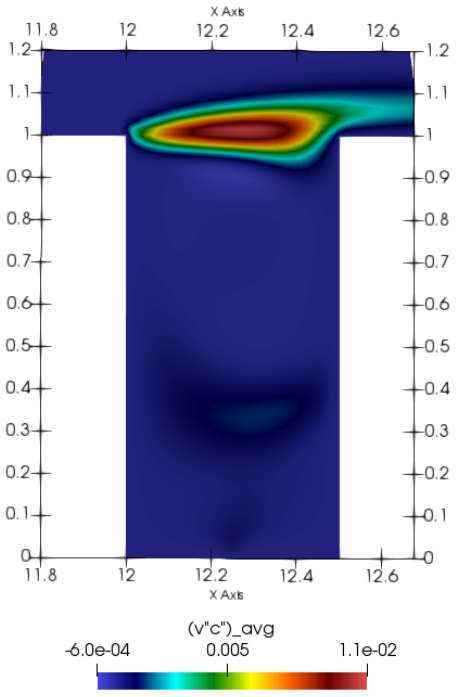

Figure 5.54: Dimensionless mean vertical pollutant flux, AR=2.00

During the whole thesis we have been stating that AR=2.00 street canyons have a completely different flow structure compared to the other cases. Regarding to the mean pollutant fluxes it is not different. In *Figure 5.53* and *Figure 5.54* we can appreciate how the highest pollutant flux levels are found at ground-level and in the connection between the two primary recirculations. This is generated because the turbulent transport in between recirculations is key for surpassing the boundary of the lower vortex and move tot the upper one, where, despite of the obvious lack of ventilation, a part of the pollutant will finally join

the free-stream. For this geometry configuration the pollutant fluxes also follow the flow recirculations, and different from other aspect ratios we have that the vertical pollutant flux maps shows a middle zone where higher levels of turbulent flux are given, because of the presence of turbulent transport in between recirculations. During the *Validation* section we will talk about it and in the *Appendix* the LES results of previous studies will be presented

5.3.2 Validation

Now that all the results have been presented, it is time to do the validation of them by comparing all the plots with previous studies done. To do that we are using three papers as main information sources: the study done by *Xian-Xiang Li, Chun-Ho Liu and Dennis Y.C. Leung*[13] in 2005, called *"Development of a $k-\varepsilon$ model for the determination of air exchange rates for street canyons"*; this study is so interesting to be used as a 2D RNG k-epsilon model is used and the post-processing resources obtained are the same as chosen for this thesis. Moreover, two additional sources are used where the comparison in between RANS simulations and LES ones is carried out, by using the same geometry. These are: *"On the prediction of air and pollutant exchange rates in street canyons of different aspect ratios using large-eddy simulation"*[19] and *"Large-Eddy Simulation of Flow and Pollutant Transport in Street Canyons of Different Building-Height-to-Street-Width Ratios"*[11].These last two papers are also interesting because of the different data analysed and the emphasis on the pollutant distribution.

If we analyse and compare the vertical and horizontal velocities in street canyons of the different studied aspect ratios, it is clear that the level of precision is high. Using the information given in [13] we appreciate how for all aspect ratios, the vertical and horizontal velocities general structures are the same, having captured some interesting phenomena such as all the gradients generated at windward roof-level or the secondary recirculations of AR=1.00. On the other hand, while comparing our RNG k-epsilon model vertical velocity contours with the reference, we can appreciate how in our study the two different velocity sides (upward and downward) of the lower primary recirculation are more defined and differentiated.

Regarding to the spatial contours of dimensionless mean stream functions, again the level of precision is high but with the same main differences as we have been noticing before. Something interesting to mention is the difference in between the secondary recirculations

at ground-level size plotted by us and the ones obtained in [13]. The windward recirculation obtained in the literature goes from -1 to 0 horizontally, while our goes from 12 to 12.3 approximately. In general, for the three aspect ratios, the secondary recirculations have been under-predicted, as expected, because the use of an RNG k-epsilon model and because of the wall treatments; it creates an under-prediction of mean velocities at ground and roof-level that can affect to the secondary vortexes strength. Additionally, the secondary recirculations found at leeward roof-level in the LES simulations have not been found by our study, neither in the RANS simulation carried out in [13].

When it comes to the turbulent kinetic energy contours there is more difference detected as in here some key factors take part:

- Reynolds stress tensors (velocity fluctuations): as detected in *Chapter 4*, the highest level of inaccuracy while performing the validation was at the second order terms. As turbulent kinetic energy is directly calculated by using them, this is important to take into account as it has been shown that RANS models are not the best choice to compute second order terms.
- Turbulent kinetic energy boundary conditions: apart from the handicap of using this kind of method for solving the Navier-Stokes equations, the boundary conditions regarding to k, in the inlet but also in the walls, affect to the final solution.
- Mesh: the grid size is a key factor that needs to be taken into account as it generates error compared to meshes with almost ten times more cells as in the mentioned studies.

After having mentioned the most relevant factors which mainly affect the Reynolds stresses, it is time to talk about mean pollutant concentration distribution. Before doing the validation of it, it is important to mention that in isolated flows, like the studied, the turbulent transport is the most important way of pollutant transport and it is directly related to the previously mentioned issues.

Figure 5 in [11], shows the spatial variation of dimensionless mean pollutant concentration in street canyons of AR=0.50, AR=1.00 and AR=2.00, respectively. If we compare them with the mean pollutant concentration contours obtained after our simulations and post-processing have been done, the general distribution is achieved but some differences

are shown. All these differences were expected as, apart from the turbulence, there is also a possible discrepancy regarding the pollutant modelling. There are some parameters, such as the molecular diffusion coefficient and the initial value of pollutant concentration in the pollutant source, that may differ from the literature mentioned. The key fact that makes these values noticeably different is the way how the pollutant source has been modelled: in the literature used for validating our results the source has been taken as a volumetric source with a certain flux. On the other hand, in this thesis the pollutant has been included in the *Dirichlet* boundary condition of the $0.045m^2$ cell, where pollutant concentration has been configured with an initial fixed and uniform value of 1.00. These discrepancies make our study appropriate for doing a comparison in between our own results, among the different AR canyons, and to compare the general pollutant distribution, but not for conducting a deep analysis and contrasting our results directly with the literature.

Finally, for concluding this validation section, we can state that the pollutant flux values, obtained after our RNG k-epsilon simulation, differ from the ones showed in [11]. The reasons are the same as mentioned during the mean pollutant concentration study, as this values just depend on the fluctuating velocities and pollutant concentration fluctuations. Despite of the general differences, the obtained maps and contours allow us to identify with precision the zones where the pollutant fluxes are high, which means that by focusing on the vertical flux we can visualize the roof-level zones with more pollutant removal levels. Anyway, some of the resources used in this section will be included in the *Appendix* of this thesis. Despite of not having obtained the exact results, in the mean pollutant concentration sections presented we have reached a good level of detail and precision, as some key factors for the pollutant removal from the canyons have been found. Some of these factors are the high turbulent fluctuations found at roof-level for the three aspect ratios, the fluctuations originated after the pollutant is generated at the source. the noticeable pollutant flux detected where the two recirculations are united in AR=2.00, among others. All these phenomena can be observed and validated with the data attached in the *Appendix*.

Chapter 6

Discussion

In this section all the results presented in *Chapter 4* and *Chapter 5* are discussed in order to extract all the valuable information that the maps, contours, streamlines, ... offer us but that need a further physical interpretation. After putting in common the RNG k-epsilon results, from simulations of AR=0.50, AR=1.00 and AR=2.00, we can conclude and understand how the flow structures and pollutant transport are in our cities' street canyons. To improve the understanding of the mentioned phenomena and corroborate our statements we include a new parameter in our study: the air exchange rate, *ACH*.

Air exchange rate is very useful when it comes to the study of air ventilation and pollutant dilution in street canyons, for this reason in this section it is explained in order to ensure a good understanding of the concept. The first thing that we have to take into account is that, as has been showed using the streamlines in the three studied cases, the vortexes generated in the street canyons are isolated from the free-stream. That means that if we obtained the data along an horizontal line at roof-level, the mean vertical velocity would be zero.

Despite of being zero the mean vertical velocity, the roof-level fluctuating vertical velocity is not zero and for this reason it is the main responsible of pollutant transport and dispersion. Because of this phenomenon, caused by turbulence, the pollutant generated in one street canyon can move downstream and barely ventilate and renew the airflow in the street canyon.

As we have performed a RANS simulation, the fluctuations computed using an averaged method are expected not to be precise and exact, but representative for comparing the results in between our three different aspect ratio studies. The needed information to be

obtained using *OpenFoam* is the one regarding the vertical velocity fluctuations at roof-level $\overline{(v''v'')}_{y=1.00}$, which in our software are modelled as $R_average$: 1, different from $Uprime2Mean\_YY$ which is the "solved" part of the fluctuations, and are obtained by using a plot over a line. With this method we can get the necessary information for integrating the fluctuating vertical velocity along the ventilation area *(A)* (which is calculated as $A = wL$, being w the street canyon's width and *L=1.00m* the length of a 2D canyon). Applying the *Mass conservation principle* in the control volume of one street canyon, if we integrated both the positive and negative fluctuating velocities, we would obtain a total air exchange rate of zero. For this reason we are just focusing on the positive part, ACH_+, which is the air removal from the canyon, as the Y direction velocity vector has the same direction as the normal surface vector of the air ventilation area (both pointing outside the canyon). The negative air exchange rate, ACH_-, is the free of pollutant air that comes from the free-stream and has the same value as the air removal from the street canyon.

As we are considering the canyon's transient air exchange is divided in two processes, one for the inflow and another for the outflow in a 2D street canyon with averaged results, the expression that governs this simplified air exchange is the following:

$$\overline{ACH_+} = \overline{ACH_-} = \frac{1}{2}\int_A (\overline{v''v''})^{\frac{1}{2}}\, dA \tag{6.1}$$

For obtaining the non-dimensional values we can directly use the volume of the street canyon and the reference time scale:

- Volume: $V = HwL$
- Reference time scale: $T = H/U_{ref}$ being $U_{ref} = U_{inlet}$

The only value that changes depending on the AR of the case studied and that it is not always the unit, is the street canyon's width, w. As the final expression obtained is $\frac{ACH_+}{\frac{HwL}{T}} = \frac{ACH_+}{w}$ for AR=0.50 the values are doubled and for AR=2.00 are reduced to the half. This information given by the air exchange rates coincides with the pollutant flux levels seen during the post-processing sections.

Applying all this concepts to a *Matlab* code, we have finally obtained the values of X/w vs ACH_+. All these plots help us discuss all the results presented in the previous chapters and corroborate the physical interpretation previously given to the maps.

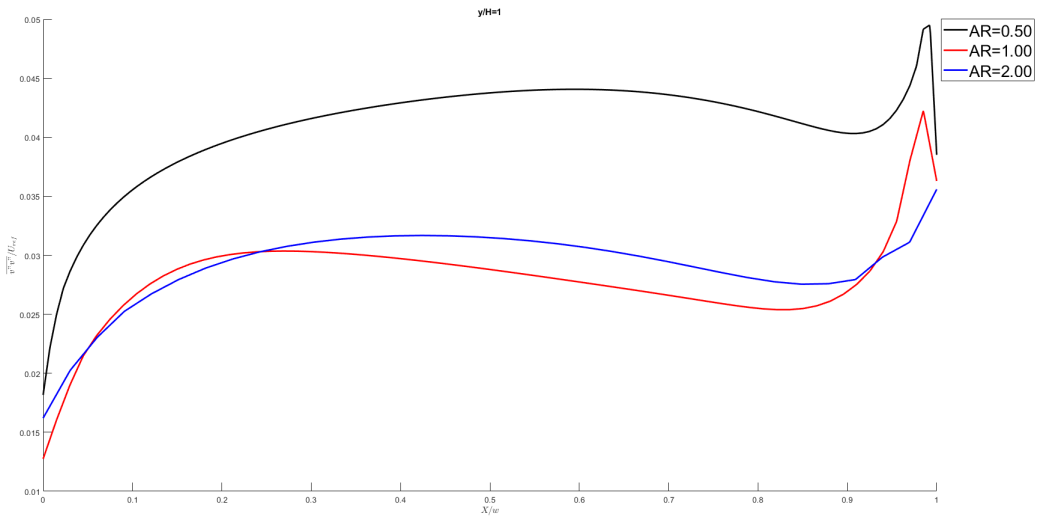

Figure 6.1: ACH_+ comparison along the 2D street canyons of AR=0.50, AR=1.00 and AR=2.00

In here we can see how the integration has just been done of the positive vertical fluctuating velocities and the X axis has been made dimensionless in order to perform a more precise comparison. It can be appreciated how the highest vertical fluctuations are found at windward side and the distribution for AR=1.00 and AR=2.00, are quite similar and noticeably lower than the AR=0.50 case. This is completely expected as we have already commented the relation in between the AR and the pollutant removal from the street canyon, the lowest the aspect ratio, the highest pollutant removal levels. All of this is summarized in *Table 6.1*:

Aspect ratio *(AR)*	**ACH/(HwL/T)**	
	$RNGK-\varepsilon$	**LES**
0.50	0.1010	0.1200
1.00	0.0835	0.0500
2.00	0.0852	0.0500

Table 6.1: Dimensionless air exchange rate (ACH) comparison in between this thesis RNG k-ε obtained results and the LES simulation from [13]

The results obtained using our RNG k-ε configuration are quite acceptable compared to

the LES. The difference in between results for AR=1.00 was expected as during the validation section in *Chapter 4*, for the AR=1.00 street canyon without pollutant source, we found that, despite of having obtained very precise results regarding to the velocity profiles, the second order fluctuating terms were over-predicted. This discrepancy is generated, apart from the possible improvements that could be implemented in the turbulence configuration in *OpenFoam*, by the error or lack of accuracy that generates the computation of fluctuations by using a Reynolds Averaged model and the possible need of a mesh refinement for a better computation. Because of this difference, the results showed in *Figure 6.1* are just used as a resource for comparing our own results among the three different street canyons configurations. If we changed some parameters such as the turbulent kinetic energy at the inlet, the mesh refinement, the schemes and solvers, etc. the precision of these results could be improved.

Another interesting plot used for improving this discussion is the comparison in between the vertical mean velocities at roof-level. We can contrast the maps of vertical velocities and the obtained data.

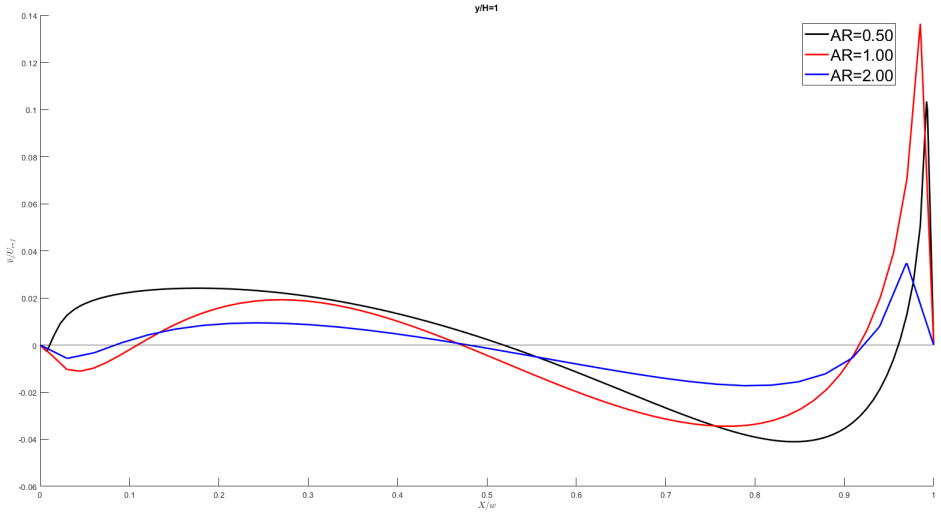

Figure 6.2: Vertical velocity comparison along the 2D street canyons of AR=0.50, AR=1.00 and AR=2.00

Despite of the integral of these velocities along the flow exchange surface is null, this

gives us a solid idea about the zones with inflow and outflow and where is the highest velocity.

Using these plots combined with the *vertical velocity maps*, *mean pollutant concentration flux maps* and *streamlines* from previous chapters, it is obvious that there is a relation in between street canyons' aspect ratio and the level of pollutant removed from them. When analysing the ACH plots we can appreciate the similarity in between the distribution of air exchange for AR=1.00 and AR=2.00. On the other hand, AR=0.50 is different, having an air exchange rate that almost doubles the other two.For the three cases there is a peak of air exchange rate at windward level, coinciding where the highest vertical velocity levels are also detected. After this analysis and looking at *Table 6.1* we can conclude that the ACH is an important value regarding to the pollutant levels and combined with the mean pollutant concentration maps we can state that the pollutant removal decreases when the AR increases.

The mean vertical pollutant concentration flux plots corroborate these statements: the pollutant removal of an AR=2.00 canyon is considerably lower than for AR=0.50 and the highest value is found at leeward; in [11] the pollutant retention in street canyons of aspect ratios of 0.50, 1.00 and 2.00 is quantified , and the calculated values are 95%, 97% and 99%, respectively.

Despite of what could be expected by looking at *Figure 6.1*, the biggest part of the pollutant is removed by turbulent transport at leeward. The peak of velocity fluctuations found at windward are caused by the increase of turbulent kinetic energy generated by the mechanical wind shear.

Moving on to the vertical velocity plots and maps, both of them give us the same information: there are two differentiated zones, one with positive and another with negative velocity, governed by the primary recirculations. There are flow disturbances at roof-level level, which are located at corners and the velocity and fluctuations peaks found are generated by the interference of the flow with the buildings. This produces a flow deviation, that at the same time is the main cause of the TKE increase, and consequently of the velocity fluctuations, at this point.

We are finishing this discussion talking about *mean pollutant concentration*. The reason why it is a good way to finish this discussion is because it summarizes all the previously

mentioned phenomena explained in this section and, at the same time, allows us to visualize the effect of the two primary recirculations in the pollutant transport of an AR=2.00 street canyon, which is the most different and complicated to study case. Pollutant concentration distribution is directly affected by all the physics involved in the street canyons' airflow: velocity and pressure, diffusion coefficients, turbulent transport, secondary recirculations, primary vortexes... and many other factors that have influence in the flow structure.

One important aspect to take into account is that for AR=0.50, because of the under-prediction of the secondary recirculations magnitude (present for the three aspect ratios), the leeward secondary recirculation does not cover the street canyon to the mid-part, where the pollutant source is, but in the results obtained by LES simulations it does. Despite of it, for an AR=0.50 street canyon the pollutant follows the primary recirculation moving to the leeward side, then, at roof-level via turbulent transport, a part of it joins the free-stream and it is removed from the canyon at leeward. The secondary recirculations act like a low-pollutant concentration bubbles, specially the windward side one. If we look to the complete domain, it is clear that if the pollutant removal from the source canyon is big, the gaseous substances that arrive to the down-stream canyons is also greater than for bigger aspect ratios.
Regarding to the primary vortex's center, it is located approximately at $X = 13.3m$ and $Y = 0.6m$, an expected result as the geometry of the canyon and the flow direction originate this displacement. This produces the windward secondary vortex's dimension reduction, which is considerably smaller than the leeward one.

For AR=1.00 we have performed the study necessary to appreciate the importance of turbulent transport when it comes to pollutant diffusion and distribution. The higher the diffusivity is, the higher the street canyons' affected part by the pollutant. Again, the pollutant follows the main vortex and at leeward roof-level a part of it leaves the canyon thanks to the vertical velocity fluctuations, as seen with the ACH plot. The pollutant transport to the other canyons is lower than for an AR=0.50, as the air exchange rate is also lower, and the primary recirculation is approximately centered in the canyon at $X = 12.5m$ and $Y = 0.50m$.

Finally the analysis of street canyons with an aspect ratio of 2.00 is conducted. We have mentioned many times the difficulty that the flow structure of these canyons add to the study. This is mainly caused by the two primary recirculations created, one upper vortex which is

clock-wise rotating and another lower counter-clock wise rotating vortex. As the pollutant source has to follow an "S" shaped path and has to go from one isolated recirculation to another, just via turbulent transport and diffusion, the levels of pollutant that arrive at roof-level are so low. This is also corroborated by the vertical velocity fluctuations and vertical velocity plots, which show that the air exchange at roof-level is very insignificant compared to the lower aspect ratios cases.

Additionally, as the lower recirculation is counter-clock wise rotating the pollutant at ground level is transported to the windward wall and then, a part goes to the upper vortex and the other part continues in the lower one. This generates a massive pollutant concentration at pedestrians-level, reducing the air quality.

Regarding to the transport of pollutant from one canyon to another, as expected is almost nonexistent because of the lack of air ventilation. The vortexes locations are: $X = 12.25m$ and $Y = 0.20m$ for the lower recirculation, $X = 12.30m$ and $Y = 0.75m$ for the upper one.

Now that all the results obtained from our RNG k-ε simulation are presented and discussed, it is obvious the effect that aspect ratio has on airflow and pollutant transport in street canyons. In these flow structures, where the recirculations generated inside the canyons are completely isolated from the free-stream, we notice the big effect and importance of turbulence in pollutant transport, regarding to the pollutant turbulent transport originated by the velocity fluctuations at roof level and between recirculations for AR=2.00 canyons.

Chapter 7

Conclusion

After having performed all the process to study the airflow and pollutant transport in urban street canyons by using a *RNG* $k-\varepsilon$ model, it is time to obtain some relevant conclusions, which can be the basis for future possible study improvements and development of the case. This thesis has covered all the steps necessary for conducting a CFD simulation, from the geometry and mesh creation to the validation and discussion of the results, allowing us to have a global but precise vision of the whole process and of the physics behind the pollutant transport in our cities, in particular of a flow with $Re = 12000$ and $Sc = 0.72$.

First of all it is important to mention that all the previsions and general results, expected after having performed a deep study of the street canyon's airflow state of the art, have been corroborated. It has been shown that aspect ratio (AR) is a determining factor when it comes to the airflow structure and pollutant removal from street canyons. We have confirmed that for all the three studied aspect ratios the recirculations inside of the canyons are isolated from the free-stream, which make it difficult to ventilate and remove the inert gaseous pollutants generated by cars.

Apart from it, we have shown how the aspect ratio affects the vortexes generated, going from one primary recirculation, for canyons whose aspect ratio is 0.50 and 1.00, to two vertical counter-rotating primary recirculations in a canyon of $AR = 2.00$. Moreover, the secondary recirculations generated at ground-level have also been detected and studied. This first phenomenon can be directly translated to a higher level of pollutant removal for low aspect ratios and an almost complete pollutant retention in street canyons with a high aspect ratio; this is because in isolated flows the main way to remove pollutant is via the turbulent transport generated by the velocity fluctuations. In street canyons, with low

velocities and turbulence levels, the fluctuations are not high, and if we add more than one primary recirculation forcing the pollutant to follow an $S - shaped$ path, the situation gets worse. All of that leads to a retention of approximately the 95%, 97% and 99% of the pollutant in street canyons with an aspect ratio of 0.50, 1.00 and 2.00, respectively. This information, as we do not dispose of the necessary resources, has been extracted from [11] but carefully evaluated and contrasted with our own results. It leaves an open path for further studies.

Aspect ratio also affects the zones of the street canyon which are more affected by the pollutant: it has been shown that for $AR = 0.50$ and $AR = 1.00$, the path done by the pollutant is so similar, as it follows the primary recirculation, increasing the pollutant concentration at leeward, mainly. On the other hand, for $AR = 2.00$, the pollutant is mostly concentrated at windward ground-level, worsen the air quality. For all of the studies the point where the highest part of the pollutant has been removed from the canyon is the leeward roof-level. These interpretations and by having analysed the mean pollutant concentration maps, pollutant concentration flux maps, air exchange rate plots, etc. drive us to find coherent and logic the mentioned pollutant retention percentages.

Additionally, the effect of diffusion in gaseous pollutants transport has been appreciated after performing a comparison in $AR = 1.00$ canyons: a simulation without turbulent diffusion and another with it have been performed. There is no doubt about the important role that diffusivity has in pollutant transport throughout street canyons, as when increasing the diffusion coefficient, the space polluted in the source canyon and the affectation of the ones which are down-stream increase substantially.

Finally, this thesis could not be finished without talking about model chosen for solving the *Navier-Stokes* equations. *RNG* $k - \varepsilon$ is a $RANS$ turbulence model that has shown good results in solving the flow around street canyons, but which has many drawbacks. It is a fact that we have been able to obtain really good velocity results compared to the LES and experimental ones showed in the literature. On the other hand, as expected, using a *Reynolds Averaging* model for solving velocity fluctuations is not the best choice. The second order terms, corresponding to the *Reynolds Stress Tensor*, which are crucial for modelling pollutant transport, have been well approximated when collecting data in vertical lines, but are over-predicted at the roof-level horizontal line . This error is not only attributed to the model itself, but also to the model configuration in *OpenFoam*. It is because the

implementation of the model in the software needs a certain level of experience in order to correctly chose the flow and turbulence configuration such as the turbulent kinetic energy and (k) and the energy dissipation rate (ε), the conditions at the inlet, boundary conditions, the mesh refinement, etc. By improving some of these parameters the obtained results might be closer to the experimental and computational data available to validate the case.

This opens a new window and uncountable opportunities for continuing improving and developing this project. The same process followed using a $RANS$ model could be done with a LES, some other aspect ratios could be evaluated, the pollutant exchange rate could be computed *(PCH)* the 3D simulations could be carried out, the building's geometry could be changed in order to increase the similarity of the case with a real street-canyon, we could implement a case with two pollutant sources at ground level representing two car lanes, we could repeat the whole process by using a refined mesh if we had more computational resources, etc. Additionally, as has been mentioned, the possibility to perform the simulations using a steady solver, such as *simpleFoam*, is a good test to do, as it would save computation time and finer meshes could be used with no need to increase the computational resources too much.

In conclusion, the next steps that could be followed are:

- Compute the PCH with the actual mesh and configuration.
- Study the possibility to use *simpleFoam* instead of *pisoFoam* by doing some test simulations with AR=1.00, as we have its initial validation done.
- Study the relation in between the mesh refinement and the results obtained. If a mesh refinement results in a results improvement, repeat the already done process for the other aspect ratios. If despite of the mesh refinement we cannot reach the desired results, improve the case setup, boundary conditions, solvers, schemes, etc.
- Once the desired results are reached and we have all the information validated, some further changes and implementations already mentioned could be done:
  - Change the way how the pollutant source is modelled.
  - Add a second pollutant source and do the study with two symmetric pollutant sources from the street canyon's center.

  - Apply changes in the geometry: not symmetric street canyons, other aspect ratios, add realism to the buildings, etc.

- Once all the improvements and studies using the RANS study and the*RNG k-ε* turbulence model are done, move on to DES and/or LES simulations.

All these improvements drive us to the same point: continue developing and studying a field that concerns all of us and generates great impact, pollution. By now, with the information and knowledge acquired during this thesis, we can state that the best and most feasible action that could be taken in order to improve the air quality in street canyons is the pollutant reduction from the root. It is clear that the levels of ventilation and pollutant removal in urban street canyons are so low, for this reason the most direct and logic step to follow is try to move to clean transport.

Nevertheless, if it did not have the obvious physic, logistic and construction drawbacks, reducing the aspect ratio of street canyons would be a good way to improve the air quality in street canyons. As, by now, it is not feasible, some studies could be conducted for contrasting and observing how the geometry and characteristics of canyons affect to it, without the need to change the aspect ratio.

Bibliography

[1] Area guide: The eixample – time out barcelona. https://www.timeout.com/barcelona/things-to-do/the-eixample, 21/06/2021.

[2] Vista aérea de la ciudad china — foto gratis. https://www.freepik.es/foto-gratis/vista-aerea-ciudad-china_1283809.htm, 21/06/2021.

[3] Definition of leeward — chegg.com. https://www.chegg.com/homework-help/definitions/leeward-8, 21/06/2021.

[4] T. R. Oke. Street design and urban canopy layer climate. *Energy and Buildings*, 11:103–113, 1988.

[5] Flow and turbulence in an urban canyon in: Journal of applied meteorology and climatology volume 50 issue 1 (2011). https://journals.ametsoc.org/view/journals/apme/50/1/2010jamc2525.1.xml, 21/06/2021.

[6] Supratik Banerjee. Compressible turbulence in space and astrophysical plasmas: Analytical approach and in-situ data analysis for the solar wind. page 194, 2014.

[7] Turbulence models: Which should i select for my cfd analysis. https://www.simscale.com/blog/2017/12/turbulence-cfd-analysis/, 21/06/2021.

[8] Turbulence models in cfd - rans, des, les and dns. https://www.idealsimulations.com/resources/turbulence-models-in-cfd/, 21/06/2021.

[9] Combustion Cfd, Aiaa Modeling. Cfd for combustion modeling heinz pitsch and suresh menon georgia institute of technology orlando , fl day 2 : Summary of presentations.

[10] Basics of y plus boundary layer and wall function in turbulent flows — learncax. https://www.learncax.com/knowledge-base/blog/by-category/cfd/

basics-of-y-plus-boundary-layer-and-wall-function-in-turbulent-flows, 21/06/2021.

[11] Mary C. Leung Dennis Y.C. Liu, Chun Ho Barth. Large-eddy simulation of flow and pollutant transport in street canyons of different building-height-to-street-width ratios. pages 1410–1424, 2004.

[12] Dennis Y.C. Liu Chun Ho Lam K. M. Li, Xian Xiang Leung. Physical modeling of flow field inside urban street canyons. pages 2058–2067, 2008.

[13] Dennis Y.C. Leung Xian-Xiang Li, Chun-Ho Liu. Development of a k-ε model for the determination of air exchange rates for street canyons. 39:7285–7296, 2005.

[14] Jordi Gal. Air distribution in street canyons : a cfd study. 2019.

[15] Sandrine Mestayer Patrice G. Sini, Jean François Anquetin. Pollutant dispersion and thermal effects in urban street canyons. *Atmospheric Environment*, 30:2659–2677, 1966.

[16] Liu Jianguo Sang Boyin Zhang Yujun, Jiang Huizhi. Numerical and experimental studies on flow and pollutant dispersion in urban street canyons. *ADVANCES IN ATMOSPHERIC SCIENCES*, 24:111–125, 2007.

[17] Sandrine Mestayer Patrice G. Sini, Jean François Anquetin. Pollutant dispersion and thermal effects in urban street canyons. *Atmospheric Environment*, 30:2659–2677, 1966.

[18] Michael Pavageau, Michel Schatzmann. Wind tunnel measurements of concentration fluctuations in an urban street canyon. *Atmospheric Environment*, 33:3961–3971, 1999.

[19] Dennis Y.C. Barth Mary C. Liu, Chun Ho Leung. On the prediction of air and pollutant exchange rates in street canyons of different aspect ratios using large-eddy simulation. *Atmospheric Environment*, 39:1567–1574, 2005.

[20] R. A Banerjee, T. Christian. Three dimensional analysis of pollution dispersion in street canyon. *World Academy of Science, Engineering and Technology*, 81:863–869, 2011.

[21] A. Chung. Title on the mechanism of air pollutant removal in two-dimensional idealized street canyons: a large-eddy simulation approach. pages 241–253, 2013.

[22] Richard Fuller Christina H. Kumar Prashant Gill Laurence W. McNabola Aonghus Gallagher, John Baldauf. Passive methods for improving air quality in the built environment: A review of porous and solid barriers. *Atmospheric Environment*, 120:61–70, 2015.

[23] R. N. Yataghene M. Fellouah H. Saleh F. Boufadel M. C. Lateb, M. Meroney. On the use of numerical modelling for near-field pollutant dispersion in urban environments - a review. pages 271–283, 2016.

[24] nor Azwadi Che Salim Salim Mohamed Saqr Khalid M. Yazid, Afiq Witri Muhammad Sidik. A review on the flow structure and pollutant dispersion in urban street canyons for urban planning strategies. *Advances in neural information processing systems*, 90:892–916, 2014.

[25] Bernard E.A. Pericleous Koulis Gonzalez-Flesca Norbert Vardoulakis, Sotiris Fisher. Modelling air quality in street canyons: A review. pages 155–182, 2003.

[26] Aspect ratio - wikipedia. (n.d.). retrieved march 29, 2021. https://en.wikipedia.org/wiki/Aspect_ratio, 29/03/2021.

[27] Michael M Kost Karen M Sataloff, Robert T Johns. Oke boundary layer.

[28] Turbulence. (n.d.). https://en.wikipedia.org/wiki/Turbulence, 29/03/2021.

[29] Turbulent flow — definition, characteristics, facts — britannica (n.d.). https://www.britannica.com/science/turbulent-flow, 29/03/2021.

[30] Hrvoje Jasak. Turbulence modelling for cfd:numap-foam summer school. 2009.

[31] Robert Castilla. Brief introduction to open source computational fluid dynamics course 2018-19. 2018.

[32] Finite volume method - wikipedia. (n.d.). https://en.wikipedia.org/wiki/Finite_volume_method, 27/03/2021.

[33] Gustavo Raush. Verification validation in cfd and numerical calculations.

[34] Ronaldo G. Glasgow Larry A. Bonifacio, Henry F. Maghirang. Numerical simulation of transport of particles emitted from ground-level area source using aermod and cfd. 8:488–502, 2014.

[35] Generic scalar transport equation – cfd-wiki, the free cfd reference. (n.d.). https://www.cfd-online.com/Wiki/Generic_scalar_transport_equation, 27/03/2021.

[36] Navier-stokes equations. (n.d.). https://www.grc.nasa.gov/www/k-12/airplane/nseqs.html, 27/03/2021.

[37] Strain-rate tensor - wikipedia. (n.d.). https://en.wikipedia.org/wiki/Strain-rate_tensor, 27/03/2021.

[38] Reynolds number. https://en.wikipedia.org/wiki/Reynolds_number, 12/05/2021.

[39] Prandtl number. https://en.wikipedia.org/wiki/Prandtl_number, 12/05/2021.

[40] Turbulence models in cfd - rans, des, les and dns. (n.d.). https://www.idealsimulations.com/resources/turbulence-models-in-cfd/, 29/03/2021.

[41] Conservative vector field (n.d.). https://en.wikipedia.org/wiki/Conservative_vector_field#Irrotational_vector_fields, 02/05/2021.

[42] Direct numerical simulation - wikipedia. (n.d.). https://en.wikipedia.org/wiki/Direct_numerical_simulation, 29/03/2021.

[43] Large eddy simulation - wikipedia. (n.d.). https://en.wikipedia.org/wiki/Large_eddy_simulation, 29/03/2021.

[44] Reynolds-averaged navier–stokes equations - wikipedia. (n.d.). https://en.wikipedia.org/wiki/Reynolds-averaged_Navier\OT1\textendashStokes_equations, 29/03/2021.

[45] Introduction to turbulence/reynolds averaged equations – cfd-wiki, the free cfd reference. https://www.cfd-online.com/Wiki/Introduction_to_turbulence/Reynolds_averaged_equations, 30/03/2021.

[46] Turbulence modelling simulation. https://transat-cfd.com/download/release/5.7/manuals/TransAT_turbulence_handbook.html#x1-30001, 17/06/2021.

[47] One equation turbulence models – cfd-wiki, the free cfd reference. https://www.cfd-online.com/Wiki/One_equation_turbulence_models, 30/03/2021.

[48] Two equation turbulence models – cfd-wiki, the free cfd reference. https://www.cfd-online.com/Wiki/Two_equation_models, 30/03/2021.

[49] Rng k-epsilon model – cfd-wiki, the free cfd reference. (n.d.). https://www.cfd-online.com/Wiki/RNG_k-epsilon_model, 30/03/2021.

[50] Yu Khaing Thet, Mon Soe San. Comparison of turbulence models for computational fluid dynamics simulation of wind flow on cluster of buildings in mandalay. 7:337–350, 2017.

[51] Wall functions — introduction to cfd. (n.d.). https://cfd.blogs.upv.es/turbulence/wall-functions/, 06/04/2021.

[52] Schmidt number. https://en.wikipedia.org/wiki/Schmidt_number, 12/05/2021.

[53] Jesse Yu, Hesheng Thé. Simulation of gaseous pollutant dispersion around an isolated building using the k– sst (shear stress transport) turbulence model. pages 517–536, 2017.

[54] Ansys fluent 12.0 user's guide - 6.2.2 mesh quality. https://www.afs.enea.it/project/neptunius/docs/fluent/html/ug/node167.htm, 29/03/2021.

[55] Openfoam v6 user guide: 4.1 openfoam case directory. https://cfd.direct/openfoam/user-guide/v6-case-file-structure/, 06/04/2021.

[56] Openfoam: User guide: controldict. https://www.openfoam.com/documentation/guides/latest/doc/guide-case-system-controldict.html, 06/04/2021.

[57] Openfoam: User guide: pisofoam. https://www.openfoam.com/documentation/guides/latest/doc/guide-applications-solvers-incompressible-pisoFoam.html, 06/04/2021.

[58] Practical cfd modeling: Judging convergence — datawave marine solutions. https://www.dmsonline.us/practical-cfd-modeling-judging-convergence/, 15/04/2021.

[59] S. Cavaleri, L. Zecchetto. Reynolds stresses. pages 443–448, 1985.

[60] How to add a passive scalar to your openfoam simulations. https://cfd-training.com/2018/08/14/how-to-add-a-passive-scalar-to-your-openfoam-simulations/, 018/04/2021.

[61] Molecular transport equations. (n.d.). https://slideplayer.com/slide/7057670/, 29/04/2021.

[62] Chun-Ho C Leung Dennis Y Li, Xian-Xiang Liu. Large-eddy simulation of flow and pollutant dispersion in high-aspect-ratio urban street canyons with wall model. 129:249–268, 2008.

—- This page has been intentionally left blank —-

Air distribution in street canyons: a CFD study

Thesis submitted in partial fulfillment of the requirements for the degree

of

Bachelor's degree in Industrial Technologies Engineering

by

Pau Garcia Moreno

Under the supervision of

Ivette María Rodríguez Pérez

UNIVERSITAT POLITÈCNICA DE CATALUNYA
BARCELONATECH
Escola Superior d'Enginyeries Industrial, Aeroespacial i Audiovisual de Terrassa

Department of Heat engines and machines

Polytechnic University of Catalonia, ESEIAAT

Date: June 22, 2021